Condensed Phase Properties of Platinum Group Metal Complexes from Computational Simulations

by

M.R. Burger

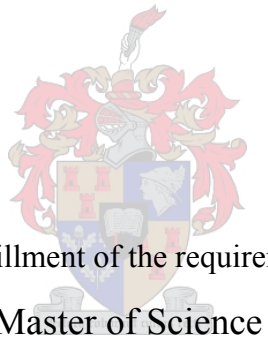

Thesis presented in fulfillment of the requirements for the degree of

Master of Science

in Chemistry at the

University of Stellenbosch

Supervisor: Prof. K.R. Koch (S.U.)
Co-supervisor: Prof. K. Naidoo (U.C.T.)

Stellenbosch
April 2004

Declaration

I the undersigned hereby declare that the work contained in this thesis is my own original work and that I have not previously in its entirety or in part submitted it at any university for a degree.

Signature:

Date:

Summary

A variety of computational techniques are used to calculate structural, thermodynamic and transport properties of two specific Platinum Group Metal (PGM) complex systems. The first system consists of a PGM complex ($[PdCl_4]^{2-}$; $[PtCl_4]^{2-}$; $[PtCl_6]^{2-}$ or $[RhCl_6]^{3-}$) with sodium counter-ions in a water solution at 30ºC and at a concentration of 0.106 mol/dm^3. The second system under consideration is that of a PGM complex ($[PdCl_4]^{2-}$; $[PtCl_4]^{2-}$; $[PtCl_6]^{2-}$ or $[RhCl_6]^{3-}$) with sodium counter-ions in a water solution in the presence of four poly (ethylene oxide) (PEO) chains at 30ºC and at a concentration of 0.013 mol/dm^3. A conformational study of the two types of dihedral angles in a PEO chain (-C-O-C-C- and -O-C-C-O-) is performed and the extreme flexibility of the polymer is confirmed. Dihedral angle distributions of the two dihedral angles are calculated and explained in terms of the potential energy surface obtained from the conformational study. The solvation geometries of the PGM complexes are confirmed and the results are contrasted with those in the system where the polymer (PEO) is present. It is concluded that the effect of the polymer on the structure and degree of solvation is negligible. The free energy of solvation values of the PGM complexes are calculated to provide insight into their structural characteristics such as solvation shell volume and geometry. The structural and thermodynamic properties of the PGM complexes in solution are also used to explain the trends observed in the calculated diffusion coefficients. Comments are made on the accuracy of the calculated diffusion coefficients as well as the legitimacy of the mechanistic speculations which results from them. Suggestions regarding possible future improvements to the computational methods are made.

Opsomming

Verskeie berekenings tegnieke is aangewend om die strukturele, termodinamiese en verplasings eienskappe van twee spesifieke Platinumgroep Metaal (PGM)-kompleks sisteme te bereken. Die eerste sisteem bestaan uit die PGM-kompleks ($[PdCl_4]^{2-}$; $[PtCl_4]^{2-}$; $[PtCl_6]^{2-}$ of $[RhCl_6]^{3-}$) met natrium teen-ione in water by 30ºC en met ‘n konsentrasie van 0.106 mol/dm^3. Die tweede sisteem bestaan uit die PGM-kompleks ($[PdCl_4]^{2-}$; $[PtCl_4]^{2-}$; $[PtCl_6]^{2-}$ of $[RhCl_6]^{3-}$) met natrium teen-ione in water in die teenwoordigheid van vier poli-etileenoksied (PEO) kettings by 30ºC en met ‘n konsentrasie van 0.013 mol/dm^3. ‘n Studie is gemaak van die konformasies van die twee soorte dihedrale-hoeke in ‘n PEO-ketting (-C-O-C-C- en -O-C-C-O-) en die insense buigbaarheid van die polimeer is hiermee bevestig. Die dihedrale-hoek-verspreidings van die twee tipes dihedrale hoeke is bereken en word verduidelik in terme van die potensiële energie kromvlakke soos bereken tydens die konformasie analiese. Die geometrie van die solvasie van die PGM-komplekse is bereken en vergelyk met die sisteme waar die polimeer (PEO) teenwoordig is. Hieruit word afgelei dat die effek van die polimeer op die struktuur en graad van solvasie van die komplekse minimal is. Die vrye energie van solvasie van die PGM-komplekse is bereken met die doel om insig in te win oor die stukturele eienskappe soos byvoorbeeld die volume van die solvasie sfeer en die geometrie daarvan. Die strukturele en termodinamiese eienskappe van die PGM-komplekse in oplossing word ook gebruik om die neigings in die berekende diffusie koëffisiente te verduidelik. Opmerkings word gemaak aangaande die akkuraatheid van die berekende diffusie koeffisiente asook die geldigheid van die meganistiese spekulasies wat daaruit gemaak word. Voorstelle word ook gemaak rakende toekomsige verbeterings aan die reken tegnieke.

Acknowledgements

I would like to express my gratitude to the following persons, without whom this work would not have been possible:

My supervisor, Prof. Klaus R. Koch (Stellenbosch University), for his support as well as his insight and enthusiasm which inspires everybody around him.
My co-supervisor, Prof. Kevin Naidoo (UCT), for his guidance, patience, support and encouragement as well as providing me with the opportunity to work at UCT.
Dr. Dave Robinson (Anglo Platinum), for his interest and creative suggestions.
Dr. Michelle Kuttel (UCT), for her generosity in sharing her knowledge and experience.
Chas Simpson (UCT), for making me feel welcome and at home at UCT as well as for him sense of humor.
Jeff Chen and Dr. Anton Lopis for their support and conversation.
The National Research Foundation for financial support.
My parents for their everlasting interest, patience and understanding.
My friends who have kept me sane throughout.

Index

Chapter 1

INTRODUCTION

Chapter 2

COMPUTER SIMULATIONS TO DETERMINE STRUCTURAL AND TRANSPORT PROPERTIES

Chapter 6

PRELIMINARY DIFFUSION STUDIES

Chapter 1

INTRODUCTION

1.1 Developing a model to predict Platinum Group Metal (PGM) separation

Several attempts have been made to design and build columns in order to separate a variety of Platinum Group Metal (PGM) complexes [1-6] . However, very little effort has been invested into understanding the mechanisms involved in these separations. The design of an effective column, which would be capable of separating these PGM complexes with high resolution, relies heavily on a thorough understanding of the solvation structure and thermodynamic properties of the PGM complexes as well as the structure and interaction energies of these complexes with the stationary phase. In order to obtain structural and thermodynamic data for these systems several computational methods can be employed.

1.2 Possible separation mechanisms

1.2.1 Anion Exchange and liquid-liquid extraction

In this section the important concepts related to anion-exchange separations by liquid-liquid extraction will briefly be mentioned. To some extent, these principles are parallel to those of ion-pair extraction processes. A brief description of the physical factors relevant to anion solvent-extraction methods is presented. Numerous reviews and books [7-9] have thoroughly treated these concepts and will be referenced appropriately. Several separation processes exists (especially in industry) which are based almost exclusively on these physical and chemical phenomena [7]. An understanding is needed of how the underlying chemical driving forces can be manipulated or exploited to achieve better separations. The driving forces in simple solvent extraction processes are those of solvation and electrostatics. In turn, these effects are functionally dependant on ion-properties such as size, symmetry, hydrophobicity and charge. The principles of electrostatics are quite effective when used to explain solvent-extraction processes [9, 10]. This is due to the fact that the solvation of anions involves hard-hard interactions almost exclusively. Several expressions have been developed which can be used to make useful predictions, such as solvation free energies etc. The dependence of these predictions on anion dimensions (size and symmetry) and solvent dielectric constants etc. will be discussed in chapter 3. The concept of primitive selectivity phenomena, such as *size bias*, is briefly explained in this section. The factors which could be used to influence the direction of the bias are also mentioned. A positional separation of anions from one phase to another implies that the mechanism of the transfer of ions across phase boundaries needs to be investigated. The change in ion-solvation characteristics which results from this transport is important, because the overall driving force and selectivity of the system are influenced by these changes.

In this discussion we assume that electrostatic interactions are predominantly responsible for the selectivity in anion exchange separations. That means that selectivity is a function of physical properties such as the size of the ion and the dielectric constant of both solute and solvent. To illustrate the concept of bias we focus temporarily on simple spherical anions. For these anions a clear pattern exists within a set charge type. The extractive preference increases with increasing anion size. From this it is apparent that no specific recognition is involved, but rather a bias towards bigger anions. Recognition separation demands receptor species with three-dimensional qualities such as appropriate bonding sites and complimentary structural features [10]. In recognition extraction the effect of size bias is also present, but is seen as *baseline selectivity*. Therefore, an understanding of bias in a system is also important when we want to evaluate the relative merit of receptors. Selectivity in anion exchange systems do not benefit from stable coordinate bonding, but relies solely on physical interactions and solvation. There are certain effects (steric interactions, multiple hydrogen bonding and unique organization of the extraction complex) which results in departure from the strict definition of

bias. These effects are classified as primitive aspects of recognition. Numerous industrial separation processes have been developed based on size and solvation bias.

The table below summarizes the factors characteristic of the two types of selectivity. (Table reproduced from [10])

Bias	***Recognition***
1) Monotonic trend	1) Peak preference
2) Little geometrical preference	2) Geometry sensitive
3) Physical variables important	3) Bonding Character important
4) Solvation important	4) Shielding from solvent
5) No host	5) Host-guest interaction
6) Simple ligand	6) Multifunctional ligand

1.2.2 Chromatographic methods and principles

The techniques used to separate these PGM complexes cover a variety of chromatographic methods. Reversed-phase liquid chromatography can be used [6] where the adsorption on the boundary surface between the mobile and stationary phase is governed by the polarities of the components involved. For such a column the retention is influenced by characteristics of the components one wants to separate as well as properties of the stationary and mobile phases. Retention decreases with: (1) an increasing solubility in water of the component, (2) an increase in polarity of the component and (3) a decrease in ionic character of the component. Retention is also decreased by an increasing concentration of organic eluent. The choice of organic eluent also has an influence on the selectivity of the column. The functional groups present on the stationary phase have a profound effect on retention. Reversed-Phase LC is a very powerful mode of LC, because of its accuracy, repeatability and reliability [11, 12] . This mode is however of limited use for ionic compounds which can be dealt with more effectively by using Ion Pair LC.

The concepts behind solvent extraction can be used to derive the principle of Ion Pair Chromatography [13, 14] . An ion in aqueous solution can be extracted by an organic solvent if the charge on the ion is compensated by an organic counter-ion. A typical organic counter-ion has an apolar chain with an ionic group. The organic ion pair that results is neutral and therefore dissolves in the organic phase. In Chromatography the counter-ion is generally added to the mobile phase. Retention is influenced by the nature of the counter-ion, the concentration of the counter-ion, the polarity of the mobile phase, the temperature, the pH and the concentration of the ionic component.

Another method that deals effectively with water-soluble ions is Ion-Exchange LC [4] . An ion exchange column generally consists of a macromolecular matrix on which ionogenic groups are bonded. An aqueous solution of an electrolyte is normally used as the mobile phase. In the case of a cation exchanger, the electrolyte (M^+) functions as counter-ion to the anionic group A^- on the stationary phase. The cation, X^+, which we want to separate, can displace the counter-ion M^+ from the stationary phase. In the case of an anion exchanger the same principle applies, but the signs of the charges are reversed. Chemical equilibria play a big role in Ion-Exchange Chromatography. This method is therefore very dependant on the temperature, which influences the position of the equilibrium. The exchanger column has the greatest affinity for ions with higher charge and ions with a smaller solvated volume due to the electrostatic nature of the interactions and their dependence on charge and dimension.

Gel Permeation Chromatography (GPC) [1] and Gel Filtration Chromatography (GFC) are both classified as Size-Exclusion LC. In cases where there is a significant difference in the form, size or the solvated volume of the component molecules this technique may prove effective. GFC is mostly used to isolate large biomolecules, such as proteins. Water is normally used as the mobile phase, which makes this technique both cheap experimentally and easy to simulate computationally. The stationary phase used in GPC consists of porous particles which are synthesized in such a way that the diameter of the pores lies between specific limits. The separation mechanism in GPC is very dependent on the size and diffusion of the components which we want to separate [15] . Elution takes place in order of decreasing size. Smaller molecules or molecules with a smaller solvated volume are more accessible to

diffuse into the pores of the stationary phase. The molecules are temporarily trapped and therefore experience more retention.

Computational techniques exist which allows us to investigate these mechanisms at the molecular level. The free energy of solvation (relevant for Reversed-phase LC) can be determined computationally. Factors such as temperature, pressure, pH and ionic strength can be manipulated. From a Molecular Dynamics (MD) trajectory one can extract useful information such as diffusion coefficients, solvated volumes, solvent accessible surface areas, pore volumes as well as structural properties of the solvated PGM's, the stationary phase and the mobile phase. The electrostatic interactions of the PGM's with the stationary phase can be quantified in terms of binding energies. The amorphous morphology of a polymer based stationary phase can be investigated in terms of surface area and pore sizes.

1.3 The ideal qualitative model to predict separation

In nearly all the methods mentioned in section 1.2 the electrostatic interactions between the PGM's and the polymeric stationary phase plays a determining role in separation. The ideal computational model to predict these separations must have certain qualities in order for it to be accurate and flexible. In such a model one must be able to introduce different functional groups on the polymeric stationary phase. The CHARMM [16] program has reliable and tested force fields available to deal with a large variety of synthetic polymers. Some of the static techniques we can use, such as the Poisson-Boltzmann method [17-19] , do not require exhaustive parameterization and new functional groups can be introduced effortlessly. The advantages and flexibility of this method will be described in section 1.4. The model must have the ability to reflect the influence of pH and ionic strength. These factors have been found to be crucial to the resolution of the separation results. An effective model must also allow the introduction of new PGM species, such as $[PtCl_3(H_2O)]^-$, $[PtCl_5(H_2O)]^-$ etc., without having to go through a full-scale parameterization process. Ideally, the model should provide at least qualitative information regarding the relative binding energies of the PGM complexes to the polymeric stationary phase. The model must be computationally inexpensive and quick so that many permutations and a large number of variables can be accommodated. It must therefore be possible to determine the predicted elution order of chosen PGM species on a specific column. Ideally, the model must provide the capability to test all possible permutations of the input variables, in order to predict the best combination which would result in the best separation.

1.4 The Poisson-Boltzmann (PB) method

The Poisson-Boltzmann [17-22] method satisfies almost all the requirements needed from a model as described in section 1.3. This method is static and treats the solvent as a structureless yet polarizable material. A solvent such as water is therefore treated as a continuum. The dielectric constant of the solvent is used to control its polarizability, which in turn determines the extent of the screening effect of the solvent on different ions in solution. A solvent with a high dielectric constant, such as water, has a greater screening effect than a solvent with a lower dielectric constant, such as methanol. Due to screening two charges in a methanol solution has a greater electrostatic effect on each other than two similar charges at the same distance in a water solution. Poisson-Boltzmann is a numerical method whereby the solute structure is put inside a three dimensional grid and the non-linear (or linear in the case of zero ionic strength) Poisson-Boltzmann equation is solved for every individual grid point. This process is iterated until the electrostatic potentials calculated at every point converge. The reader is referred to Chapter 3.3 for a thorough treatment on this subject. One of the biggest advantages of the Poisson-Boltzmann method is that it does not require complicated parameterization. New PGM species can be introduced with relative ease. The only input parameters this method requires are (1) the dielectric constants of the solvent and the solute, (2) the partial charges on all the atoms in the solute molecule, (3) the ionic strength of the solution, (4) the structural coordinates of the solute molecule and (5) the vd Waals radii of the atoms in the solute molecule. The partial charges are normally obtained from the topology file in the force field. If the force field is not defined then these values can be obtained from quantum calculations. The PB method is so fast that one can easily vary these partial charges to do a sensitivity analysis.

There are several reasons why the PB method is ideal when dealing with PGM systems. As mentioned before, this method is very fast. That means that it would be possible and realistic to extend the chemical system in order to resemble the structure of a true column (amorphous polymer surface area etc.). PB deals particularly well with systems in which long-range interactions (electrostatic) play a dominant role. Electrostatic effects are very likely to dictate the separation mechanism of the PGM complexes. Ionic strength and pH can easily be manipulated in the PB method. The PB method is most accurate when treating systems which are either very constrained or very symmetrical. This is due to the fact PB is a static method. All the PGM complexes are very symmetrical and the polymeric stationary phase is fixed or has a very slow time scale of motion. A great advantage of PB is that the method makes it possible to calculate free energy values, eg. free energy of solvation and binding energies. Other explicit solvent methods to determine free energy values, particularly solvation free energies, are extremely computationally expensive.

1.5 Chemical Systems under consideration

In this study we analysed two specific systems intensively. Structural and thermodynamic properties were determined for both systems. The first system consists of a PGM complex ($[PdCl_4]^{2-}$; $[PtCl_4]^{2-}$; $[PtCl_6]^{2-}$; $[RhCl_6]^{3-}$) with sodium counter-ions in a water solution at 30ºC and at a concentration of 0.106 mol/dm^3. A previous study [23] covered much of the structural properties of these solvated PGM complexes. These results were confirmed and extended by adding diffusion studies and thermodynamic calculations to the analysis. The purpose of investigating this system was to determine solvation geometries, free energies of solvation as well as diffusion coefficients for all the PGM species. A full description of how these systems were generated as well as details on how the simulations were performed can be found in section 4.2.

The second system under consideration was that of a PGM complex ($[PdCl_4]^{2-}$; $[PtCl_4]^{2-}$; $[PtCl_6]^{2-}$; $[RhCl_6]^{3-}$) with sodium counter-ions in a water solution in the presence of four polymer chains (Poly (ethylene oxide)) at 30ºC and at a concentration of 0.013 mol/dm^3.This investigation served several purposes, such as: (1) determining the structural behaviour of the polymer in water, (2) quantifying the change, if any, in the degree of solvation of the PGM complexes due to the presence of the polymer, (3) establishing the effect of the polymer on the diffusion of the PGM complexes and (4) calculating numerous thermodynamic properties of the system. This system should be considered as a very crude model of a possible separation column. However, this model does not accurately resemble the molecular structure of the components in a real column, and the weaknesses thereof are mentioned in section 4.2 and 3.

1.6 Information needed to lay the foundation for the model

Limited experimental data is available for the systems we considered. This section attempts to give a brief overview of these sources as well as explain the gaps that this study intends to fill. What we knew before this study commenced is based on related experimental and computational investigations. Very few computational studies on the systems described in section 1.5 are documented, but the techniques are well defined and thoroughly references in this treatment. The principles of obtaining and interpreting the conformational potential energy maps (adiabatic maps) for polymer chains are well established [24-26] . The technique for the application of simulated annealing to conformational analysis of disaccharides [27] was adjusted to be used on a polymeric (PEO) system. An interesting conformational study on PEO was performed which described the influence of Hydrogen-Bonding and polar interactions [28] . An experimental study reported on the role of hydrogen bonding in a dilute solution of PEO and water [29] . The development of the poly(ethylene oxide) force field [30] was verified for the CHARMM [16] program. This study [30] describes (1) the parameterization process and methodology for this polymer, (2) the force field validation process, (3) the PVT behaviour of PEO oligomers, (4) the cohesive properties of PEO, (5) dihedral angle distributions as well as (6) end-to-end distance distributions. The force field validation process in this study was almost exactly duplicated. The above mentioned paper is definitive in describing the PEO force field development and validation. Other computational studies of PEO [31] focussed on its amorphous properties such as its glass transition temperature, condensed phase conformational triads population analysis, radial distribution functions and helical structure analysis.

Several computational studies investigating a PEO-based polyelectrolyte system were performed. These papers are uniquely relevant as they describe the techniques to obtain information such as (1) diffusion coefficients of ionic species in condensed media [32] [33] , (2) binding properties of ions by the polymer [34] , (3) ion pairing in amorphous PEO [35] , (4) adiabatic maps and vibrational spectra [36] . These techniques were used as guidelines to perform similar simulations on the systems described in section 1.5. Despite the usefulness of the method descriptions, these investigations were performed on different systems. No prior free energy calculations have been performed on the systems we are interested in, but the techniques are well defined [17-22, 37-46] and have been applied to other systems. Before an effective model to predict PGM separation can be designed, we need information regarding energy, structure and thermodynamics of the systems described above. The following sections (1.6.1 to 3) broadly outline these requirements.

1.6.1 Information from Molecular Dynamics (MD) simulations

Molecular Dynamics [47] simulation is a useful tool to obtain many of these properties, especially those related to potential energy and structure. In order for the Poisson-Boltzmann model to succeed, we need to be sure that the behaviour of the system (in terms of binding interactions and preferred conformational states) is governed by electrostatic effects. By analysing the energy profiles in a MD trajectory this crucial prerequisite can be confirmed. The model also requires suitable average structures for both the polymer (PEO) and the solvated PGM. A conformational study of the two dihedral angles in a PEO chain (-C-O-C-C- and -O-C-C-O-) is necessary to obtain information on the flexibility (ie. the accessibility of conformational space) of the polymer. A dihedral angle distribution of these two dihedral angles can also be calculated to serve as a map to generate starting structures for the polymer chains. These angles are randomly assigned along the chain according the calculated probability distributions. By calculating the end-to-end distance (ie. the distance between two terminal groups of the polymer chain) time series we can establish the relative ease with which the polymer folds as well as quantifying the time scale of motion. The study mentioned in section 1.5 [23] provides almost all the information needed about the solvation geometries of the PGM complexes. These results need to be compared and contrasted with those of a system where the polymer is present. If these results are quantitatively consistent it can be assumed that the polymer does not significantly interfere with the solvation structures. By integrating the probability density function of the ether oxygens on the polymer chain to the metal centre of the complex we can quantify how many ether oxygens are involved in a possible interaction. This could give a crude indication of binding or the degree of repulsion. Finally, the equilibrated MD trajectories can be used to calculate mean square displacement values over time. These projections can be used to calculate the diffusion coefficients of the PGM complexes.

1.6.2 Information from explicit solvent thermodynamic simulations

Explicit solvent free energy simulations are computationally very expensive, but produce useful data. The difference in the solvation free energies of two PGM complexes can be calculated by using the thermodynamic integration method [37] . This $\Delta\Delta G$ value can be compared with the same difference in values calculated with the Poisson-Boltzmann method. If these values are similar, it would be a big step towards validating the use of the PB method for these systems. Component analysis should be performed to establish whether the solvation free energy is dominated by enthalpic or entropic effects. A dominant enthalpic effect would favour the PB method which neglects to incorporate the entropic penalty of solvent rearrangement and cavity creation upon solute insertion.

1.6.3 Information from continuum solvent thermodynamic simulations

The Poisson-Boltzmann method can be used to generate electrostatic potential contour maps from which electric field lines and free energy values can be calculated. The free energy of solvation of the PGM complexes, with and without the polymer present, can be determined. Most importantly, the binding energies of the PGM complex to the polymer can be calculated.

1.7 Challenges involved with calculating the diffusion coefficient

Calculating diffusion coefficients [48] from MD trajectory data is a challenge due to the relatively short time intervals over which the mean square displacements are collected. This problem can be solved by simulating longer trajectories (over 5 ns). Several mathematical and statistical techniques exist that might also help to clarify the integrity of the results obtained.

1.8 The objectives of this work

The objective of the opening two chapters (chapter 2 and chapter 3) is to present a very brief theoretical description of the various techniques which will be used in later chapters to generate data from which structural, thermodynamic and transport related information can be deduced. Discussions will focus exclusively on those techniques which should to be treated in a unique way due to the specific demands of the PGM systems which will be investigated.

The objective in chapter 4 is to describe computational techniques which can be employed to determine a variety of properties; specifically those related to potential energies and solvation structures of PGM chloro-complexes in water and poly (ethylene oxide) solutions. Two specific system types are to be simulated and analysed intensively. The first system consists of a PGM complex ($[PdCl_4]^{2-}$; $[PtCl_4]^{2-}$; $[PtCl_6]^{2-}$; $[RhCl_6]^{3-}$) with sodium counter-ions in a water solution at 30ºC and at a concentration of 0.106 mol/dm^3. The second system under consideration is that of a PGM complex ($[PdCl_4]^{2-}$; $[PtCl_4]^{2-}$; $[PtCl_6]^{2-}$; $[RhCl_6]^{3-}$) with sodium counter-ions in a water solution in the presence of four polymer chains (poly (ethylene oxide)) at 30ºC and at a concentration of 0.013 mol/dm^3.

The aim in chapter 5 is to describe the procedures and results obtained from two independent computational techniques which can be used to calculate thermodynamic properties of the solute molecules in PGM systems. The systems on which these thermodynamic analysis will be performed involves a variety of PGM Chloro-Complexes ($[PdCl_4]^{2-}$, $[PtCl_4]^{2-}$, $[PtCl_6]^{2-}$ and $[RhCl_6]^{3-}$) with the appropriate number of counter ions in a water solution. Thermodynamic properties (particularly free energy of solvation values) will be calculated to provide insight into the structural characteristics observed in chapter 4 (solvation shell volume and geometry) as well as the diffusion coefficients which will be calculated and reported in chapter 6. The thermodynamic results will then be used to clarify the observed trends or phenomena and offer possible explanations for their occurrence. Chapter 5 should therefore complement chapter 4 and chapter 6 by validating the structural and diffusion results and offering unique mechanistic insight.

The objective in chapter 6 is to investigate the influence of physical and thermodynamic properties on the diffusion coefficient. Special attention will be given to those properties which can be calculated computationally. The two systems types which will be investigated in this chapter are (1) the PGM chloro-complexes in water and polymer (PEO) solution, and (2) the PGM chloro-complexes in water solution. The aims are also to comment on the accuracy of the calculated diffusion coefficients as well as the legitimacy of the mechanistic speculations which results from this and previous chapters. This chapter is a preliminary investigation and should contain suggestions regarding possible future improvements to the computational method.

References

1. B. Limoni-Relis and G. Schmuckler, *Intersepararion of platinum metals in concentrated solution by gel permeation chromatography.* Separ. Sci. Techn., 1995. **30**(3): p. 337-346.
2. A.V. Pirogov and J. Havel, *Determination of platinum, palladium, osmium, iridium, rhodium and gold as chloro complexes by capillary zone electrophoresis.* J. Chromatogr. A, 1997. **772**: p. 347-355.
3. A.R. Timerbaev, A. Kung and B.K. Keppler, *Capillary electrophoresis of platinum-group elements.* J. of Chromatogr. A, 2002. **945**(1-2): p. 25-44.

4. J. Kramer, W.L. Driessen and K.R. Koch, *Highly selective extraction of platinum group metals with silica-based (poly)amine ion exchangers applied to industrial metal refinery effluents.* Hydrometallurgy, 2002. **64**(1): p. 59-68.
5. X. Chang and Y.F. Li, *Synthesis and characterization of a macroporous poly(vinyl-aminoacetone) chelating resin for the preconcentration and separation of traces of gold, palladium, rhodium and ruthenium.* Talanta, 1992. **39**(8): p. 937-941.
6. L.V. Bogacheva, L.A. Kovalev and T.I. Tikhomirova, *Sorption of palladium on hyrophobic polymers in the presence of alkylamines.* Sep. Purif. Technol., 2002. **29**(1): p. 33-40.
7. Y. Marcus and A.S. Kertes, *Ion Exchange and Solvent Extraction of Metal Complexes*. 1969, New York: Wiley Interscience.
8. J. Rydberg, C. Musikas, and G.R. Choppin, *Principles and Practices of Solvent Extraction*. 1992, New York.
9. T. Sekine, *Solvent Extraction Chemistry: Fundamentals and Applications*. 1977, New York: Marcel Dekker.
10. A. Bianchi and K. Bowman-James, *Supramolecular Chemistry of Anions*. 1997, New York: Wiley-VCH.
11. I. Halasz, *Columns for Reversed Phase Liquid Chromatography.* Anal. Chem., 1980. **52**(1393A).
12. P.E. Antle and L.R. Snyder, *Selecting Columns for Reversed-Phase HPLC.* Lig. Chromatogr. HPLC Mag., 1985. **3**(98).
13. E. Tomlinson, T.M. Jefferies, and C.M. Riley, *Ion-Pair High-Performance Liquid Chromatography.* J. Chromatogr., 1978. **159**(315).
14. R. Gloor and E.L. Johnson, *Practical aspects of Reversed Phase Ion Pair Chromatography.* J. Chromatogr. Sci., 1977. **15**(413).
15. S.A. Borman, *Recent Advances in Size Exclusion Chromatography.* Anal. Chem., 1983. **55**(384A).
16. B.R. Brooks, D. Janezic, R.M. Venable and M. Karplus, *CHARMM:A program for macromolecular energy,minimization,and dynamics calculations.* J. Comput. Chem., 1983. **4(2)**: p. 187-217.
17. J. Shen. and A. Quiocho, *Calculation of binding energy differences for receptor-ligand systems using the Poisson-Boltzmann method.* J.Comput.Chem., 1995. **16**(4): p. 445-448.
18. K. Sharp, *Inorporating solvent and ion screening into molecular dynamics using the finite-difference Poisson-Boltzmann method.* J.Comput.Chem, 1991. **12**(4): p. 454-468.
19. K. Sharp and B. Honig, *Calculating total electrostatic energies with the nonlinear Poisson-Boltzmann equation.* J.Phys.Chem., 1990. **94**: p. 7684-7692.
20. A. Nicholls and B. Honig , *A rapid finite difference algorithm,utilizing successive over-relaxation to solve the Poisson-Boltzmann equation.* J. Comput. Chem., 1991. **12**(4): p. 435-445.
21. M.E. Davis and J.A. McCammon, *Solving the finite difference linearized Poisson-Boltzmann equation:A comparison of relaxation and conjugate gradient methods.* J.Comput.Chem., 1989. **10**(3): p. 386-391.
22. M.J. Holst and F. Saied, *Numerical solution of the nonlinear Poisson-Boltzmann equation:developing more robust and efficient methods.* J.Comput.Chem., 1995. **16**(3): p. 337-364.
23. K.J. Naidoo, G. Klatt and K.R. Koch, *Geometric Hydration Shells for Anionic Platinum Group Metal Chloro Complexes.* Inorg. Chem., 2002. **41**: p. 1845-1849.
24. A.R. Tiller, *Towards first-principles prediction of polymer configurational statistics.* Polymer, 1994. **35**(21): p. 4511-4520.
25. A.R. Leach, *A survey of methods for searching the conformational space of small and medium-sized molecules.* Comp.Chem.II, 1991: p. 1-55.
26. S. Fujiwara and T. Sato, *Molecular dynamics simulations of structural formation of a single polymer chain:Bond-orientational order and conformational defects.* J.Chem.Phys., 1997. **107**(2): p. 613-623.
27. K.J. Naidoo and J.W. Brady, *The application of simulated annealing to the conformational analysis of disaccarides.* Chem. Phys., 1997. **224**: p. 263-273.
28. G.D. Smith and D. Bedrov, *A Molecular Dynamics Simulation Study of the influence of Hydrogen-Bonding and Polar Interactions on Hydration and Conformations of a Poly(ethylene oxide) Oligomer in Dilute Aqueous Solution.* Macromolecules, 2002. **35**(14): p. 5712-5719.

29. E.E. Dormidontova, *Role of Competitive PEO-Water and Water-Water Hydrogen Bonding in Aqueous Solution PEO Behavior.* Macromolecules, 2002. **35**: p. 987-1001.
30. D. Rigby, H. Sun, and B.E. Eichinger, *Computer Simulation of Poly(ethylene oxide): Force Field, PVT Diagram and Cyclization Behaviour.* Polymer International, 1997. **44**(3): p. 311-330.
31. H. Dong, J.K. Hyun and C. Durham, *Molecular dynamics simulations and structural comparisons of amorphous poly(ethylene oxide) and poly(ethylenimine) models.* Polymer, 2000. **42**(18): p. 7809-7817.
32. J. Ennari, I. Neelov, and F. Sundholm, *Estimation of the ion conductivity of a PEO based polyelectrolyte system by molecular modeling.* Polymer, 2001. **42**(19): p. 8043-8050.
33. J. Ennari, M. Elomaa, and F. Sundholm, *Modelling a polyelectrolyte system in water to estimate the ion-conductivity,.* Polymer, 1999. **40**(18): p. 5035-5041.
34. F. Muller-Plathe and W. van Gunsteren, *Computer simulation of a polymer electrolyte:lithium iodide in amorphous poly(ethylene oxide).* J.Chem.Phys., 1995. **103**(11): p. 4745-4757.
35. J.W. Halley and Y. Duan, *Lithium perchlorate ion pairing in a model of amorphous polyethylene oxide.* J. Chem. Phys., 1999. **111**(7): p. 3302-3308.
36. J. Ennari, J. Hamara, and F. Sundholm, *Vibrational spectra as experimental probes for molecular models of ion-conducting polyether systems.* Polymer, 1996. **38**(15): p. 3733-3744.
37. D.A. Pearlman and P.A. Kollman, *Free energy perturbation calculations:problems and pitfalls along.* J.Chem.Phys., 1994. **94**: p. 101-118.
38. D.L. Severance, J.W. Essex, and W.L. Jorgensen, *Generalized alteration of structure and parameters:a new method for free energy perturbations in systems containing flexible degrees of freedom.* J. Comput. Chem., 1994. **16(3)**: p. 311-327.
39. U.C. Singh, F.K. Brown, P.A. Bash and P.A. Kollman, *An approach to the application of free energy perturbation methods using molecular dynamics.* J.Am.Chem.Soc, 1987. **109(6)**: p. 1607-1614.
40. M. Souaille and B. Roux, *Extension to the weighted histogram analysis method: combining umbrella sampling with free energy calculations.* Comp. Phys. Comm., 2001. **135**: p. 40–57.
41. R.V. Stanton, S.L. Dixon, and K.M. Merz, *General formulation for a quantum Free Energy Perturbation study.* J. Phys. Chem., 1995. **99**: p. 10701 - 10704.
42. J. Mouesca, J.L. Chen and D.A. Case, *Density functional/Poisson-Boltzmann calculations of redox potentials for ion-sulfur clusters.* J.Am.Chem.Soc., 1994. **116**: p. 11898-11914.
43. C. Viebke, J. Borgstrom and I. Carlsson, *A differential scanning calorimetry study of k-carrageenan in the NaCl/CsCl/NaI/CsI systems and analysis by Poisson-Boltzmann.* Macromolecules, 1998. **31**: p. 1833-1841.
44. T. Simonson, G. Archontis, and M. Karplus, *Free Energy Simulations Come of Age: Protein-Ligand Recognition.* Acc. Chem. Res., 2002. **35**: p. 430-437.
45. C. Höög and G. Widmalm, *Free Energy Simulations of D-Xylose in Water and Methyl D-Xylopyranoside in Methanol.* J. Phys. Chem. B, 2001. **105**: p. 6375-6379.
46. H. Schafer, W.F. van Gunsteren, and A.E. Mark, *Estimating Relative Free Energies from a Single Ensemble: Hydration Free Energies.* J. Comput. Chem, 1999. **20**(15): p. 1604]1617.
47. W.F. van Gunsteren and H.J.C. Berendsen, *Molecular dynamics simulations: Techniques and approaches.* Molecular Liquids - Dynamics and Interactions, 1983: p. 475 - 500.
48. I.M.J.J. van de Ven-Lucassen, T.J.H. Vlugt and A.J.J. van der Zander, *Molecular Dynamics Simulation of Self-Diffusion Coefficients in Liquid Mixtures of Methanol and Water.* Mol. Simulat., 1999. **23**: p. 79-94.

Chapter 2

COMPUTER SIMULATIONS TO DETERMINE STRUCTURAL AND TRANSPORT PROPERTIES

This chapter presents a very brief theoretical description of the various techniques used to generate data from which structural and transport related information can be deduced. The purpose of this is to provide the reader with a convenient reference which could facilitate a better understanding of both theory and practical application. Discussions are focused exclusively on those techniques which had to be treated in a unique way due to the specific demands of the PGM systems we are interested in. Section 2.1 covers the concepts behind Molecular Dynamics which are both general and specific to its application in solvated PGM systems. The reader will note that a general explanation of Molecular Mechanics and force fields were omitted. A very thorough treatment of these concepts exits elsewhere [1]. Particular importance is assigned to the use and application of the Ewald summations method which is a prerequisite when working with charged species, such as PGM chloro-complexes and their counter ions. Section 2.2 describes how Conformational Analysis can be used to determine the potential energy surface of a molecule, dictated by chosen degrees of freedom. Special attention is given to the concept of Simulated Annealing and its significance when dealing with polymeric compounds. Two analytical techniques which can be used to determine solvent structure are discussed in section 2.3. Diffusion Analysis theory is treated quite thoroughly in section 2.4. In this case an understanding of the theory contributes substantially our appreciation of the practical stumbling blocks when calculating diffusion coefficients.

2.1 Molecular Dynamics Simulation Methods

2.1.1 Newton's second law:

Molecular dynamics is based on the numerical solution of Newton's second law of motion, $F=ma$, for a many bodied system [2] . Here F is the force on the particle, m is its mass and a its acceleration. From the force on each atom its acceleration in the system can be determined. By integrating these equations of motion a trajectory that describes the positions, velocities and accelerations of the particles can be obtained as they vary with time. From these values, averages of certain properties can be calculated. Equation (1) illustrates how the force, F_i on particle i, is equal to the gradient of the potential energy, V. In equations (2) the derivative of the potential energy is related to the changes in position of the particles as a function of time [1] . In equation 2 the mass of particle i is represented by m_i and the position by r_i.

$$F_i = -\nabla_i V \qquad (1)$$

$$\frac{-dV}{dr_i} = m_i \frac{d^2 r_i}{dt^2} \qquad (2)$$

There are several examples of numerical algorithms to do the required integration. Amongst the lower order methods are the Verlet, Leap-frog and Velocity Verlet algorithms [3] . The Predictor-Corrector method is an example of a higher order algorithm [3] .

2.1.2 The role of Statistical Mechanics:

A many bodied system containing N atoms requires $6N$ values to define the state of the system. A single point in this $6N$-dimensional phase space is defined by one of the $3N$ position and $3N$ momenta combinations [1]. A Molecular Dynamic simulation provides information at the microscopic level, like atomic positions and velocities. Statistical Mechanics is now used to convert the microscopic information to observable macroscopic properties, such as pressure, energy and heat capacities [4] . These macroscopic properties are then related to the distribution and movements of the atoms and molecules of the system.

2.1.3 Ensemble averages

An ensemble is a collection of points in phase space which conforms to the conditions of a specific thermodynamic state [2] . A molecular dynamics (MD) simulation generates a time sequence of these points in phase space. All these points belong to the same ensemble. In other words, an ensemble is a collection of all possible systems with identical macroscopic (thermodynamic) states, but different microscopic states. For a system of N atoms with a volume of V, a pressure of P and an energy of E the following ensembles are most common:

1. Microcanonical ensemble (NVE): N, V and E are fixed. This resembles an isolated system.
2. Canonical ensemble (NVT): N, V and T are fixed.
3. Isobaric-Isothermal ensemble (NPT): N, P and T are fixed. The method and theory of how this is accomplished is discussed below.

Experimental observables are defined in terms of ensemble averages sampled over all of phase space. Let A be the observable of interest, where A is a function of the momenta and positions of the system in question. A can for example be potential energy or kinetic energy. To calculate $\langle A \rangle_{ensemble}$ is difficult however, because all possible states must be taken into account. It is therefore necessary that the MD simulation pass through all the possible states in accordance with the particular thermodynamic constraints that the ensemble demands. Running a MD simulation results in a series from which a time average, $\langle A \rangle_{time}$ can be calculated. The ergodic hypothesis [1] states that the ensemble average of property A is equal to the time average of that property.

$$\langle A \rangle_{ensemble} = \langle A \rangle_{time} \tag{4}$$

Therefore, if the system progresses in infinite time, it will pass through all the possible states. An important condition of an MD simulation is to generate enough representative conformations. Only then can experimentally relevant structural, dynamic and thermodynamic properties be calculated.

2.1.4 The NPT ensemble

Most experimental measurements are made under constant temperature and pressure conditions and are therefore directly comparable to results generated via the NPT ensemble. Implementation of the NPT ensemble is done via two methods. In the first method the temperature of a system is related to the time average of its kinetic energy which is a function of the particle velocities [5] . In the same way, the pressure of a system is related to the volume of the system. Therefore, to alter the temperature or pressure of a system all we need is to alter the velocities or volume respectively. The second method maintains a system at a constant temperature by introducing an external "heat bath". This heat bath scales the velocities in such a way that the rate of change of temperature is proportional to the difference in temperature between the heat bath and the system. In a similar way a constant pressure can be maintained by using a "pressure bath". The pressure bath scales the volume so that the rate of change of pressure is proportional to the difference in pressure in the pressure bath and the system. The above two methods fail to generate satisfactory canonical averages. The overall temperature of the system can be maintained at its desired level quite well, but these methods result in a temperature difference between the solvent and the solute (this is known as the "hot solvent, cold solute" phenomenon). One of the methods to solve this problem was developed by Nose and extended by Hoover [1] . Again the constant temperature and constant pressure methods work on the same principle. In a sense the system is "extended" by including an additional degree of freedom to represent a thermal (or pressure, in the case of constant pressure), reservoir. Both the potential and the kinetic energy of this reservoir can be calculated as a function of this additional degree of freedom.

2.1.5 The Ewald summation method

Long-range forces have to be dealt with carefully, particularly when charged species are present. Interactions which decays slower than r^{-n} (n is the system dimension) present a problem which cannot be dealt with using standard cutoff lists. This is because the range of these interactions is greater than half the box size. An example of this is charge-charge interactions, which decays as r^{-1}.

What follows is a brief description of the technique that the Ewald summation method [6] employs to solve this problem. The total charge-charge contribution, V, to the potential energy comprises of:

(I) Interactions within the central box (cube).
(II) Interactions of the central box with all the image boxes.
(III) Interaction of the image boxes with the surrounding medium.

An expression which incorporates all these interactions is expressed in equation (5). In this equation the left most series excludes i = j terms for $\mathbf{n} = 0$. The number of charges per image box is N, while r_{ij} is the minimum distance between charges q_i and q_j. A box is generally positioned at a cubic lattice point $\mathbf{n}$ defined as: (n_xL,n_yL,n_zL) where L is the length of the cube.

$$V = \frac{1}{2}\sum_{|\mathbf{n}|=0}^{\infty}\sum_{i=1}^{N}\sum_{j=1}^{N}\frac{q_i q_j}{4\pi\varepsilon_0 |\mathbf{r}_{ij}+\mathbf{n}|} \tag{5}$$

The problem with this summation is that it is conditionally convergent. This means that the sum of the positive terms in the series is divergent and therefore doesn't have a finite result. The same applies for the sum of all the negative terms in the series. The sum of a conditionally convergent series therefore depends on the order of the terms - and herein lies the trick of the Ewald summation method. The summation above is therefore converted into separate summations, each of which individually converges much faster. The initial set of charges is surrounded by a Gaussian distribution of equal magnitude but opposite sign (calculated in real space) to which a canceling set of distributions must be added (calculated in reciprocal space). The functional form of these Gaussian distributions can be modified by the parameter α.

A+B:
$$V = \frac{1}{2}\sum_{|\mathbf{n}|=0}^{\infty}\sum_{i=1}^{N}\sum_{j=1}^{N}\frac{q_i q_j erfc(\alpha|\mathbf{r}_{ij}+\mathbf{n}|)}{4\pi\varepsilon_0 |\mathbf{r}_{ij}+\mathbf{n}|} \tag{6}$$

Where equation (7) is the complementary error function and has the following functional form:

$$erfc(x) = \frac{2}{\sqrt{\pi}}\int_x^{\infty}\exp(-t^2)dt \tag{7}$$

This summation (the “real space” summation), as expressed in equation (6), converges rapidly and its convergence rate depends on the width of the Gaussian distributions (if the distributions are wider it converges faster). The parameter, α, should therefore be chosen in such a way that the only terms in the series are those for which $|\mathbf{n}| = 0$.

C: A second series of distributions, equation (8), which exactly cancels the first series is now added. This summation is performed in “reciprocal space” and the vectors, $\mathbf{k}$, are defined as $\mathbf{k} = 2\pi\mathbf{n}/L^2$.

$$V = \frac{1}{2}\sum_{k\neq 0}^{\infty}\sum_{i=1}^{N}\sum_{j=1}^{N}\frac{q_i q_j}{4\pi\varepsilon_0}\frac{1}{\pi L^3}\frac{4\pi^2}{k^2}\exp(-\frac{k^2}{4\alpha^2})\cos(\mathbf{k}.\mathbf{r}_{ij}) \tag{8}$$

This calculation is done in reciprocal space. The series converges slower however if the distributions are wider. This effect is therefore to be balanced with that in A + B.

D: A + B includes the interaction of each Gaussian with itself, and this must be subtracted, as expressed in equation (9):

$$V = -\frac{\alpha}{\sqrt{\pi}}\sum_{k=1}^{N}\frac{q_k^2}{4\pi\varepsilon_0} \tag{9}$$

E: A correction term, equation (10), is needed to account for the medium that surrounds the image boxes. This correction is applicable only if the surrounding medium has a permittivity of 1 (vacuum).

$$V_{correction} = \frac{2\pi}{3L^3}\left|\sum_{i=1}^{N}\frac{q_i}{4\pi\varepsilon_0}\mathbf{r}_i\right|^2 \tag{10}$$

The final result is expressed in equation 11.

$$V = A + B + C + D + E \tag{11}$$

The total charge-charge contribution to the potential energy is therefore obtained by adding all the appropriate terms.

2.2 Conformational Analysis

2.2.1 General introduction and concepts

The object of this analysis is to obtain an overall picture of the potential energy surface defined by specific degrees of freedom, usually dihedral angles [7] . A conformational search is done to determine the preferred conformations of a molecule. Once such an adiabatic map of the potential energy surface is obtained useful information can be extracted [8] such as the global and local minima conformations, transition state conformations and their corresponding barriers heights as well as kinetic pathways of conformational transitions. Most conformational searches focus on finding the minimum energy conformations. Energy minimization algorithms are therefore very important in any conformational analysis. The problem with normal energy minimization methods is that the algorithms are designed to move to the minimum point closest to that of the starting structure. However, to cover the whole of conformational space it is necessary to utilize a separate algorithm which generates starting structures that would subsequently deliver all the appropriate minima. One of these algorithms is Simulated Annealing [9] .

2.2.2 Simulated Annealing

Simulated annealing is a useful technique in solving any problem which has a large number of possible solutions, e.g. a potential energy surface with more than one local minimum [10]. This computational technique attempts to mimic the physical process of annealing where careful temperature control at the liquid-solid transition phase is used and subsequent quenching results in perfect crystals at the global minimum of the free energy. Simulated annealing uses internal energy as a cost function. Molecular dynamics is used to bring a system to thermal equilibrium at a relatively high temperature. Here, the system can freely occupy any region of conformational space, as it has enough energy to pass over any potential energy barriers. This step creates a unique starting structure. Molecular dynamics is also used to lower the temperature in a very controlled fashion. The probability of a specific energy state to be occupied is governed by the Boltzmann distribution. Note that simulated annealing cannot guarantee the finding of the global minimum.

2.3 Analytical Methods

2.3.1 Pair Distribution Function

The localized structure of a solvent is of interest especially when investigating solute solvation. A method which provides useful insight into solvation properties is the pair distribution function (PDF), g(r) [11] . This function, equation (12), is defined as the probability of finding two atoms at a distance *r* apart, relative to the probability of finding them at distance *r* in a completely random distribution.

$$g(r) = \frac{1}{4\pi\rho r^2}\frac{dN(r)}{dr} \tag{12}$$

In equation (12) ρ is the bulk density and N(r) is the number of molecules within a sphere of radius r around the solute. The function is also normalized so that, in the case of water, the value of one corresponds to bulk solvent density. Molecular dynamics simulations provide us with the system trajectories from which g(r) can be deduced and plotted and information can be extracted such as the distance of the nearest neighboring atoms to the atom in question as well as the total number of atoms which form part of the "solvation shell". This number is calculated by integrating g(r) (which needs to be properly normalized).

A. Solvent-Solvent pair distribution functions:
When molecular solvents, such as water, are considered the site-site distributions can be calculated, eg. O-O or O-H PDF's. These pair distributions can easily be related to structural factors calculated using X-ray and neutron diffraction [12] [13] . Therefore, to validate a solvent model the PDF's can be compared with experimentally measured data.

B. Solvent-Solute pair distribution functions:
The distribution of solvent around solute sites can be analyzed using a site-site g(r) with a solute atom or residue as one of the sites [14] . These results cannot be obtained directly from experiment due to the radial averaging of the experimental observables.

Although PDF's give valuable insight into the structure of liquids, they are unsuitable for investigating anisotropic liquid structuring. This is because the PDF's are radially averaged and are therefore limited to give information about the number of neighbors to each site as well as their distance from the site. Information about the precise location of solvent molecules around the solute therefore requires a three dimensional treatment.

2.3.2 Three-Dimensional Solvent Structure around Solute molecules

There are several methods available, the most popular of which is the calculation of a three dimensional probability density matrix for a particular solute conformation [15] . This matrix can be contoured using three dimensional graphing packages [16] . When the solute molecule exists in several conformational forms it is important not to average over all these conformations, but only to consider similar conformations. When considering a solute with a fixed or very rigid conformation this averaging problem disappears.

Related solute conformations are selected out of the trajectory data. Only these frames will be considered when calculating the densities. To eliminate translational and rotational diffusion the selected frames are all rotated and translated in turn to fit a reference position. The solvent site of interest is accordingly binned into a three dimensional grid which is mapped onto the reference position. Depending on the resolution required the number of bins in the grid can be increased. A Gaussian function, representing each nucleus and its surrounding electron density is used to proportion the binning over neighboring bins. The Gaussian is chosen so that the function drops to 10% of its maximum value at the van der Waals radius. These densities are normalized in reference to a random bulk distribution.

2.4 Diffusion Analysis

2.4.1 Introduction

Transport in general is normally described by the following linear equation:

$$Flux = -coefficient \times gradient \tag{13}$$

The flux gives the transfer per unit area in unit time. The coefficient quantifies the resistance to flow, while the gradient provides the driving force for the flux. This equation can be applied whether it is mass, energy or momentum that moves through the system. Macroscopically, these laws are normally applied and observed in non-equilibrium situations. An example of this is a concentration gradient across a membrane which offers a "resistance" to the flux which results. However, in an equilibrated

system molecules redisperse and aggregate to spontaneously create local density fluctuations. The fluctuation-regression hypothesis which Onsager [17] formulated states that these fluctuations are proportional to the local gradients. This means that these fluctuations obey Fick's law [17] . The trajectory data extracted from MD simulations can therefore be used to calculate transport coefficients like the diffusion coefficient. Fick's law describing one-dimensional diffusion is represented in equation (14).

$$N\dot{x} = -D\frac{\partial N}{\partial x} \tag{14}$$

Where:

$$Flux = N\dot{x}$$
$$Diffusion\ coefficient = D$$
$$Number\ of\ atoms\ per\ unit\ volume = N(x,t) = N$$
$$Velocity\ at\ (x,t) = \dot{x}$$

From the continuity of mass the following is true:

$$\frac{\partial N}{\partial t} + \frac{\partial (N\dot{x})}{\partial x} = 0 \tag{15}$$

Therefore, from eq. (14) and eq. (15):

$$\frac{\partial N}{\partial t} = D\frac{\partial^2 N}{\partial x^2} \tag{16}$$

Equation (16) is known as the diffusion equation and can be solved by calculating the function N(x,t) for which eq. (16) applies. Say that N_0 atoms are present at position x = 0 and at time t = 0, then by solving eq. (16) the following one-dimensional equation results:

$$N(x,t) = \frac{N_0}{2\sqrt{\pi Dt}}\exp\left[\frac{-x^2}{4Dt}\right] \tag{17}$$

From this can be seen that, for t > 0, the atoms diffuse away from the origin with time, according to a Gaussian distribution. The second moment of eq. (17) gives the mean-square displacement of atoms.

$$< [x(t) - x(0)]^2 >= \frac{1}{N_0}\int x^2 N(x,t)dx \tag{18}$$

Substituting eq. (17) in eq. (18) followed by integration results in the one-dimensional Einstein relation:

$$< [x(t) - x(0)]^2 >= 2Dt \tag{19}$$

This equation is significant because it directly connects the mean-square displacements to the diffusion coefficient [17] . This is valuable as the mean-square displacements can easily be calculated from the trajectory data. Note that eq. (19) is a linear equation where the slope is 2D and the line cuts through the origin. A simple strategy to calculate the diffusion coefficient would therefore be to calculate the mean-square displacements for different time delays, and plotting the linear equation over time.

The three-dimensional version of eq. (19) is:

$$< [r(t) - r(0)]^2 >= 6Dt \tag{20}$$

To prevent distortions resulting from atom-atom collisions, it is important that the time delays considered when calculating the slope must be as large as possible relative to average collision times. It can be a complicated problem to decide where the slope should be taken. Several things should be considered:

1. The linear line goes through the origin.
2. A time delay range which is significantly greater than the average collision times must be used. These collisions result in directional changes. For very short time delays (time delay < collision time) the displacement resembles the actual distance traveled and the slope represents the speed. The real interest lies in the displacement over time where change in direction due to collisions is included.

Therefore:
$$\lim_{t->\infty} \frac{<[r(t)-r(0)]^2>}{6t} = D \qquad (21)$$

The averages over a specific time delay are calculated over different time origins.

This is an example of a fluctuation-dissipation equation. The Einstein relation shows the relationship of diffusion to time and ensemble averages.

References:

1. A.R. Leach, *Molecular Modelling: Principles and Applications*. First ed. 1996, Singapore: Longman. 595.
2. W.F. van Gunsteren and H.J.C. Berendsen, *Computer Simulation of Molecular Dynamics: Methodology, Applications, and Perspectives in Chemistry.* Angew. Chem. Int. Ed., 1990. **29**: p. 992-1023.
3. W.F. van Gunsteren and H.J.C. Berendsen, *Algorithms for Macromolecular Dynamics and Constraint Dynamics.* Mol. Phys., 1977. **34**: p. 1311-1327.
4. A. Ben-Naim, *Statistical mechanics of aqueous fluids*, in *Prog. in Liq. Physics*, C.A. Croxton, Editor. 1978: Wiley NY. p. 429-451.
5. M.P. Allen and D.J. Tildesley, *Computer Simulation of Liquids*. First ed. 1989, Oxford: Oxford Science Publications.
6. J.D. Adams, *On the use of the Ewald Summation in Computer Simulation.* J. Chem. Phys., 1982. **78**(5): p. 2585 - 2590.
7. A.R. Leach, *A survey of methods for searching the conformational space of small and medium-sized molecules.* Comp.Chem.II, 1991: p. 1-55.
8. B.J. Hardy, S. Bystricky and P. Kovac, *Conformational analysis and molecular dynamics simulation of (1-2)and(1-3)linked rhamnose oligosaccharides:Reconcilliation with optical rotation and NMR experiments.* Biopolymers, 1997. **41**: p. 83-96.
9. S. Kirkpatrick, C.D. Gelatt, and M.P. Vecchi, *Optimization by simulated annealing.* Science, 1983. **220**(4598): p. 671-680.
10. S.R. Wilson, *Conformational analysis of flexible molecules:locaton of the global minimum energy conformation by the simulated annealing method.* Tetrahedron letters, 1988. **29**: p. 35.
11. A. Lienke, G. Klatt, D.J. Robinson, K.R. Koch and K.J. Naidoo, *Modeling Platinum Group Metal Complexes in Aqueous Solution.* Inorg. Chem., 2001. **40**: p. 2352-2357.
12. G.W. Neilson and J.E. Enderby, *Neutron Diffraction experiments of Cl- in water.* Annu. Rep. Prog. Chem., Sect. C, 1979. **76**: p. 185.
13. T. Yamaguchi, K. Hidaka, and A.K. Soper, *The structure of liquid methanol revisited: a neutron diffraction experiment at -80^{O}C and +25^{O}C.* Mol. Phys., 1999. **96**(8): p. 1159-1168.
14. K.J. Naidoo and M.M. Kuttel, *Water Structure about the Dimer and Hexamer Repeat Units of Amylose from Molecular Dynamics Computer Simulations.* J. Comput. Chem., 2001. **22**(4): p. 445-456.
15. K.J. Naidoo, G. Klatt and K.R. Koch, *Geometric Hydration Shells for Anionic Platinum Group Metal Chloro Complexes.* Inorg. Chem., 2002. **41**: p. 1845-1849.
16. L. Laaksonen, *gOpenMol*, . 2000, Center for Scientific Computing: Espoo, Finland.

17. J.M. Haile, *Static Properties*, in *Molecular dynamics simulation: "Elementary Methods"*, J. Wiley, Editor. 1992: New York. p. 224 - 275.

Chapter 3

COMPUTER SIMULATIONS TO DETERMINE THERMODYNAMIC PROPERTIES

There are numerous challenges when calculating thermodynamic properties (particularly free energy values) using computational techniques. This chapter attempts to clarify the theoretical requirements as well as stipulate the practical difficulties implied by these requirements. Section 3.1 describes the fundamental concepts and continues by introducing the two methods used in Chapter 6 to calculate the solvation free energy values. These methods are discussed in terms of their shortcomings and applicability regarding a variety of systems. Section 3.2 and section 3.3 reports respectively on these two methods. These sections focus specifically on the theoretical foundation of the techniques as well as describing the methods of mathematical approximation needed to convert pure theory to practical application. Once again, a thorough understanding of these theories facilitates a better appreciation of the accuracy and relevance of the results and conclusions as reported in Chapter 6.

3.1 General introduction

The free energy profile of a molecule determines its behavior in terms of conformational preferences, binding etc. Several methods are employed to calculate free energies [1-16] . Most methods use the equations of classical statistical mechanics to relate the free energy difference of two molecular states, eg. vacuum vs. solvated, or conformational change, to a thermodynamic ensemble average, eq. 1, of the potential energy of these states.

$$\Delta G = f(\textit{ensemble average function of the potential energy}) \tag{1}$$

Calculating a converged value for these ensemble averages are very demanding since multiple solvent molecules must be averaged over all possible configurations. In this chapter we consider two very different methods of calculating free energies. The first method uses an explicit solvent (water) model, while the second method uses a continuum or implicit solvent model which is more empirical in nature.

Systems where a continuum solvent model is particularly useful are the following:

1. Very big systems where computation time would be excessive if an explicit solvent model was used. Using a continuum solvent model radically reduces computation time.
2. Systems where the effect of ionic strength and long-range electrostatic interactions play a particularly important role. The Poisson-Boltzmann method [17, 18] , which will be discussed later, is very effective in treating such properties.
3. When investigating highly constrained systems where very little conformational change occur it can be redundant to work with explicit solvent molecules.

Systems where an explicit solvent model is useful:

1. A system where specific solvent molecules play a unique role in solvation or conformation (eg. specific hydrogen bonds in carbohydrate conformations).
2. Systems where the detailed solvation shell structures and geometries are of particular interest.
3. Any system where we are interested in the time-dependent properties of the solute, such as diffusion coefficients. The continuum model overestimates these rates because frictional effects of the solvent are neglected. The continuum model implies instantaneous structural rearrangement of the solvent.

3.2 Free Energy Changes in Solution: Thermodynamic Integration

The thermodynamic integration method [16, 19-21] can be derived from basic statistical mechanical equations. The free energy, G, of any system can be related to the integral of the Boltzmann factor over

coordinate (**x**) and momentum (**p**) phase spaces. By applying elementary statistical mechanics for the canonical ensemble (constant NVT) the following equation results:

$$G_{NVT} = -RT \ln Q \tag{2}$$

$$Q_{NVT} = C \iint \exp\left(\frac{-H(x,p)}{RT} \right) dx dp \tag{3}$$

where: R = the gas constant
T = the temperature
Q = the classical configuration partition function
C = a constant related to the number of unique atoms.
H(**x**,**p**) = the Hamiltonian giving the energy of the system as a function of positions, **x**, and momenta, **p**.

The free energy calculated from a canonical ensemble delivers the Helmholtz free energy. These equations can be derived for other ensemble types including the isobaric ensemble (constant NPT) which leads to the Gibbs free energy. In order to simplify the derivation the NVT partition function is used. When the expressions for the free energy differences are defined all the differences in the partition functions of the various ensemble types are cancelled out. The Hamiltonian incorporates both the potential and kinetic energy functions. The potential energy function is not dependent on the momenta however and the kinetic energy function can therefore be treated separately. The kinetic energy contribution is normally assumed to be zero. This implies that the Hamiltonian can be reduced to the potential energy function V(**x**).

Let's consider the free energy difference between two systems, A and B. The first step of the thermodynamic integration method is to define a series of non-physical intermediate points between the two physical endpoints, A and B. Free energy can be calculated via any pathway between A and B since it is a state function. Therefore the total free energy of going from physical state A to B is the sum of the free energies of the intermediate states. These intermediate points are defined by introducing a parameter λ into the potential energy function. The value of λ varies from zero to one and V(λ,**x**) is defined so that:

$$V(0,\mathbf{x}) = V_A(\mathbf{x}),\ V(1,\mathbf{x}) = V_B(\mathbf{x}) \text{ and } V(\lambda,\mathbf{x}) = (1-\lambda)V_A(\mathbf{x}) + V_B(\mathbf{x}) \tag{4}$$

The Hamiltonian H in equation (3) can therefore be replaces by the λ-dependent potential energy function V(λ,**x**). The first derivative of equation (2) is therefore:

$$\frac{dG}{d\lambda} = -\left[\frac{RT}{Q} \right] \left[\frac{dQ}{d\lambda} \right] \tag{5}$$

Differentiation and substitution leads to equation 6.

$$\frac{dG}{d\lambda} = \frac{\int \left(\frac{dV(\lambda,x)}{d\lambda} \right) \exp\left(-V(\lambda,x)/RT\right) dx}{\int \exp\left(-V(\lambda,x)/RT\right) dx} = \left\langle \frac{dV(\lambda,x)}{d\lambda} \right\rangle_{\lambda} \tag{6}$$

The $\langle \rangle_{\lambda}$ notation defines the average within the brackets as determined from the ensemble for the λ state. Integrating this equation gives:

$$\Delta G = \int_0^1 \left\langle \frac{dV(\lambda,x)}{d\lambda} \right\rangle_{\lambda} d\lambda \tag{7}$$

The thermodynamic integration method uses equation 7 to calculate the free energy differences.

3.3 Poisson-Boltzmann based continuum methods

3.3.1 Introduction

In a continuum model substances are treated as structureless, homogeneous dielectric media, which can be polarized by electric charges. Therefore, rather than explicitly representing each molecule in the solvent, a dielectric constant is used which is a parameter measuring the bulk polarizability of the media. The dielectric constant, as can be seen in equation 8, is therefore also related to the extent to which the coulomb forces between two charges are weakened due to the screening effect of the solvent.

$$F = \frac{q_1 q_2}{\varepsilon R} \tag{8}$$

The more polar the solvent the higher the dielectric constant and the more significant the screening effect.

Solvent:	*Dielectric constant, ε*:
Vacuum	1.0
Ethylether	4.3
Methanol	32.6
Water	78.5

3.3.2 Continuum models of solvation and electrostatics

The free energy of solvation of a molecule is understood as the transfer of the molecule from vacuum to water.

Three energy factors contribute to this value, as expressed in eq. 9:

1. The electrostatic contribution to the free energy.
2. The entropy penalty attributed to the creation of the cavity in the solvent to allow solute insertion. This value represents the work done in solvent rearrangement and reorientation as well as the energy involved in the actual solute insertion.
3. The van der Waals interaction energy between solute and solvent.

$$\Delta G_{solvation} = \Delta G_{vdWaal} + \Delta G_{cavity} + \Delta G_{electrostatic} \tag{9}$$

Continuum methods can be categorized into Analytical and Numerical methods.

3.3.2.1 Analytical Methods:

In these methods the response of the continuum dielectric to the electrostatic multipoles is solved analytically. The Born model is such an example. The Born model only considers the zeroeth order electric moment. The ion is treated as a uniformly charged sphere which exclusively interacts via its charge.

$$\Delta G_{electrostatic} = -\frac{\varepsilon - 1}{2\varepsilon}\frac{q^2}{R} \tag{10}$$

In equation 10: R is the ion radius, ε is the dielectric constant and q represents the charge.

The Onsager Model is another analytical method that is often used. This model was founded on the second term in the electric multipole expansion. As with the Born model the solute is treated as spherical (radius=R), but the sphere is allowed a dipole, μ and a polarizability factor, α .

$$\Delta G_{electrostatic} = -\frac{\varepsilon - 1}{2\varepsilon + 1}\frac{\mu^2}{R^3}\left[1 - \frac{\varepsilon - 1}{2\varepsilon + 1}\frac{2\alpha}{R^3}\right]^{-1} \tag{11}$$

The Debye-Hückel Theory investigates the long-range forces acting between ions of a strong electrolyte. Consider a system with a positive reference ion in solution with a mixture of other positive and negative ions. Let q_p and q_n be the charges of the positive and negative surrounding ions respectively. The corresponding concentrations (at a distance far enough from the reference ion so that the potential felt from the reference ion is zero) of these ions are represented by $C_p(\infty)$ and $C_n(\infty)$. In turn $C_p(r)$ and $C_n(r)$ are the respective concentrations at distance r from the reference ion. It can be shown that:

$$C_p(r) = C_p(\infty)e^{\left[-\frac{q_p e\phi(r)}{kT}\right]} \tag{12}$$

$$C_n(r) = C_n(\infty)e^{\left[-\frac{q_n e\phi(r)}{kT}\right]} \tag{13}$$

In equation 12 and 13, ø(r) represents the potential at distance r from the positive reference ion. Since $q_p > 0$ and $q_n < 0$ it is clear that $C_n(r) > C_p(r)$, which is what we would expect. More negative than positive ions are found in the vicinity of the positive reference ion and vice versa. Every ion in solution therefore has a "counter ion atmosphere". It is important therefore to get an appropriate expression for ø(r), especially in dilute solutions containing more than two ion types. It can be shown that:

$$\phi(r) = \frac{q_i e}{\varepsilon r} - \frac{q_i e\kappa}{\varepsilon} \tag{14}$$

where:

$$\kappa^2 = \frac{8\pi e^2}{\varepsilon kT} \times I \tag{15}$$

The ionic strength of a solution, I, is defined as:

$$I = \frac{1}{2}\sum_i C_i q_i^2 \tag{16}$$

The equation for the potential can also be written as:

$$\phi(r) = \frac{q_i e}{\varepsilon}\frac{1}{r} - \frac{q_i e}{\varepsilon}\frac{1}{1/\kappa} \tag{17}$$

The first term in equation 17 is the potential (due to the reference ion itself) at distance r from the reference ion in the absence of other ions. The second term is the potential (due to the "counter ion atmosphere") at "distance" 1/κ from the reference ion. This "distance" is known as the "debye length" and plays the same role in the second term as r plays in the first term.

3.3.2.2 Numerical methods: Solving the Poisson-Boltzmann equation:

This continuum method calculates the electrostatic potential, ø(r), across a three dimensional grid. Once the electrostatic potential has been calculated, the following properties can be derived:

(i) The electrostatic field: $-\frac{d\phi(r)}{dr}$

(ii) The electrostatic energy of charge q: $q\,\phi(r)$
(iii) Equilibrium constants at any point in space.
(iv) The electrostatic contribution to the solvation free energy.
(v) The electrostatic contribution to the binding free energy.

Poisson's equation shows the relationship between the electric displacement, D(r), and the charge density, ρ(r).

$$\nabla \cdot D(r) = 4\pi\rho(r) \tag{18}$$

Consider the equations for both the electrostatic field, E, and the electrostatic displacement, D.

$$E(r) = -\nabla \cdot \phi(r) \tag{19}$$
$$D(r) = \varepsilon(r) \cdot E(r) \tag{20}$$

where:
E(r) = electrostatic field; D(r) = electrostatic displacement; ø(r) = electrostatic potential; ε(r) = dielectric function; r = position vector.

By substituting eq.(19) and eq.(20) into eq.(18) we get:

$$\nabla \cdot \left[\varepsilon(r) \cdot \nabla \cdot \phi(r)\right] + 4\pi\rho(r) = 0 \tag{21}$$

Both the internal and external charges contribute to the value of the charge density ($\rho = \rho_{int} + \rho_{ext}$). The internal charge distribution, ρ_{int}, refers to the fixed positions of all the charges in the molecule. These values are taken as the partial charges, as used in the force field, of all the atoms in the molecule. The external charge distribution, ρ_{ext}, refers to the redistribution of the ions due to the impact of the electrostatic potential. Boltzmann's distribution can be used to express this distribution which delivers eq.(22).

$$4\pi\rho_{ext} = (-\kappa'^2)\sinh\left[\phi(r)\right] = (-\kappa'^2)\phi(r)\left[1 + \frac{\phi(r)^2}{6} + \frac{\phi(r)^4}{120} + \ldots.\right] \tag{22}$$

where:

$$\kappa' = \sqrt{\varepsilon}\kappa = \left[\frac{8\pi e^2 N_A I}{1000kT}\right]$$

ø = electrostatic potential (kT/e)
I = ionic strength (mol/dm^3)
T = temperature
κ = Debye inverse length

By substituting these equations into the Poisson equation (18) we get the non-linear Poisson-Boltzmann equation:

$$\nabla \cdot \left[\varepsilon(r) \cdot \nabla \cdot \phi(r)\right] - \kappa'^2_0\,\phi(r)\left[1 + \frac{\phi(r)^2}{6} + \frac{\phi(r)^4}{120} + \ldots\right] + 4\pi\rho_{\text{int}}(r) = 0 \tag{23}$$

where:

$$\kappa'^2_0 = 0 \quad \textit{if r inside the solute}$$
$$\kappa'^2_0 = \kappa \quad \textit{if r inside the solvent}$$

The values of ø(r) can be solved numerically with the following input parameters (All these parameters are dependent on the structural positions of the atoms):
ε(r): The value of ε is equal to the dielectric constant of the solvent when r is located inside the solvent area but equal to that of the solute when r is inside the solute area.
ρ_{int}(r): These values correspond to the partial charges of the atoms at their fixed positions.

κ: These values are only relevant when r is outside the solute area. To calculate this value we need to know the ionic strength of the solution.

From this it is apparent that the numerical solution of the Poisson-Boltzmann equation will incorporate both the effect of varying dielectric media as well as the impact of the ionic strength in solution. The output upon solving the Poisson-Boltzmann equation is the spatial distribution of the electrostatic potential, ø(r) (in units of kTe^{-1}). The solution of the Poisson-Boltzmann equation can be used to calculate the electrostatic contribution to the free energy of solvation.

What follows is a brief description of how this is accomplished [11]. In order to calculate these free energy values it is necessary to derive the spatial distribution of the solvent reaction potential, $ø^x(s)$. This distribution represents the responding potential acting back at any point s in the solute.

$$\phi^x(s) = \int_v \left(P(r) \cdot \nabla \frac{1}{|s-r|} + \frac{\rho^{ext}(r)}{|s-r|} \right) dv \tag{24}$$

In this equation P(r) is the solvent polarization:

$$P(r) = \frac{(\varepsilon(r)-1)E(r)}{4\pi} \tag{25}$$

The electrostatic contribution to the free energy of solvation is represented in the following equation:

$$\Delta G_{solv}^{elec} = \sum_i \int_0^{q_i} \phi_i^x \delta q_i \tag{26}$$

This equation sums over all the solute charges (which are treated as changing integrals) in their reaction potentials. It is easier to calculate this sum when the equation is rewritten as the integral over the volume of the solvent.

$$\Delta G_{solv}^{elec} = \int_V \left(\rho^{\text{int}}(r)\phi(r) - \varepsilon(r)E^2(r)/8\pi - \sum_i c_i \exp(-z_i\phi(r)) \right) dV \tag{27}$$

The sum within the integral is over all ionic species of valence z_i, and bulk concentration c_i.

The electrostatic force can be calculated from the derivative of the solvation free energy. These expressions can be used to calculate a variety of molecular properties including pK_a shifts, redox potential shifts, binding energies and association rates.

3.3.2.3 The Finite Difference approximation:

The DelPhi program [22] was used to calculate the electrostatic potential as well as all the other properties that can be derived from it. The method DelPhi uses to accomplish this is called the Finite Difference Approximation [23] . What follows is a very brief discussion on how DelPhi practically implements the finite difference approximation. Because this method and the consequences of its implementation are so central to the parameters chosen for a DelPhi run, a fuller description will be given in Chapter 6.2.

The solute molecule is superimposed onto a three-dimensional cubical grid. The spacing between grid points as well as the size of the entire grid impacts on the accuracy of the calculation. The continuous functions for ø, ρ and ε as defined before are replaced by their respective values at the grid points. This approximation therefore replaces all derivatives by finite differences over the adjacent grid points. Each grid point (i) is assigned a value for: charge (q_i), Debuy-Huckel inverse length (κ_0) and electrostatic potential ($ø_i$). The midpoints of the lines between grid points are assigned the relevant values for the dielectric constant (ε_i).

The following equation can be derived which represents the electrostatic potential value at grid point m. The distance between two grid points, l, plays a big part in the overall accuracy of the approximation. This approximation simplifies the solution to the PB equation considerably as only the six neighboring grid points are considered when calculating the electrostatic potential at grid point m.

$$\phi_m = \frac{\sum_{j=1}^{6} \varepsilon_j \phi_j + 4\pi \frac{q_m}{l}}{\sum_{j=1}^{6} \varepsilon_j + \kappa_0^2 l^2 N} \tag{28}$$

This equation can be looked at as the finite difference version of the Poisson-Boltzmann (PB) equation. The iterative procedure works as follows: The first iteration calculates the electrostatic potential at every grid point in the three dimensional grid. Because the neighboring values of the electrostatic potential changes, new values are calculated in the second iteration. This process is repeated until the differences in consecutive iterations are small enough to meet the convergence criteria.

For the linear PB equation: N = 1 (this equation cannot incorporate the effect of ionic strength.)
For the non-linear PB equation: N = $(1 + ø_m^2/3! + ø_m^4/5! + \ldots)$

3.3.2.4 Calculating various electrostatic energies using the finite difference approximation.

The solution to the Poisson-Boltzmann equation delivers the total electrostatic potential, ϕ^{total}. Delphi refers to this as the Grid Energy of the system. The total electrostatic potential consists of the following components:

(i) The Coulomb potential, ϕ^{own}, generated by the charges in the molecule itself.

(ii) The Coulomb potential, $\phi^{coulomb}$, generated by the direct interaction of the different charged species in solution. The energy calculated from this is referred to as the Coulombic Energy of the system.

(iii) The potential, $\phi^{reaction}$, that originates from the response (dipolar reorientation and electric polarization) of the solvent molecules and ions to the field generated by each charge in the solute. In turn, this response generates a field at the positions of the original charges. All the charges in the system, including the charge from which the reaction field originates, are exposed to this reaction field. The energy calculated from these potentials is referred to as the reaction field energy.

Once DelPhi has calculated the total electrostatic potential at every grid point, it can derive the following energy values from that:

(a) The Reaction Field Energy

This energy results from the interaction of the solute molecule with its own reaction field. Formally it is defined as the transfer energy from a medium that has the same dielectric constant as the solute molecule to a medium with a dielectric constant of the solvent.

$$G_R(\varepsilon_s, \varepsilon) = G_E(\varepsilon_s, \varepsilon) - G_E(\varepsilon_s, \varepsilon_s) \tag{29}$$

DelPhi uses a unique algorithm to calculate this energy. A series of surface polarization charges are calculated and positioned at the solvent-solute boundary positions. DelPhi does this by first locating all

points on the dielectric boundary surface. The effective surface charge at each of the points can then be calculated from the electrostatic potential at that point. The reaction field energy can be calculated from this by summing over both the number of surface charges and the number of actual charges as follows:

$$G_R = \frac{1}{2}\sum_{i=1}^{n}\sum_{j=1}^{m}\frac{\delta_i q_j}{\varepsilon_s r_{ij}} \tag{30}$$

where: n = the number of surface charges
m = the number of real charges
δ_i = the i^{th} surface charge
q_j = the j^{th} actual charge
ε_s = the dielectric constant of the solvent
r_{ij} = the distance between δ_i and q_j.

(b) The Self-reaction Field Energy

This energy is defined as the transfer of all atoms from vacuum (a dielectric constant of 1) to a homogeneous media with dielectric constant equal to that of the solute molecule.

$$-G_R(\varepsilon_s,1) = G_E(\varepsilon_s,\varepsilon_s) - G_E(\varepsilon_s,1) \tag{31}$$

This energy is useful when calculating the electrostatic energy of solvation.

(c) The Electrostatic Solvation Free Energy

The free energy of solvation can be described as the transfer energy of a solute molecule from vacuum to a medium with the dielectric constant of the solvent. This energy can be calculated by adding the self-reaction field energy to the reaction field energy. We refer to this as the Reaction Field Method.

$$\Delta G_{E(solvation)} = G_R(\varepsilon_s,80) - G_R(\varepsilon_s,1) \tag{32}$$

This results in: $\Delta G_{E(solvation)} = G_E(\varepsilon_s,80) - G_E(\varepsilon_s,1)$, which is consistent with the definition.

There is a second, less accurate way of calculating the free energy of solvation. This method will be discussed together with the Total Electrostatic Energy. We refer to this as the Grid Energy Method.

(d) The Total Electrostatic Energy

It is useful to calculate this energy, especially when comparing different conformations of the solute molecule. This energy can be defined as:

$$G_E = \frac{1}{2}\sum_i q_i\left(\phi_i^{coulomb} + \phi_i^{reaction}\right) \tag{33}$$

DelPhi, as mentioned before, calculates the following:

$$G_E = \frac{1}{2}\sum_i q_i\left(\phi_i^{coulomb} + \phi_i^{reaction} + \phi_i^{own}\right) \tag{34}$$

It is important to realize that $\phi^{coulomb}$ and ϕ^{own} are not a function of the dielectric constant and therefore their values stay the same regardless of the medium in which they are present. This is where we briefly mention the alternative method of calculating the free energy of solvation. If the G_E values of two

identical systems, which only differ in their dielectric media, were subtracted from each other, the $ø^{coulomb}$ and $ø^{own}$ values would be cancelled.

$$\Delta G_E = G_E(\varepsilon_s,80) - G_E(\varepsilon_s,1) \tag{35}$$

This would give us the free energy of solvation. In order to get the Total Electrostatic Energy of the system however, we need to add the Coulombic energy back in.

References:

1. P. Bash, M. Fields, and M. Karplus, *Free Energy Pertubation Method for Chemical Reactions in the Condensed Phase: A Dynamical Approach Based on the Combined Quantum and Molecular Mechanical Potential.* J. Am. Chem. Soc., 1987. **109**(26): p. 8092-8094.
2. C.I. Bayly and P.A. Kollman, *Molecular dynamics and free energy calculations on the peculiar bimodal alkali ion selectivity of an 8-subunit cavitand.* J.Am.Chem.Soc., 1994. **116**: p. 697-703.
3. B.J. Berne and J.E. Straub, *Novel methods of sampling phase space in the simulation of biological systems.* Current Opinion in Structural Biology, 1997. **7**: p. 7.
4. T.C. Beutler and W.F. van Gunsteren, *Umbrella sampling along linear combinations of generalized coordinates. Theory and application to a glycine dipeptide.* Chem. Phys. Lett., 1995. **237**: p. 308-316.
5. S. Boresch, G. Archontis, and M. Karplus, *Free energy simulations:The meaning of the individual contributions from a component analysis.* Proteins, 1994. **20**: p. 25-33.
6. P. Cieplak, D.A. Pearlman, and P.A. Kollman, *Walking on the free energy hypersurface of the 18-crown-6 ion system using free energy derivatives.* J.Chem.Phys., 1994. **101(1)**: p. 627-633.
7. L.X. Dang and P.A. Kollman, *Molecular dynamics simulations study of the free energy of association of 9-methyladenine and 1-methylthymine bases in water.* J.Am.Chem.Soc., 1990. **112**: p. 503-507.
8. J. Gao, *Absolute Free Energy of Solvation from Monte Carlo Simulations Using Combined Quantum and Molecular Mechanical Potentials.* J. Phys. Chem., 1992. **96**: p. 537-540.
9. J.K. Hwang, G. King, S. Creighton and A. Warshel, *Simulation of free energy relationships and dynamics of SN2 reactions in aqueous solution.* J. Am. Chem. Soc., 1988. **110**: p. 5297.
10. B. Jayaram, R. Fine, K.Sharp and B. Honig, *Free energy calculations of ion hydration : an analysis of the Bohr model in terms of microscopic simulations.* J.Phys.Chem., 1989. **93**: p. 4320-4327.
11. P. Kollman, *Free energy calculations:applications to chemical and biochemical phenomena.* Chem.Rev., 1993. **93**: p. 2395-2417.
12. P. Kollman, *Thermodynamic simulation.* Chem.Rev., 1993. **93**: p. 2395.
13. X. Kong and C.L. Brooks III, *A new approach to free energy caculations.* J.Chem.Phys., 1996. **105**(6): p. 2124-2423.
14. S. Kumar, P.W. Payne, and M. Vasquez, *Method for free-energy calculations using iterative techniques.* J. Comput. Chem., 1997. **17**(10): p. 1269-1275.
15. Lipkowitz and Boyd, *Free energy from simulation*, in *Molecular modeling and simulation*. 1993.
16. M. Mezei, *The finite difference thermodynamic integration, tested on calculating the hydration free energy difference between acetone and dimethylamine in water.* J. Chem. Phys., 1987. **86**: p. 7084-7088.
17. M.J. Holst and F. Saied, *Numerical solution of the nonlinear Poisson-Boltzmann equation:developing more robust and efficient methods.* J. Comput. Chem., 1995. **16**(3): p. 337-364.
18. K. Sharp and B. Honig, *Calculating total electrostatic energies with the nonlinear Poisson-Boltzmann equation.* J.Phys.Chem., 1990. **94**: p. 7684-7692.
19. C. Höög and G. Widmalm, *Free Energy Simulations of D-Xylose in Water and Methyl D-Xylopyranoside in Methanol.* J. Phys. Chem. B, 2001. **105**: p. 6375-6379.

20. H. Schäfer, W.F. van Gunsteren, and A.E. Mark, *Estimating Relative Free Energies from a Single Ensemble: Hydration Free Energies.* J. Comput. Chem, 1999. **20**(15): p. 1604]1617.
21. M. Souaille and B. Roux, *Extension to the weighted histogram analysis method: combining umbrella sampling with free energy calculations.* Comp. Phys. Comm., 2001. **135**: p. 40–57.
22. A. Nicholls and B. Honig , *A rapid finite difference algorithm,utilizing successive over-relaxation to solve the Poisson-Boltzmann equation.* J. Comput. Chem., 1991. **12**(4): p. 435-445.
23. M.E. Davis and J.A. McCammon, *Solving the finite difference linearized Poisson-Boltzmann equation: A comparison of relaxation and conjugate gradient methods.* J.Comput.Chem., 1989. **10**(3): p. 386-391.

Chapter 4

STRUCTURAL DESIGN OF PGM CHLORO-COMPLEXES IN WATER AND POLYMER SOLUTIONS

In this chapter we will describe several computational techniques which were employed to determine a variety of properties; specifically those related to potential energies and solvation structures of PGM chloro-complexes in water and poly (ethylene oxide) solutions. Two specific systems types were simulated and analysed intensively. The first system consists of a PGM complex ($[PdCl_4]^{2-}$; $[PtCl_4]^{2-}$; $[PtCl_6]^{2-}$; $[RhCl_6]^{3-}$) with sodium counter-ions in a water solution at 30ºC and at a concentration of 0.106 mol/dm^3. The second system under consideration was that of a PGM complex ($[PdCl_4]^{2-}$; $[PtCl_4]^{2-}$; $[PtCl_6]^{2-}$; $[RhCl_6]^{3-}$) with sodium counter-ions in a water solution in the presence of four polymer chains (Poly (ethylene oxide)) at 30ºC and at a concentration of 0.013 mol/dm^3.

The structural information obtained from the computational simulations of these systems is essential to the theoretical calculation of transport properties (diffusion coefficients in chapter 6) as well as thermodynamic property analysis (free energies of solvation in chapter 5). In order for these calculations to succeed we must first acquire a thorough understanding of the structural characteristics of the chemical systems involved. This chapter should therefore be seen as a foundation on which the chapters that follow (chapter 5 and 6) can be built. Throughout this chapter the significance of the reported results which would play a role in future chapters will be highlighted. The following paragraph gives a broad outline of these structural results and the basis they provide in the context of other computational determinations, such as thermodynamic analysis and diffusion coefficient calculations.

In order to calculate the thermodynamic and transport properties of a solute molecule, certain information regarding the structure and conformation of the specie in solution is required before any progress can be made. What follows is a list of these requirements which will be calculated and discussed in detail later in this chapter:
(1) Average, minimum and maximum energy conformations are required when calculating the free energies of solvation using a continuum solvent method (Chapter 5). Calculating the free energies of solvation for these three structures would allow us to determine a range for the values over the entire molecular dynamics trajectory.
(2) A conformational study of the two dihedral angles in a Poly (ethylene oxide) chain (-C-O-C-C- and -O-C-C-O-) is necessary to obtain information on the flexibility (the accessibility of conformational space) of the polymer. An understanding of these flexibilities would allow us to gain insight into the nature of the response of these polymer chains to electrostatic interferences, such as the presence of a PGM anion or sodium counter-ion in the vicinity of the polymer.
(3) By calculating the end-to-end distance (the distance between two terminal groups of the polymer chain) time series we can establish the relative ease with which the polymer folds as well as quantifying the time scale of motion.
(4) A dihedral angle distribution of these two dihedral angles must also be calculated to serve as a map that would enable us to generate starting structures for the polymer chains. The degree to which these starting structures reflect the true equilibrated conformations in a Molecular Dynamics simulation, will determine the computational time needed to achieve these equilibrated states.
(5) Information is needed about the solvation shell geometries of the PGM complexes. These results need to be contrasted with those of a system where the polymer, poly (ethylene oxide), is present. Based on this comparison we would be able to establish the effect (if any) of the polymer chains on the solvation of these species.
(6) By calculating the relative volumes of the hydration shells of the PGM chloro-complexes, we can form a preliminary opinion on the relative degree of solvation of these species. These relative volumes can also be used to correlate with trends observed in the free energy and diffusion coefficient results.
(7) By doing a probability analysis we can quantify how many ether oxygens in the polymer (PEO) are involved in the interactions between the PGM complex and the polymer. These results can help us to make conclusions about electrostatic affinities or repulsive interactions involving the polymer chains and the PGM chloro-complex.

4.1 Poly (ethylene oxide) Structure in the presence of PGM Chloro-Complexes and Sodium Counter-Ions (in a Water Solution)

4.1.1 Conformation Analysis in vacuum

The purpose of this investigation is twofold and corresponds to number 2 in the list above. Firstly we performed a conformational analysis on two relatively small molecules (dimethyl ether and dimethoxyethane) based on their ether linkages. These results were compared with experimental results reported in a previous study [4], thereby validating the force field which would ultimately be used. Secondly, a conformational study of the two dihedral angles in a Poly (ethylene oxide) chain (-C-O-C-C- and -O-C-C-O-) was performed. By contrasting the potential energy maps calculated for dimethyl ether and dimethoxyethane with the potential energy map of the ether linkage in a Poly (ethylene oxide) chain, we can observe the radical lowering of the energy barriers separating the different local minimum positions. From this we can make conclusions and gain insight into the flexibility (the accessibility of conformational space) of the polymer. It should be emphasizes that this study considered the polymer (PEO) exclusively (no water, PGM complexes or counter-ions were present).

4.1.1.1 Simulation Procedure

A conformational search was done to determine the preferred conformations of a molecule. These conformational searches focus on finding the minimum energy conformations. The problem with normal energy minimization methods is that the algorithms are designed to move to the minimum point closest to that of the starting structure. However, to cover the whole of conformational space it is necessary to utilize a separate algorithm which generates starting structures that would subsequently deliver all the appropriate minima. The algorithm used in this study to accomplish this is Simulated Annealing. The general steps of the conformational scan and simulated annealing [1] will briefly be discussed.

After generating the structure, a nested loop is initiated to scan systematically (from -180º to +180º) through the two designated dihedral angles, phi and psi respectively. Within the loop the phi and psi angles are constrained by putting an energy penalty to all other angles in the form of a harmonic force. An initial minimization (Steepest Descent algorithm [2] , 500 steps) is done to prepare for the molecular dynamics. The simulated annealing process consists of the following steps: Using molecular dynamics (Verlet [3]) the system is "heated" from 50 K to 900 K over 10 ps. This is followed by a 5 ps equilibration at 900 K. The system is subsequently cooled at a much slower rate from 900 K to 300 K over 20 ps. Finally a dynamic quenching is done from 300 K to 200 K over 15 ps. After these dynamic steps a final minimization (Conjugate Gradient [2]) is performed to find the local minimum. The constraints are now lifted and the computational algorithm is restarted once phi and psi are appropriately incremented by 10° steps.

4.1.1.2 Dimethyl ether (fig. 4.1)

The main objective in doing this analysis was to compare the calculated conformational energies with that obtained from experiment and other similar computer simulations [4] . For this particular molecule (dimethyl ether), simulated annealing was not performed because of its structural simplicity. The symmetry of the molecule is reflected in the potential energy map, fig. 4.4 (printed at the end of section 4.1.1), which results from the calculation.

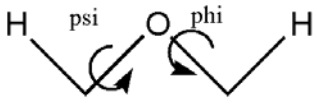

Fig 4.1 Dimethylether: The dihedral angles H-C-O-C (psi) and its symmetrical equivalent C-O-C-H (phi).

All the minimum points on the map shares an equal energy value, as would be expected for this symmetrical molecule. Global minima are found at the following (phi; psi) combinations organized according to the symmetric pairs: (180°; 180°), (60°; 60°), (60°; 180°), (180°; 60°); (60°, 300°), (300°, 60°); (180°; 300°), (300°; 180°). As expected the global minima is found where both dihedral angles

present the scattered conformation. Where the dihedral angles are eclipsed we find the global maxima. The main factor driving the shape of the potential energy map for this molecule is therefore steric hindrance. The energy barriers from one global minimum to another are all identical and the value of the transition barrier is calculated as 1.0 kcal. This value does not compare well with the experimental value [4] which is 2.72 kcal. It must be remembered that the force field used was designed for poly-ethers and is therefore not really applicable in this case. The parameters needed to make a quantitative comparison are not available for the CHARMM energy expression. It is important to observe, however, that the energy barriers separating the local minimum positions are relatively prominent, which would limit the general flexibility of the molecule.

4.1.1.3 Dimethoxyethane (Fig. 4.2)

The ether linkage in dimethoxyethane was analyzed by calculating a two-dimensional adiabatic map. From the adiabatic map, fig 4.5 (printed at the end of section 4.1.1), it is apparent that the ether linkage is extremely flexible as a huge portion of the conformational space exists at very low energy levels and the energy barriers are very low. The only high energy conformational region is at phi = 0° and/or psi = 0° which is expected due to steric hindrance. Not only are the low energy regions extensive, but these regions are also notably very flat. This means that the molecule does not need to cross any major energy barriers in order to change its conformation. The global minima is found at phi = 180° and psi = 180° for the same reasons as stated for dimethylether.

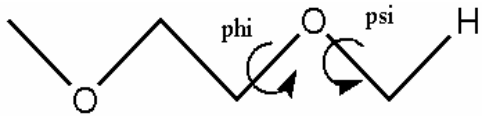

Fig 4.2 Dimethoxyethane: The dihedral angles C-O-C-C (phi) and H-C-O-C (psi) which constitutes the ether linkage are indicated.

Transition type	Calc. (kcal/mol)	Exp. (kcal/mol)
tgg	1.11	1.51
tg+g-	0.19	0.23
tgt	0.09	0.14
ttg	1.15	1.43
ttt	0.0	0.0

Table 4.1: Summary of the relevant energy barriers and a comparison with the experimental results.

It should be observed how low the energy barriers are, and that almost nothing prevents the molecule from changing conformation quite radically. From this we can conclude that by lengthening the ether chain it is possible to lower the energy barriers which separate the local energy minimum positions. This implies that the molecule has an increased accessibility to the conformational space and is therefore very flexible. It is also encouraging to observe the consistency with the experimental results [4] . This is an indication that the force field is valid.

4.1.1.4 Poly (ethylene oxide) (PEO)

As mentioned in the introduction to this chapter, a conformational study of the dihedral angles in a Poly (ethylene oxide) chain (-C-O-C-C- and -O-C-C-O-) is necessary to obtain information on the flexibility (the accessibility of conformational space) of the polymer. An understanding of these flexibilities would allow us to gain insight into the nature of the response of these polymer chains to electrostatic interferences, such as the presence of a PGM anion or sodium counter-ion in the vicinity of the polymer. The figure below illustrates the positions of the three dihedral angles on which this investigation is based.

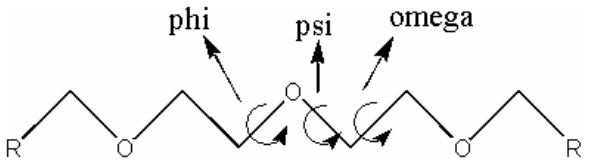

The phi and psi dihedral angles represent the ether linkage on which a two dimensional conformational analysis was performed. The potential energy map of this analysis is presented in fig 4.6. The results obtained from the conformational analysis of the dihedral angles of the ether linkage in PEO (phi and psi in the figure above) are comparable with those of Dimethoxyethane. From the adiabatic maps of the ether linkage, fig. 4.6, it is clear how low the energy barriers are, and that almost nothing prevents the molecule from changing conformation quite radically. The conformational space (combinations of phi and psi dihedral angles) surrounding the global minimum potential energy position (at phi = 180º and psi = 180º) shares the same contour level on the adiabatic map. From this it is clear that no significant local minimum potential energy positions exit, which are separated by energy barriers. Therefore, by lengthening the ether chain to an even greater extent (30 monomers in the polymer chain) the energy barriers which separate the local energy minimum positions were lowered to the extent of being almost nonexistent. As with dimethoxyethane, this implies that the ether linkage has an increased accessibility to the conformational space and is therefore very flexible. In this particular study the effect of the simulated annealing is most significant. Lower local and global minima were consistently achieved in contrast to a conformational scan with no simulated annealing.

The Newman projections of the various minimum and maximum conformations are illustrated in fig 4.3 (see on the next page). From these projections it is clear that the local and global minimum and maximum positions can be explained in terms of steric effects. The corresponding energy barriers are also quantitatively comparable (very low: < 0.1 kcal/mol). It is clear that the ether linkage enables the polymer to be very flexible, which is indeed a frequently reported [4] characteristic of poly (ethylene oxide). This characteristic affects the physical properties of the polymer significantly, such as its solubility. The flexibility of the polymer can also effect the response time the polymer would have to an external electrostatic interference, such as a PGM anion or sodium counter-ion. The reader is reminded that this conformational study was done in vacuum and its results should be seen in this context. Subsequent molecular dynamic simulations were all done with the polymer (PEO) in water.

A previous study [5] investigated the dihedral angle of the methylene linkage (O-C-C-O). A one dimensional conformational study was done and the potential energy map was calculated. From this map [5] it is clear that the energy barriers separating the local minimum potential energy positions (at the scattered conformations) are more prominent (1.5 kcal/mol) than those of the ether linkage. The energy barriers of the ether linkage are very low (< 0.1 kcal/mol) or for most transitions do not exit at all.

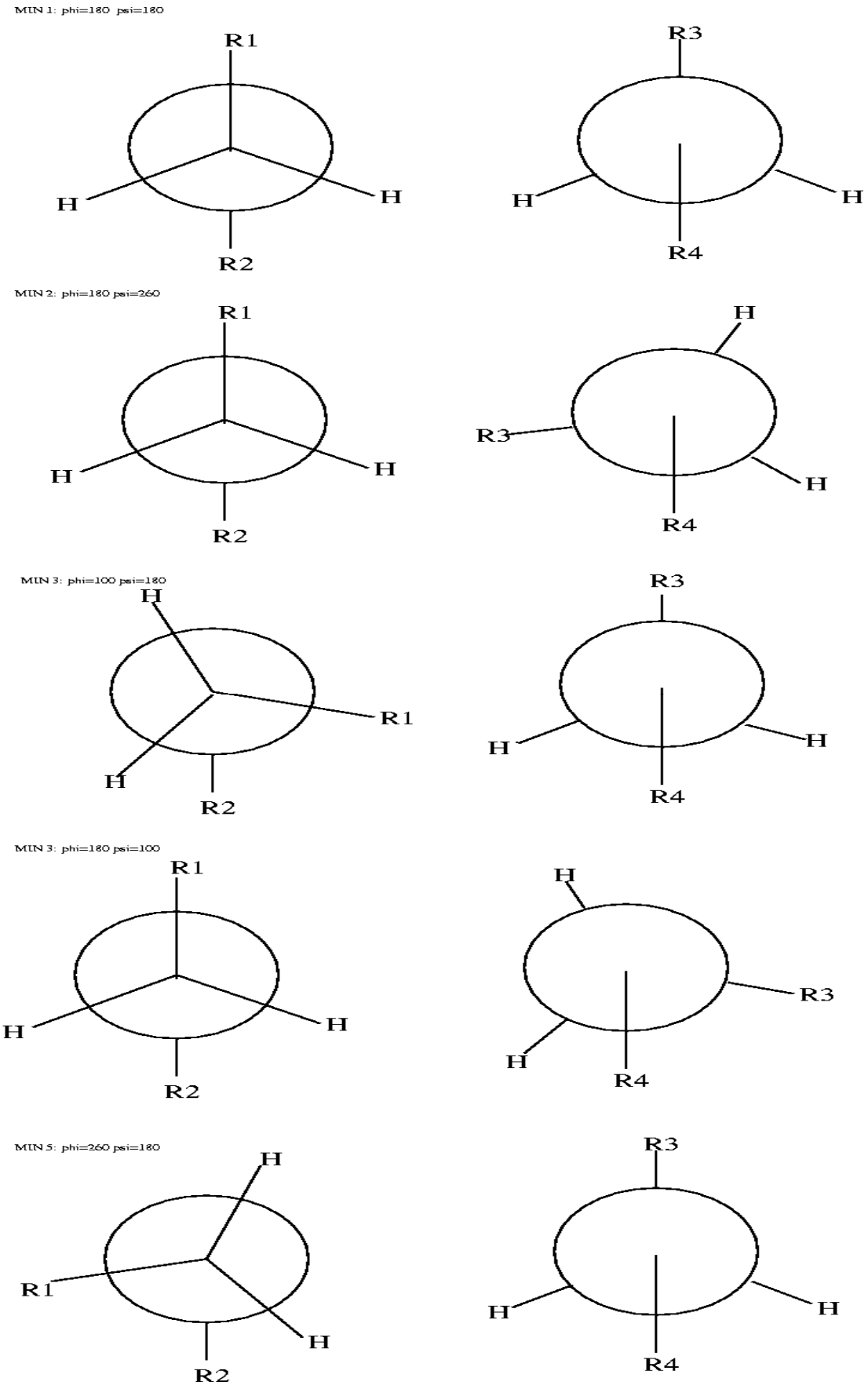

Fig. 4.3: The Newman projections of an ether linkage in PEO, where R_1=R_4=-$(CH_2$-O-$CH_2)_{15}$-…-CH_3 and R_2=R_1=-$(CH_2$-O-$CH_2)_{14}$-…-CH_3

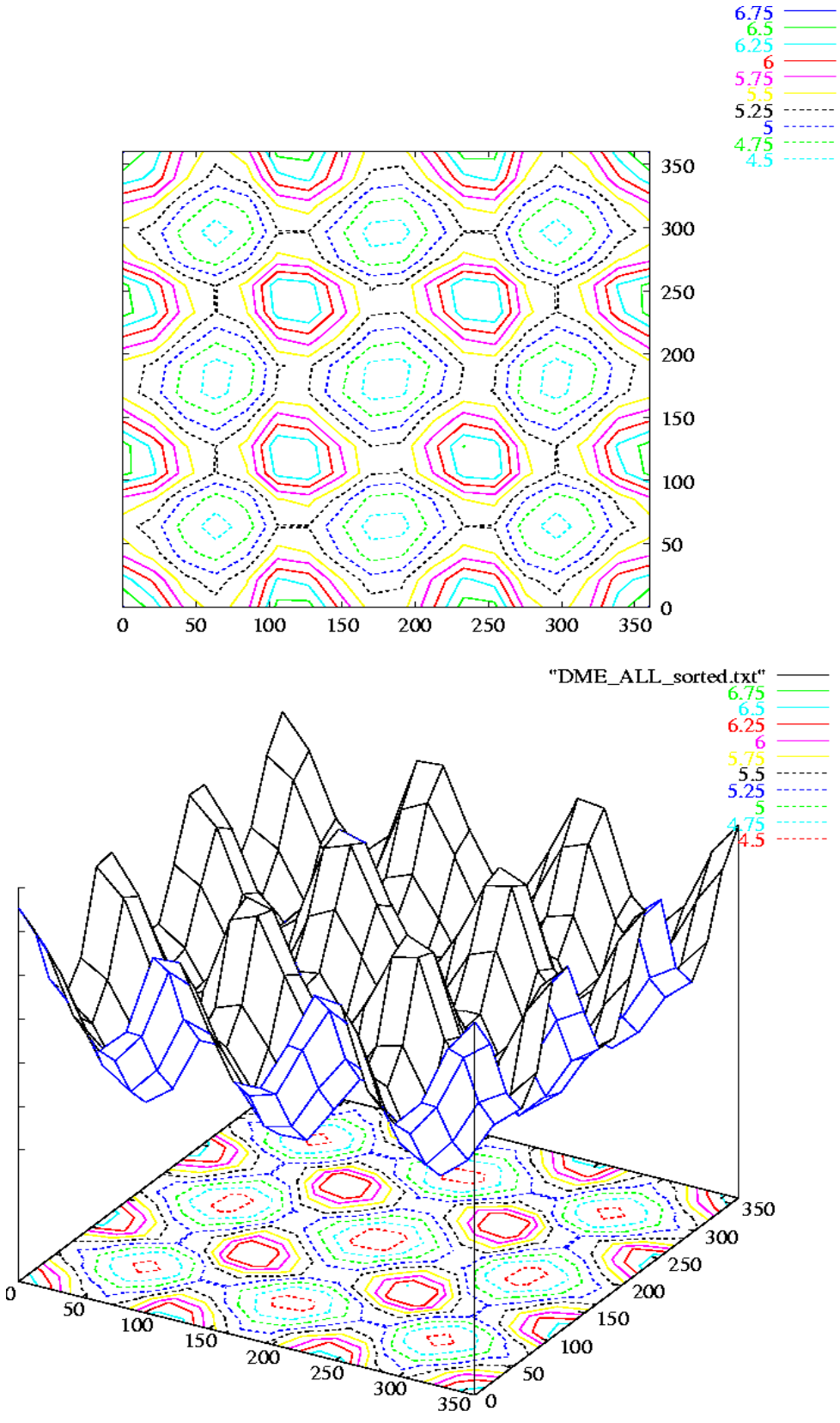

Fig 4.4: The adiabatic conformational energy map for Dimethylether in vacuum contoured at 0.25 kcal intervals.

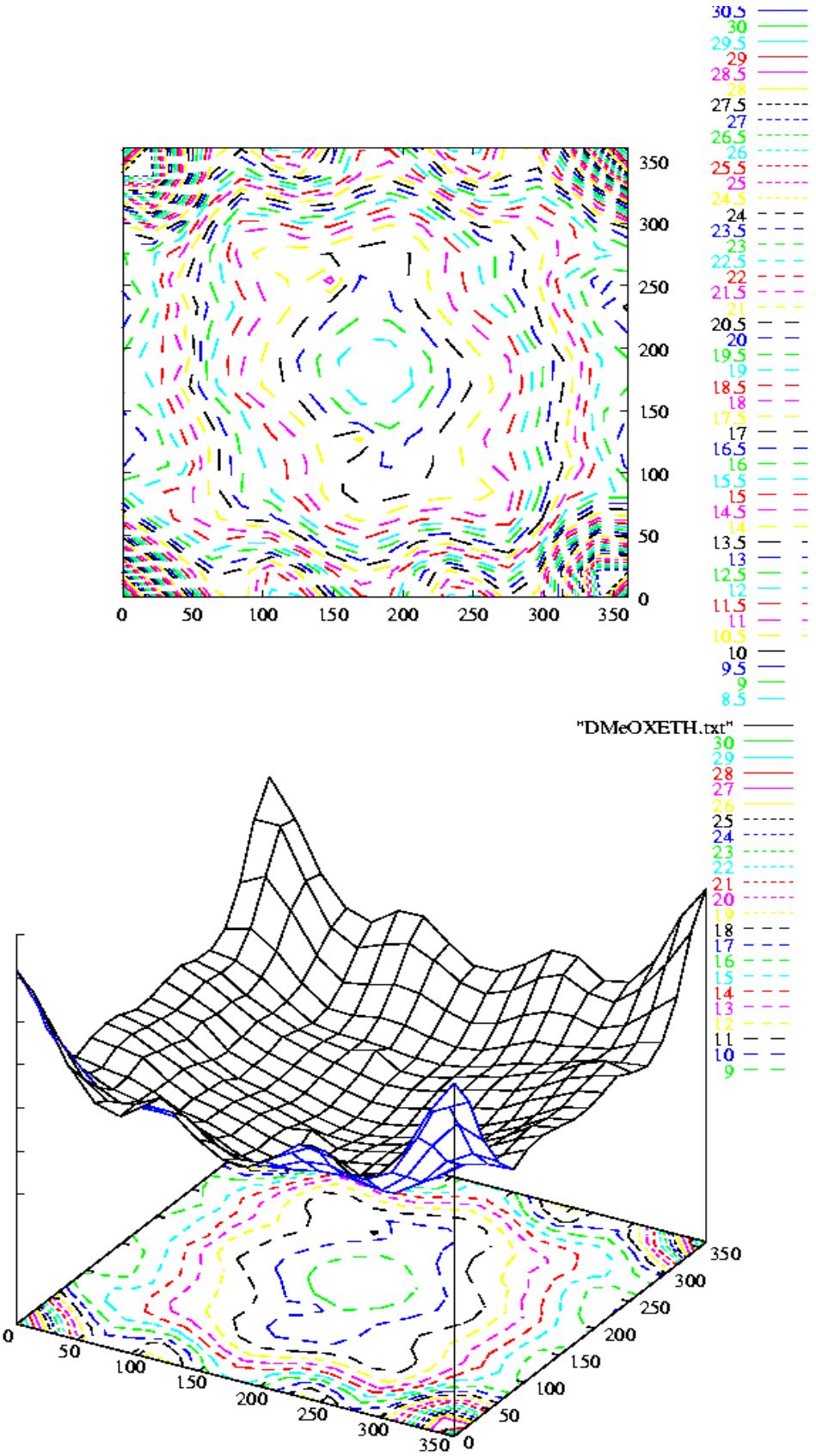

Fig 4.5: The adiabatic conformational energy map for the ether linkage of Dimethoxyethane in vacuum contoured at 0.5 kcal intervals.

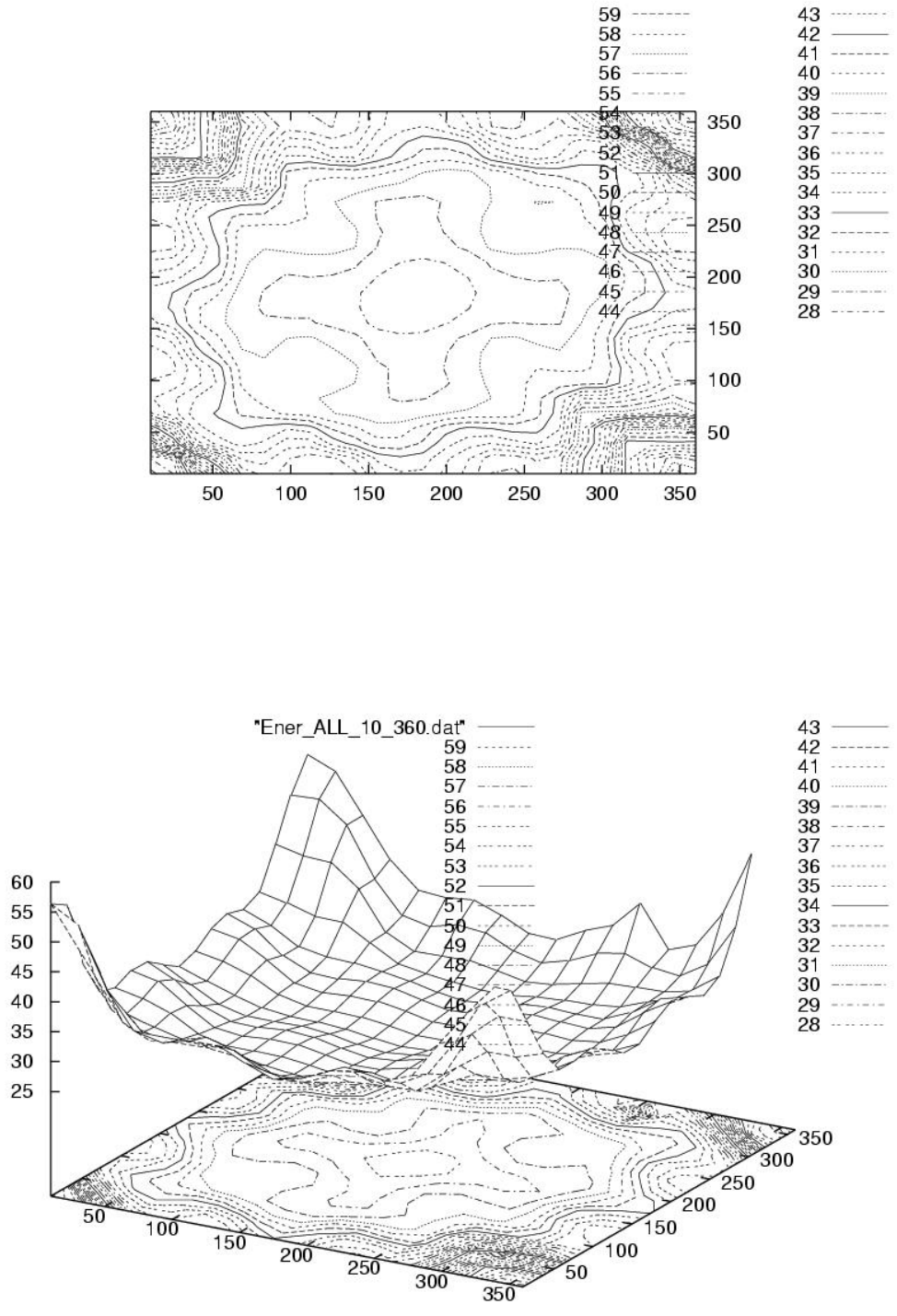

Fig 4.6: The adiabatic conformational energy map for the ether linkage of poly (ethylene oxide) in vacuum contoured at 1.0 kcal intervals.

4.1.2 Dihedral Angle Distributions of Poly (Ethylene Oxide) in water

4.1.2.1 Simulation Procedure

The molecular dynamics simulation which generated the trajectory data from which these distributions were calculated was run as part of the study of the polymer (PEO) and the PGM chloro-complexes in water. The interaction of the polymer with the PGM complex and the counter ions (sodium) has therefore most likely, partly, distorted these distributions. It is clear however that the results obtained are completely consistent with that which might be expected based on the conformational study. From the conformational study (section 4.1.1) it was clear that the ether linkages in the polymer chain are very flexible and that the potential energy barriers (separating local and global minimum positions on the adiabatic map) are easily traversed. The details of the MD simulation parameters and general setup will be discussed in section 4.3. What follows is only a brief description of the elements in system that concerns this particular analysis.

Box size: 48.7 Å cubed
Cutoff distance: 14 Å
Number of polymer chains in the box: 4 chains
Number of monomers in a single polymer chain: 30
Density of the system: 1.02 g/cm^3
Concentration of the polymer: 0.0575 mol/dm^3
Temperature of the system: 300 K
Average volume of the system: 48.7×48.7×48.7 Å^3
Image convention for water: by residue
Image convention for the polymer: by segment

A full description of how the starting structures of the polymer were generated will be discussed in section 4.3.

4.1.2.2 Discussion of the Time Series results

The results reported below represent the general pattern of dihedral angle behavior as observed throughout the various systems: a PGM complex ($[PdCl_4]^{2-}$; $[PtCl_4]^{2-}$; $[PtCl_6]^{2-}$; $[RhCl_6]^{3-}$) with sodium counter-ions in a water solution in the presence of four polymer chains (Poly (ethylene oxide)) at 30ºC and at a concentration of 0.013 mol/dm^3. No significant qualitative deviation from this pattern was observed between these systems. This is an indication that the effect of the presence of the PGM chloro-complex on the behavior of the polymer chain conformations is not significant enough to result in any observable differences in the time series results.

Characteristics of the ether linkage dihedral (C-C-O-C) time series:
It is clear from fig. 4.7 that this dihedral angle attempts frequent transitions. The potential energy surface is so flat however that the 180° dihedral is easily restored as no significant barriers exist. The transition frequency (from one local minimum position to another) of this dihedral is therefore relatively high.

Characteristics of the methylene linkage dihedral (O-C-C-O) time series:
The transition frequency of this dihedral is much lower than that of the ether linkage dihedral angle because the energy needed to cross the barriers are significantly higher. The energy barriers between the local minimum potential energy conformations for the O-C-C-O dihedral angles are 1.5 kcal/mol, as opposed to those of the C-O-C-C dihedral angles, which are almost nonexistent (< 0.1 kcal/mol). Although this dihedral angle resists frequent transitions the actual time spent at these alternative conformations are longer. The conformation gets stuck temporarily at these local minima positions before returning to the preferred global minimum. The molecule has to "wait" until the energy is high enough for the barrier to be crossed.

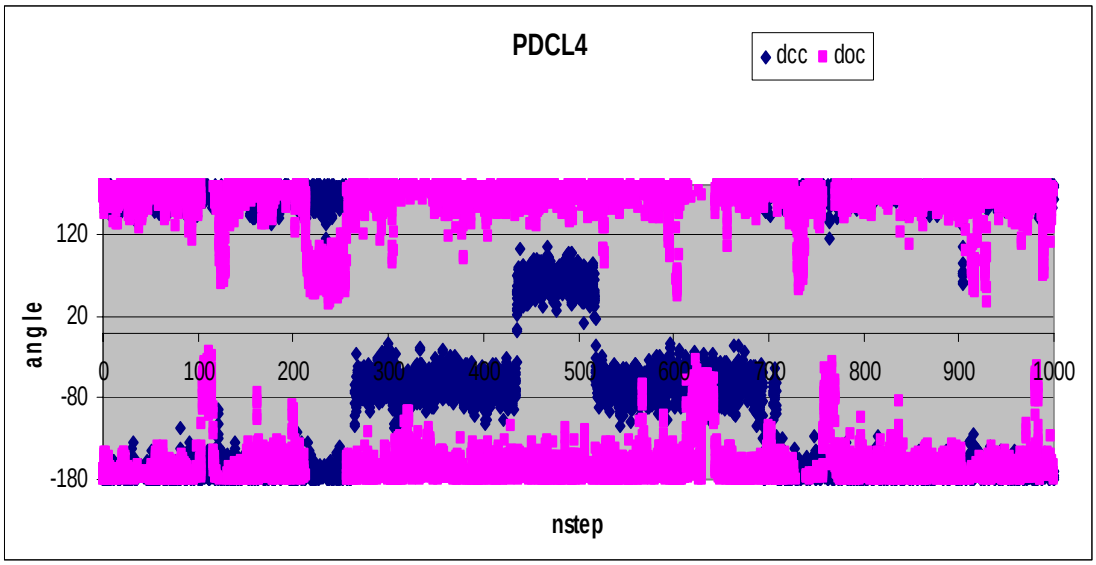

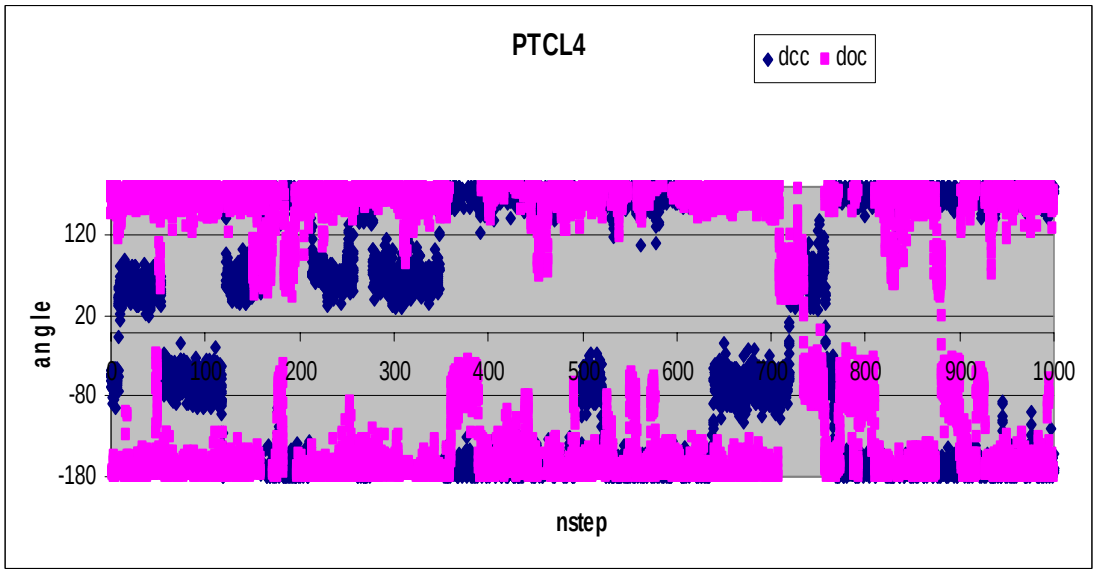

Fig. 4.7: Two examples of the typical time series observed for the two dihedral angles under consideration. The dcc (blue) curve represents the O-C-C-O dihedral, while doc (pink) is the C-C-O-C dihedral.

4.1.2.3 Discussion of the dihedral angle distribution results

The dihedral angle distributions in fig. 4.8 clearly show the effect that the shape of the potential energy surface has on the extent to which a particular dihedral angle conformation is represented in an equilibrated system. These results are similar in nature to those obtained in other computational studies [6, 7] of the same polymer. As discussed in section 4.1.1, a huge portion of the conformational space (defined by the dihedral angles constituting the ether linkage) is accessible to the polymer, without having to cross any significant energy barriers. It is therefore very easy for these dihedral angles (C-C-O-C) to rotate into their most energetically favorable conformations (the scattered conformation, at ±180°). A very small probability exists that these dihedral angles would not be at the global minimum position (±180°). Even when the dihedral angle varies slightly from this position, it is energetically easy for it to rotate back to the global potential energy minimum. The energy barriers for the methylene linkage (O-C-C-O) are more prominent however. As was seen in the previous section, this dihedral angle resists frequent transitions and the actual time spent at these alternative conformations is longer. This is because the conformation gets stuck temporarily at these local minima positions before

returning to the preferred global minimum. As is clear from fig 4.8, the probability that these alternative conformations exist is therefore higher than those of the ether linkage.

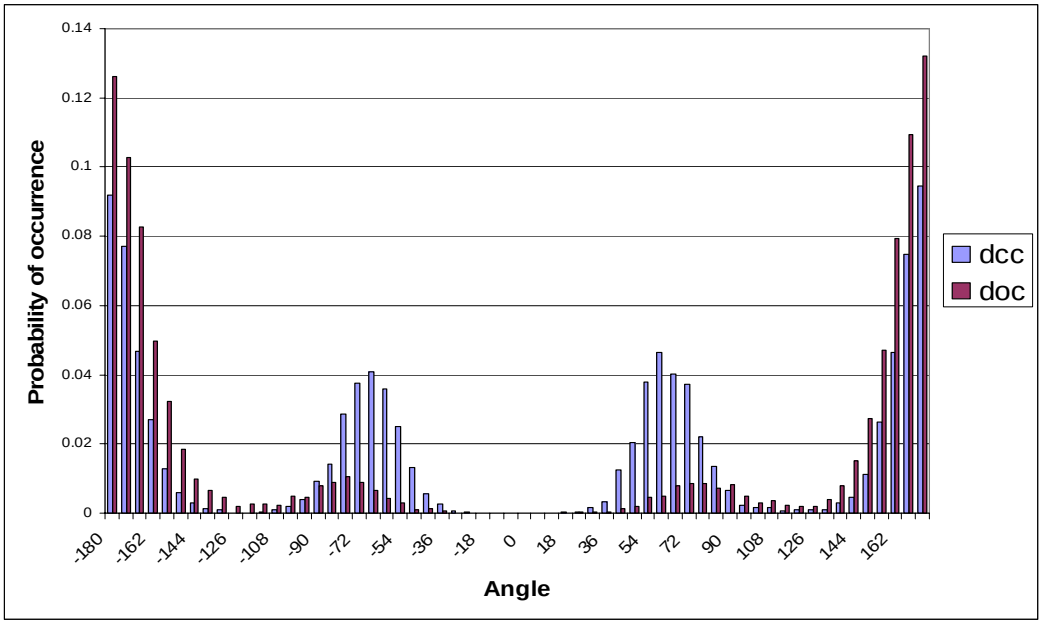

Fig. 4.8: An example of the dihedral angle distribution of the two dihedral angles under consideration. The dcc (blue) curve represents the O-C-C-O dihedral, while doc (maroon) is the C-C-O-C dihedral.

4.1.3 End to end distance time series in water

The end to end distances as measured between the two terminal carbons in the polymer chains, poly (ethylene oxide), were recorded over a 1600 ps time frame of equilibrated dynamics. These distances, the frequency and severity of their fluctuation as well as minimum and maximum values allow insight into the structure and time scale of motion of the polymer. The figures below illustrate what is meant by the concept of end to end distances.

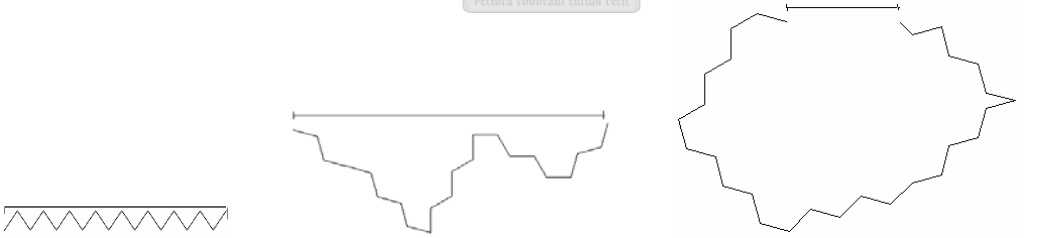

a) Straight chain b) Bended chain c) Bended chain (in circular form)

A fully stretched polymer (PEO) chain (30 monomers), where all dihedral angles in the backbone are at 180º, has a length of 110 Å. From the time series data (fig 4.9 to 12) it is clear that the polymer (PEO) chains fold and uncoil quite readily. A significant charge in the end to end distance takes place over an average period of 900 ps. This gives a rough qualitative idea of the time scale of motion within a single polymer chain at this concentration. The variation in end to end distance is quite large, ranging from 6Å to 86Å. As can be seen in the figures below, a single polymer chain can change its end to end distance over a period of 1500 ps from 30Å to 6Å and then to 42Å (fig 4.9). Another example shows a polymer chain's end to end distance changing from 40Å to 80Å and then back to 60Å (fig 4.11) over a period of 1500 ps. As is generally true with polymers of this magnitude, the time scale of motion is large relative to the time scale at which intermolecular interactions, collisions and diffusion takes place. The following paragraph describes the electrostatic interactions which could possibly play a role in the way the polymer (PEO) folds.

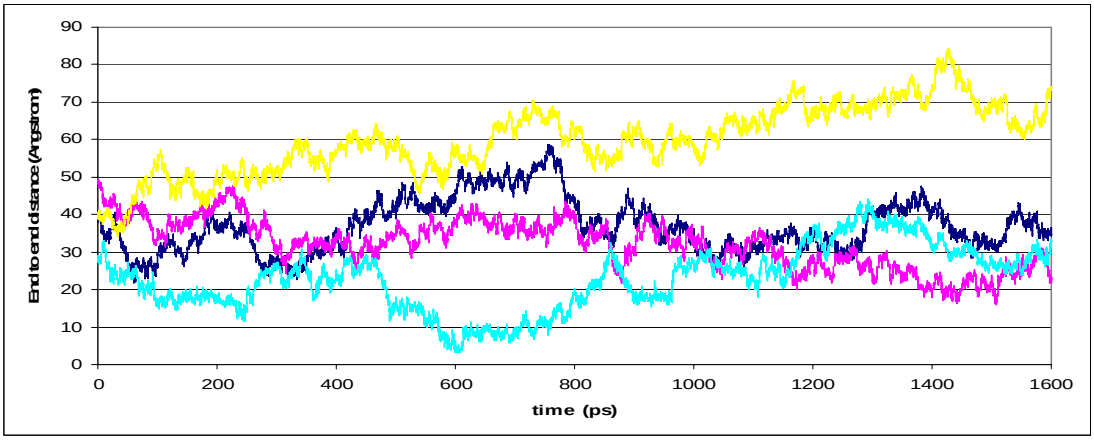

Fig. 4.9: End to end distance time series of the four individual PEO chains in water and 2$[Na]^+$ $[PdCl_4]^{2-}$ solution. Each color represents a separate polymer chain.

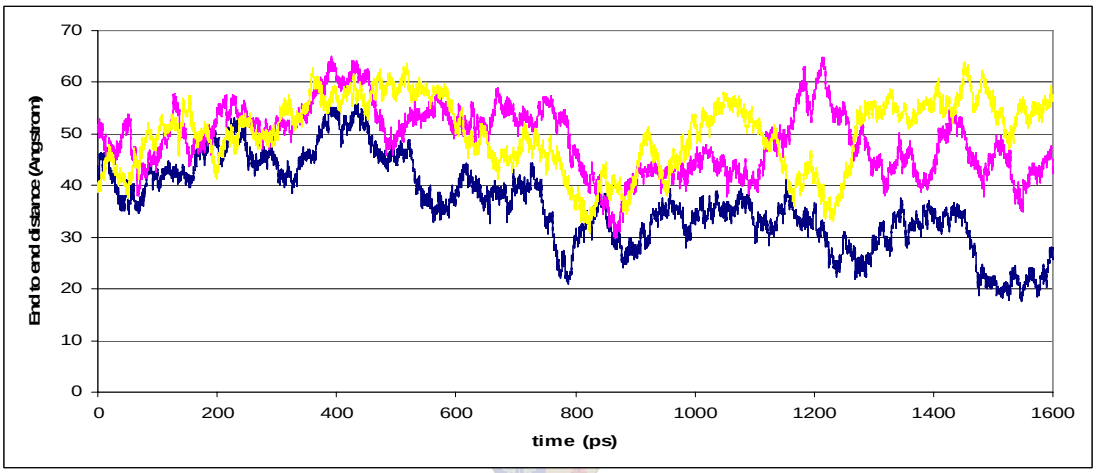

Fig. 4.10: End to end distance time series of three individual PEO chains in water and 2$[Na]^+$ $[PtCl_4]^{2-}$ solution. Each color represents a separate polymer chain.

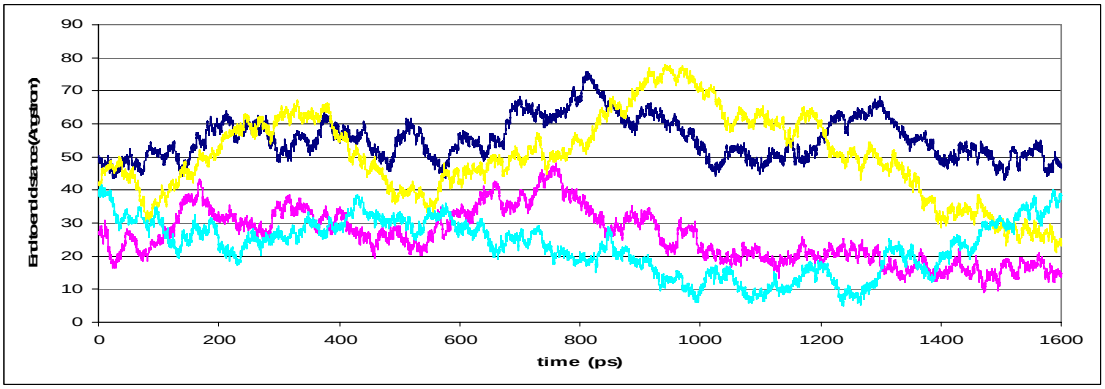

Fig. 4.11: End to end distance time series of the four individual PEO chains in water and 2$[Na]^+$ $[PtCl_6]^{2-}$ solution. Each color represents a separate polymer chain.

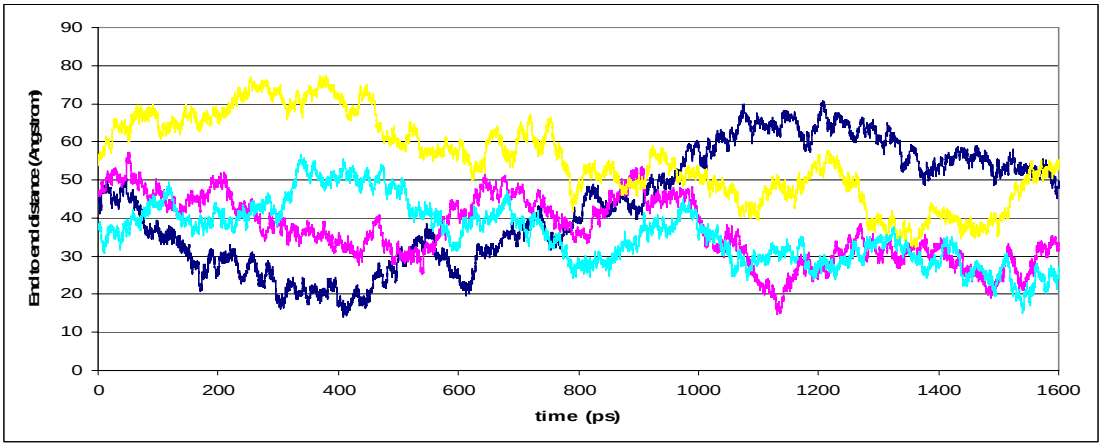

Fig. 4.12: End to end distance time series of the four individual PEO chains in water and 3$[Na]^{+}$ $[RhCl_6]^{3-}$ solution. Each color represents a separate polymer chain.

The manner in which the polymer (PEO) chains fold is also expected to be effected by the electrostatic interactions with the sodium counter-ions. The potential exists for folding to result in crown ether formations. These crown ether formations form complexes with the Na^{+} ions in the solution. In turn, these complexes, which are positively charged, would interact and associate with the negatively charged PGM chloro-complexes. The figure below illustrates a crown ether complex and its association with a PGM chloro-complex.

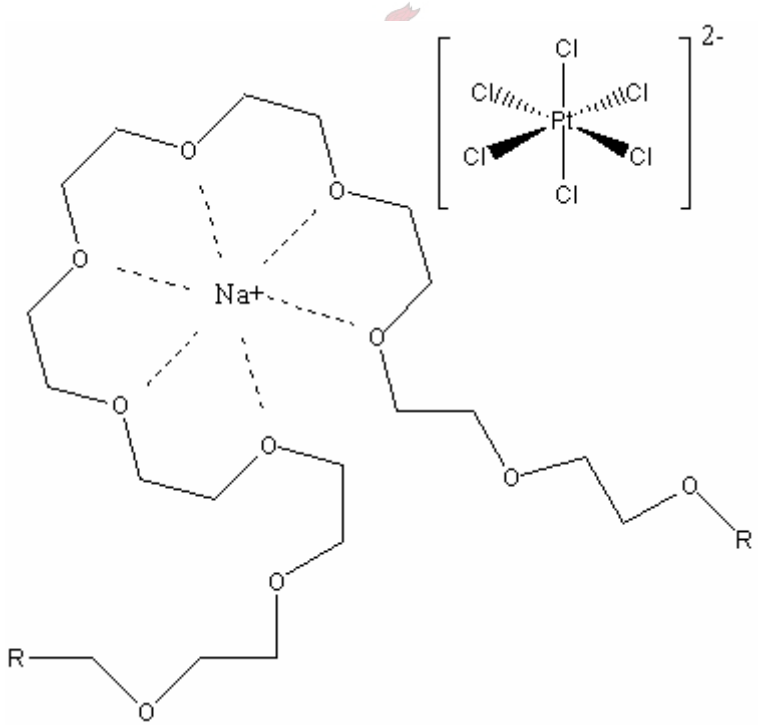

Electrostatic repulsions between the polymer chains and the PGM chloro-complexes might also influence the folding of the polymer (PEO). Due to the low concentration of these ionic species in solution (0.013mol/liter), it is less likely for these interactions to be observed within the relatively short time period of the Molecular Dynamics simulation (1.5 ns). Speculations as to the nature of these interactions and the potential effect they might have on the structural properties of the poly (ethylene oxide) chains are discussed in section 4.4.

4.2 Solvated PGM Chloro-Complex Structures

In the previous section we focused on the structural properties of poly (ethylene oxide) chains in the presence of PGM chloro-complexes and the appropriate number of sodium counter-ions (in a water solution). An attempt was made to explain these structural phenomena, such as dihedral angle distributions, in terms of the potential energy surface based on the relevant dihedral angles of the polymer (PEO). The structural effects of the electrostatic interactions of the PGM complexes and the sodium counter-ions with the polymer (PEO) chains were mostly obscured by the conformational behavior of the polymer in water. The time scale of motion of the polymer is also very slow and makes the average determination of these electrostatic interactions very computationally expensive. This section focuses on the structural characteristics, such as hydration sphere geometry, of the PGM chloro-complexes in the absence of polymer (PEO) chains. In contrast, section 4.3 will report on the structural characteristics of the PGM chloro-complexes in the presence of poly (ethylene oxide) chains.

4.2.1 Molecular Dynamics Simulation Procedure

The program CHARMM [8] was used for all Molecular Dynamics (MD) simulations. Bulk solutions of $[PtCl_4]^{2-}$, $[PtCl_6]^{2-}$, $[PdCl_4]^{2-}$ and $[RhCl_6]^{3-}$ were generated in 24.6Å×24.6Å×24.6Å cubical cells, using the TIP3P water model [8] as implemented in CHARMM. In order to maintain overall neutrality the appropriate number of sodium counter ions was added to the respective systems. To insure that the bulk density of 1.051 g/cm^3 was maintained the number of water molecules in the "box" differed for each simulated PGM solution. Periodic boundary conditions were employed and MD simulations of 500 ps equilibration were performed before production commenced. The trajectory data was collected over 1 ns of equilibrated NPT dynamics. The force field used was previously described [9] and validated against diffraction experiments and quantum mechanical calculations.

The parameters chosen in both equilibration and production are briefly described. A NPT ensemble, using the Nose-Hoover thermostat was simulated. The constant pressure calculation was performed using the extended system algorithm. The mass of the pressure piston was 500 amu and the Langevin piston collision frequency was specified as 5 per picosecond. A Nose-Hoover reference temperature of 300 K was used, while the mass of the thermal piston was 1000 kcal.ps^2. The equilibration process was therefore performed at 300 K. The temperature deviation to be allowed from the desired temperature was specified as ± 5 K. A time step of 0.001 ps was chosen for the dynamics run. A step frequency of 100 was used for stopping the rotation and translation of the molecule during dynamics. The images were updated every 10 steps. Averages and root mean square fluctuations were calculated every 100 steps.

The non-bonded interaction list was regenerated every 10 steps and the following non-bonded specifications were used: (The theoretical explanations of the concepts which these parameters represent were discussed in chapter 2)
Due to the presence of ions (PGM chloro-complexes and sodium counter-ions) in solution the Ewald summation method [10-15] was invoked to deal with these long-range interactions. The width of the Gaussian distributions used when calculating the Ewald summation was 0.32 Å. It is convention to choose this value as 4/CTOFNB which will be defined later. The Particle Mesh Ewald algorithm [15] was employed for the reciprocal space summation. The number of grid points for the charge mesh was specified as 54 for the x, y and z directions. The order of the ß-spline interpolation was 6. A spline algorithm was used for calculating the complimentary error function, erfc(x). Atom electrostatics were employed which means that interactions were computed on an atom-atom pair basis. The radial energy functional form was chosen as that of the constant dielectric where the electrostatic energy is proportional to 1/R. The distance at which the switching function takes effect is 10 Å. The shifting function which smoothly reduces the energy to zero takes effect in the 11 Å to 12 Å interval. The distance cutoff involved in generating the list of atom pairs was therefore 12 Å. The distance specified function acts per atoms and not per group which improves the accuracy of the interaction calculations. The dielectric constant used in the extended electrostatic algorithm was equal to 1 (vacuum), which is of course standard when explicit solvent models are used. The exclusion list, which prevents certain energy terms from being included in the energy calculations, was specified as 1 and 2 bond interactions. Therefore, both vd Waals and electrostatic interactions between a bonded atom pair or an atom pair separated by 2 bonds were excluded from the calculation of the energy and the forces. No scaling factor was applied to electrostatic interactions involving atom pairs separated by 3 bonds.

4.2.2 Radial Distribution Functions of the Oxygen Atoms in the Water Molecules to the PGM Complex Metal Center

A recent study has been published, describing the geometric characteristics of the hydration shells for anionic platinum group metal chloro complexes [16] . A radially averaged probability density distribution function (radial distribution function) was used to describe the geometric arrangement of water molecules around the complex chloro-anions of Pt(IV), Pt(II), Pd(II) and Rh(III). The data for this analysis was collected in a microcanonical ensemble (box size and particle number were kept constant), in contrast to the current description in which the NPT ensemble was used. This means that the respective volumes of the systems were allowed to vary in order to keen the pressure constant. The current study also has the added objective to compare and contrast the results to that obtained in a system containing polymer chains (section 4.3). The results obtained in this section are therefore very similar (qualitatively) to those obtained in the previous study [16]. There are quantitative differences that results from the use of a different ensemble type (NPT).

The radial distribution functions, calculated from the Molecular Dynamics (NPT ensemple) trajectory data, of the $[PdCl_4]^{2-}$ and $[PtCl_4]^{2-}$ complexes (both known to be square planar complexes) can be seen in fig. 4.13. The pair distribution functions, the g(r) function for the metal···O(water) configurations, for these two complexes indicate a similar solvent structure. The RDFs indicate three regions where the average distances have probabilities which vary distinctly from the bulk water structure. The region 3.1-4.1Å is not diffuse, but is the result of radial averaging. This region indicates that the oxygens atoms of the water molecules get closer to the metal center than metal···O(w) distances observed in the octahedral complexes. This can be attributed to the absence of chlorine atoms in the axial positions which allows closer access to the metal center. The closest that an oxygen atom of a water molecule gets to the metal center in the octahedral complexes is 3.8Å. The region between 4.1 and 4.5Å indicates the somewhat less diffuse extension of the inner region of solvation. This region together with the 3.1-4.1Å region constitutes the first solvation shell. In contrast to the octahedral complexes however this hydration shell is not as prominent and well defined. A second hydration shell is found in the 5.1 to 5.7Å distance region. The intensity of this region is higher because radial averaging plays a lesser role. Beyond these distances random probabilities prevail.

Although the two octahedral complexes, $[PtCl_6]^{2-}$ and $[RhCl_6]^{3-}$, have general characteristics in common, there are significant differences in terms of scale and intensities to warrant separate treatments. The general features are briefly discussed. As is clear from fig 4.14, both complexes have a very prominent inner hydration shell. In contrast to the square planar complexes, radial averaging plays a lesser role due to the octahedral symmetry. A weaker outer shell which resembles the intensities observed in those of the square planar complexes is also observed. There is a significant difference in the probability density of the inner hydration shell of these two complexes. The probability density of the inner shell of $[PtCl_6]^{2-}$ is 1.65, in contrast to that of $[RhCl_6]^{3-}$ which is 2.1. The oxygen atoms are able to get slightly closer to the Pt(IV) metal center (peak probability at 4.2Å) than they are able to for the Rh(III) metal center (peak probability at 4.4Å). The reverse is true for the respective outer shells.

The above mentioned study [16] also investigated the chlorine-O(water) RDFs for these PGM complexes. It was observed that these RDFs for the octahedral and square planar complexes resemble each other more closely than the corresponding metal-O(water) RDFs as described above. The RDFs show two prominent peaks at distances of 3.5Å and 5.9Å respectively. These distances are the same for all the complexes, regardless of symmetry. There are however clear contrasts in the intensities of these peaks. The second peak corresponding to the second hydration shell is significantly weaker for the square planar complexes in contrast with those of the octahedral complexes. The only complex which shows a convincing second hydration shell is that of Rh(III).

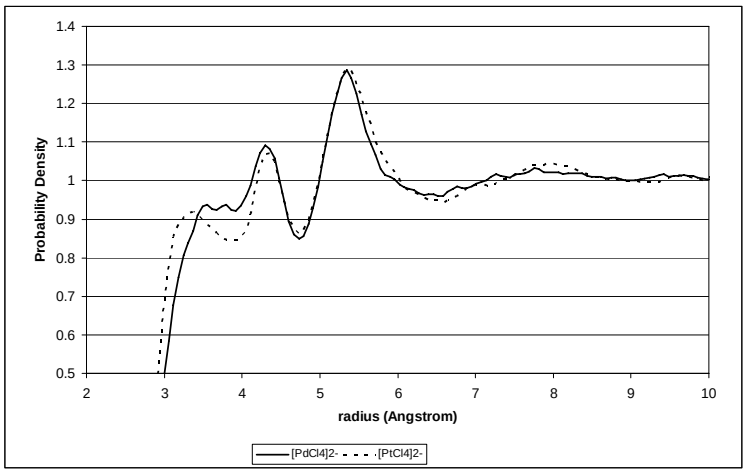

Fig 4.13: The pair distribution functions, g(r), for the metal···O(water) configuration in the two square planar complexes ($[PdCl_4]^{2-}$ and $[PtCl_4]^{2-}$).

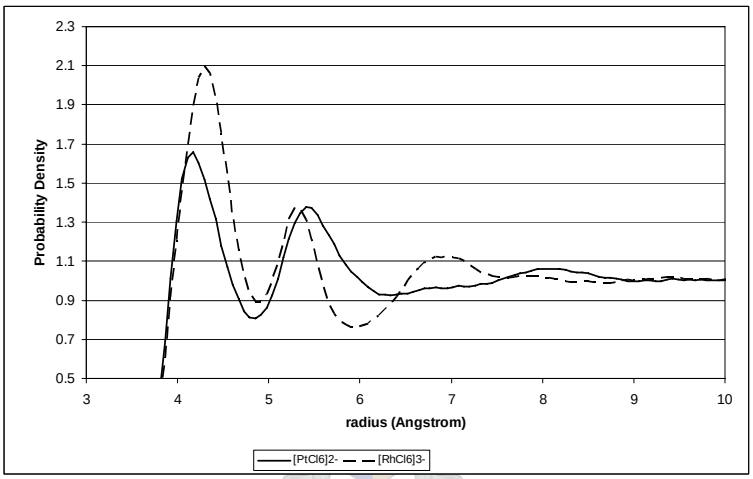

Fig 4.14: The pair distribution functions, g(r), for the metal···O(water) configuration in the two octahedral complexes ($[PtCl_6]^{2-}$ and $[RhCl_6]^{3-}$).

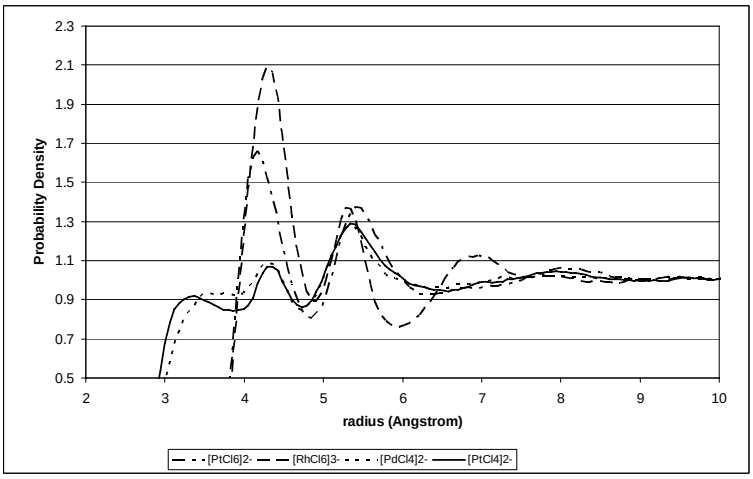

Fig 4.15: The pair distribution functions, g(r), for the metal···O(water) configuration in the following complexes ($[PtCl_6]^{2-}$, $[RhCl_6]^{3-}$, $[PdCl_4]^{2-}$ and $[PtCl_4]^{2-}$).

The relative volumes of the hydration shells were calculated by integrating over the radial distribution functions of the oxygen atoms in the water molecules to the PGM complex metal center. Levels of 20%

above bulk probability (area above 1.2 probability density in figure 4.15) were included in order to insure an accurate portrayal of the relative solvation shell volumes. These integrated functions were then expressed in relation to the integral with the lowest value. The figure below and the table adjacent to it present a summary of these results. These results are therefore a quantitative measurement of the arguments presented earlier in this section. The hydration shell of the $[RhCl_6]^{3-}$ complex has the largest volume. The fact that this complex has a higher charge (-3) than the other PGM complexes (-2) means that a greater number of water molecules can be accommodated around this complex. It is also clear that the two octahedral complexes ($[RhCl_6]^{3-}$ and $[PtCl_6]^{2-}$) have greater volumes than the square planar complexes ($[PdCl_4]^{2-}$ and $[PtCl_4]^{2-}$). This is at least partially due to the fact that the octahedral complexes in themselves have more atoms, and therefore take more space than the square planar complexes. Finally, the results show that the $[PtCl_4]^{2-}$ complex is 19% more solvated than the $[PdCl_4]^{2-}$ complex. This result will be explained in terms of the relative free energy of solvation values of these two complexes. These free energies of solvation are reported and discussed in chapter 5.

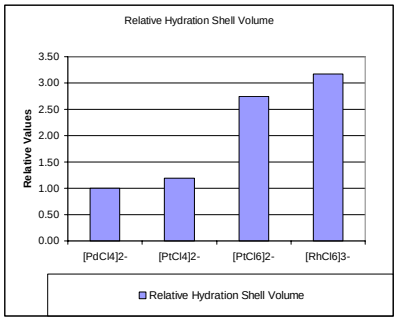

	Relative Hydration Shell Volume
$[PdCl_4]^{2-}$	100%
$[PtCl_4]^{2-}$	119%
$[PtCl_6]^{2-}$	274%
$[RhCl_6]^{3-}$	317%

4.2.3 Water Probability Density Distributions around PGM Chloro-Complex Anions

Solvation data in the form of radial distribution functions often obscures vital structural information due to the fact that it calculates radially averaged relative distances between the metal complex and the water. Important three dimensional structural characteristics of the hydration shells are therefore hidden because the distances are "smeared out". By using a technique which calculates the probability densities anisotropically valuable detail about the hydration shell symmetries can be gained. In this study the NPT trajectory data was used to perform spatial probability density calculations similar to those done in the study mentioned above [16] which used the NVE ensemble. The results obtained were almost identical and any differences are negligible. The results reported below mirror those in the above mentioned study and are only included for reference purposes. The reader is referred to the original text for a more thorough presentation. In this study only the metal···oxygen isoprobability surfaces were calculated and the metal···hydrogen surfaces were ignored. Due to the exact accordance of the metal···oxygen isoprobability surfaces data obtained with those of the previous study it can be safely assumed that the metal···hydrogen surfaces would also be similar.

Spatial probability densities for the octahedral complexes:
The isoprobability density surfaces were first analyzed at a level of 100% greater than that found in bulk water. At this level, which constitutes the first solvation shell, there are on average 8 water molecules occupying the sites centered above the 8 faces created by the 6 chlorine ligands in the octahedron. These 8 waters are therefore positioned at the corners of a cube around the metal. The dimensions of this cube are as follows: The sides and volume of the platinum complex are 4.70Å and 104Å^3 while the sides and volume of the rhodium complex are 4.65Å and 100Å^3. The distances to the chlorine ligands are acceptable as donor-acceptor distances normally found in hydrogen bonds. The Cl···O(water) distances are 3.32 and 3.27Å for the platinum and rhodium complexes respectively. These values correspond to that found in the RDF calculations as well as those obtained from neutron diffraction experiments [16] . Secondly, the isoprobability density surfaces were analyzed at a level of 50% greater that bulk water. At this level the second solvation shell is observed. There are on average 12 water molecules occupying sites directly above the saddle positions between the pairs of chlorine ligands. This framework resembles a regular 14-sided cuboctahedron. This geometry is much more prominent in the case of the rhodium complex. The volumes are 250 and 190Å^3 for the platinum and rhodium complexes respectively. While the second solvation shell of the rhodium complex is strongly

bound, the second shell of the platinum complex is much more diffuse and can only be seen at lower percentages above bulk water.

Spatial probability densities for the square planar complexes:
The isoprobability density surfaces were first analyzed at a level of 75% greater than that found in bulk water. At this level, which constitutes the first solvation shell, there are on average 8 water molecules occupying the sites equidistant from two adjacent chlorine ligands both above and below the σ_h plane. These 8 waters are therefore positioned at the corners of a tetragonal prism around the metal. The dimensions of this geometry are as follows: The sides of the platinum complex are 3.11 and 5.66Å and the volume is 55Å^3 while the sides of the palladium complex are 3.32 and 5.52Å and the volume is 61Å^3. The longer sides of this frame are perpendicular to the plane of the complexes. The distances to the chlorine ligands are acceptable as donor-acceptor distances normally found in hydrogen bonds. The Cl···O(water) distances are 3.31 and 3.29Å for the platinum and palladium complexes respectively. These values correspond to that found in the RDF calculations as well as those obtained from neutron diffraction experiments. Secondly, the isoprobability density surfaces were analyzed at a level of 50% greater than bulk water. At this level a very diffuse second solvation shell is observed. The framework of these probabilities is too weak and diffuse to classify successfully.

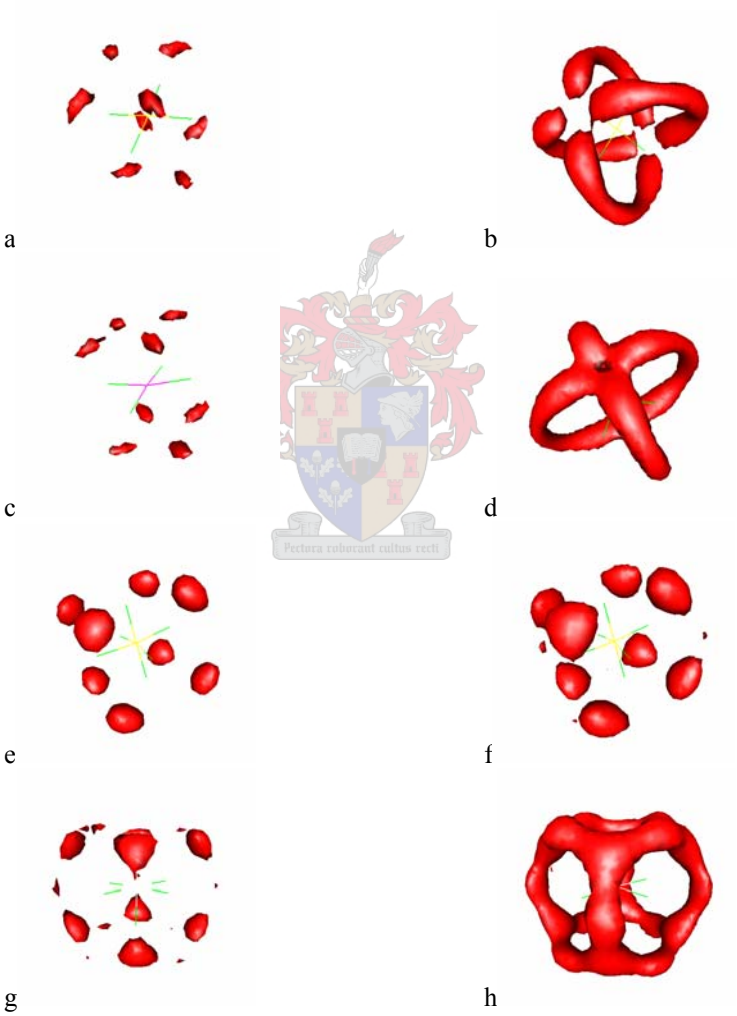

Fig. 4.16: The isoprobability density surfaces were analyzed at a level of 50% (b, d, f, h) and 100% (a, c, e, g) greater than bulk water. This was done for: $[PdCl_4]^{2-}$ (a, b); $[PtCl_4]^{2-}$ (c, d); $[PtCl_6]^{2-}$ (e, f); $[RhCl_6]^{3-}$ (g, h).

4.3 Polymer (PEO) and PGM Chloro-Complexes in a Water Solution

The previous section focused on the structural characteristics, such as hydration sphere geometry, of the PGM chloro-complexes in the absence of polymer (PEO) chains. In contrast, this section will report on the structural characteristics of the PGM chloro-complexes in the presence of poly (ethylene oxide) chains. Section 4.4 contains speculations as to the nature of possible electrostatic interactions between the polymer (PEO) and the PGM chloro-complexes. The potential effect these interactions might have on the structural properties of the poly (ethylene oxide) chains as well as on the solvation structures of the PGM chloro-complexes will also be discussed in section 4.4.

4.3.1 Simulation Procedure and Starting Structure

In order to speed up the equilibration process the solvated structures of the PGM chloro complexes ($[PtCl_4]^{2-}$, $[PtCl_6]^{2-}$, $[PdCl_4]^{2-}$ and $[RhCl_6]^{3-}$) generated in section 4.2 were used as starting structures. These boxes which were already equilibrated were superimposed onto 50Å×50Å×50Å cubical cells containing bulk water as well as four individual polymer (PEO) chains. Any overlaps were subsequently deleted. Therefore, each box contained a PGM complex as well as four separate PEO strings in bulk water. A single PEO chain consisted of 30 monomers. The polymer chain starting structures were generated by randomly assigning values to the dihedral angles in the backbone in the same proportions as was established in the dihedral angle distribution analysis. The concentration of the polymer in solution was 0.0575 mol/dm^3 while the overall density of the system was 1.02 g/cm^3. The program CHARMM [8] was used for all MD simulations. As before the TIP3P water model as implemented in CHARMM was used. In order to maintain overall neutrality the appropriate number of sodium counter-ions was added to the respective systems. To insure that the bulk density was maintained the number of water molecules in the box differed for each solution. Periodic boundary conditions were employed. The image convention used for water was per residue, but for the polymer it was implemented by segment. MD simulations of 300 ps heating followed by 500 ps equilibration were performed before production commenced. The trajectory data was collected over 1 ns of equilibrated NPT dynamics. The force field used was previously described and validated against diffraction experiments and quantum mechanical calculations [9] . The parameters chosen in both equilibration and production are as described in section 4.2. A NPT ensemble, using the Nose-Hoover thermostat was simulated. The cutoff distance used was 14Å.

4.3.2 Pair Distribution Functions of (1) the Ether Oxygen Atoms in the Polymer (PEO) chains to the PGM Complex Metal Center, as well as (2) the Oxygen atoms in the Water Molecules to the PGM Complex Metal Center

(1) Pair Distribution Functions of the Ether Oxygen Atoms in the Polymer (PEO) chains to the PGM Complex Metal Center

The PGM chloro-anions have repulsive electrostatic interactions with the ether oxygens in the polymer chains. This is because both are partially negative species. It is speculated that there would be a form of crown ether interaction between these ether oxygens and the sodium counter ions. These interactions will be discussed in section 4.4. However, this section focuses on the direct, repulsive polymer-anion interactions. The closest distances the ether oxygen ever come (over a 1 ns simulation time) to the anionic complexes can be read from fig 4.19 and 20. It has to be remembered that the volume occupied by the solvation shells of all these complexes would impact on the interaction distances. A direct interaction between the ether oxygen and the PGM chloro-complex is very unlikely. The real interaction is therefore between the solvated PGM chloro-complex and the ether oxygen in the polymer (PEO) chain. Therefore, the water molecules which make up the solvation shell of the PGM complex play a role in this interaction. The two square planar complexes, which also occupy the smallest solvated volume, allow closest contact with the ether oxygens. These distances, both at 4Å, are still bigger than the solvation shell radii for these complexes (3.62Å for $[PdCl_4]^{2-}$ and 3.58Å for $[PtCl_4]^{2-}$). The two octahedral complexes, which occupy a larger solvated volume, only allow contact with the ether oxygens at distances of 4.7Å and 5.4Å for the $[PtCl_6]^{2-}$ and $[RhCl_6]^{3-}$ complexes respectively. Of all the anions under consideration, the $[RhCl_6]^{3-}$ complex possesses the biggest solvation shell and it makes sense therefore that it should have the largest interaction distance. The $[RhCl_6]^{3-}$ complex also

has a net charge of -3 whereas the other complexes have a -2 net charge. This would make the repulsive interactions even more severe. From fig 4.19 it is clear that there is no consistent trend present that would link the RDF's of the two square planar complexes. This observation is also true for the two octahedral complexes. A possible reason for this is the time scale of motion of the polymer chains as was discussed in section 4.1.3. The polymer chains take such a long time to make significant conformational (folding) changes that it would take long simulation times to sample these distances representatively.

The RDF's were integrated in terms of the total number of oxygens participating at specific distances. Each PEO chain contains 30 ether oxygen atoms and there are four PEO chains per box. The total number of oxygens over which the integration was performed was therefore 120. Fig 4.17 shows the integration over the full range of distances and fig 4.18 focuses on those distances which could be within the electrostatic interaction range. The number of ether oxygens involved at a distance of 6Å is 4, 3, 2 and zero for the $[PdCl_4]^{2-}$, $[PtCl_4]^{2-}$, $[PtCl_6]^{2-}$ and $[RhCl_6]^{3-}$ complexes respectively. At a distance of 7Å however, the numbers of oxygens are 6, 8, 6 and 2 for the $[PdCl_4]^{2-}$, $[PtCl_4]^{2-}$, $[PtCl_6]^{2-}$ and $[RhCl_6]^{3-}$ complexes respectively. The closest, significant interaction distance is present with the $[PtCl_4]^{2-}$ complex, whereas the largest distance and most repulsive interaction is present with the $[RhCl_6]^{3-}$ complex.

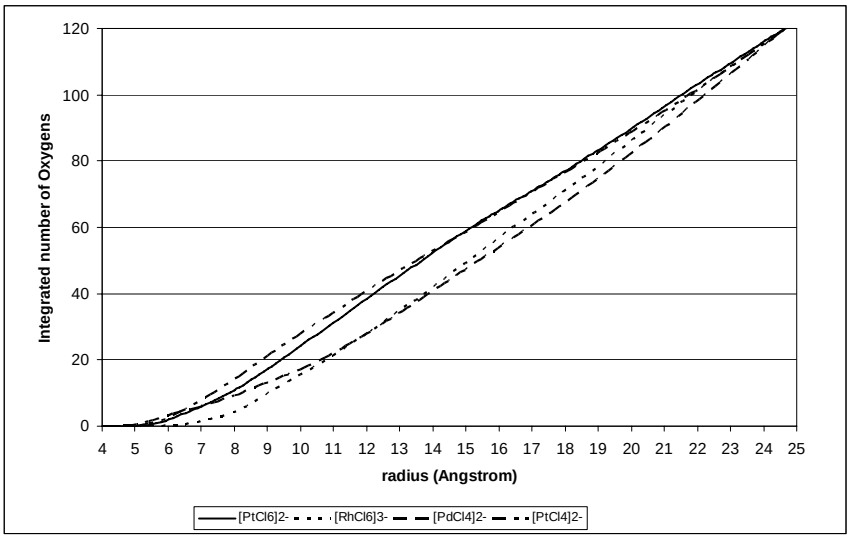

Fig 4.17: The integrated number of ether oxygens in PEO over the full range of distances.

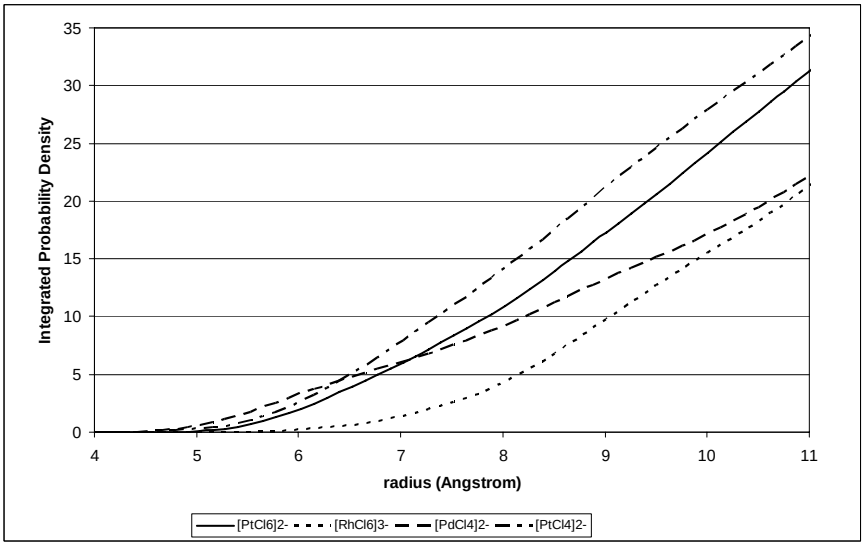

Fig 4.18: The integrated number of ether oxygens in PEO over distances within the immediate electrostatic interaction range.

Fig 4.19: RDF's of the two square planar complexes ($[PdCl_4]^{2-}$ and $[PtCl_4]^{2-}$).

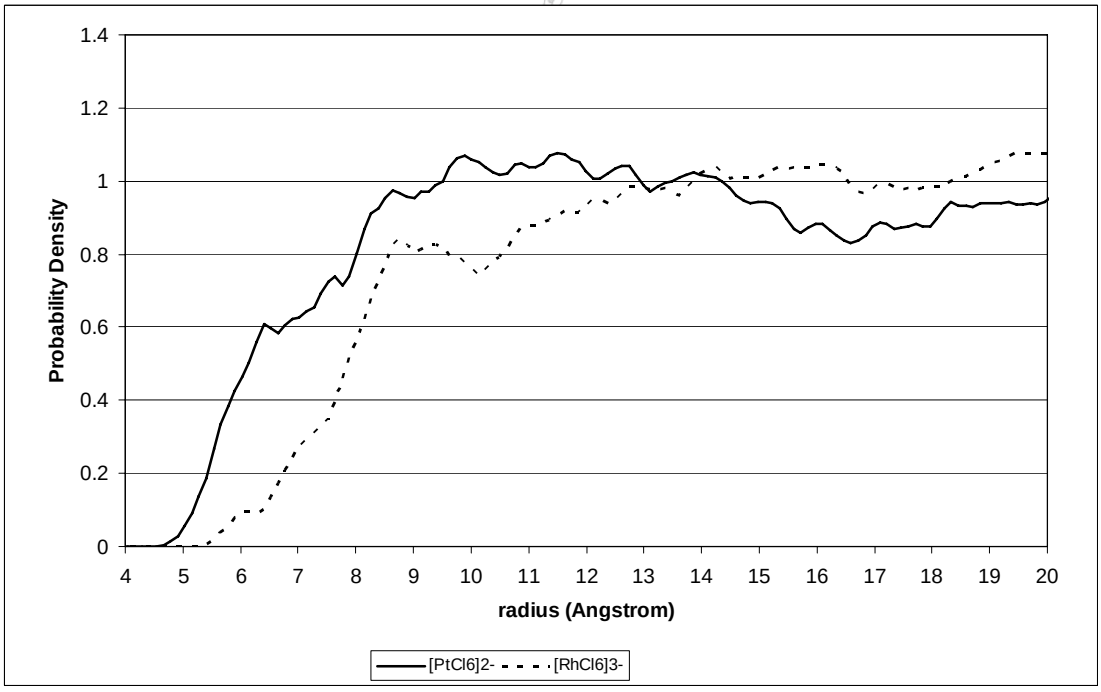

Fig 4.20: RDF's of the two octahedral complexes ($[PtCl_6]^{2-}$ and $[RhCl_6]^{3-}$).

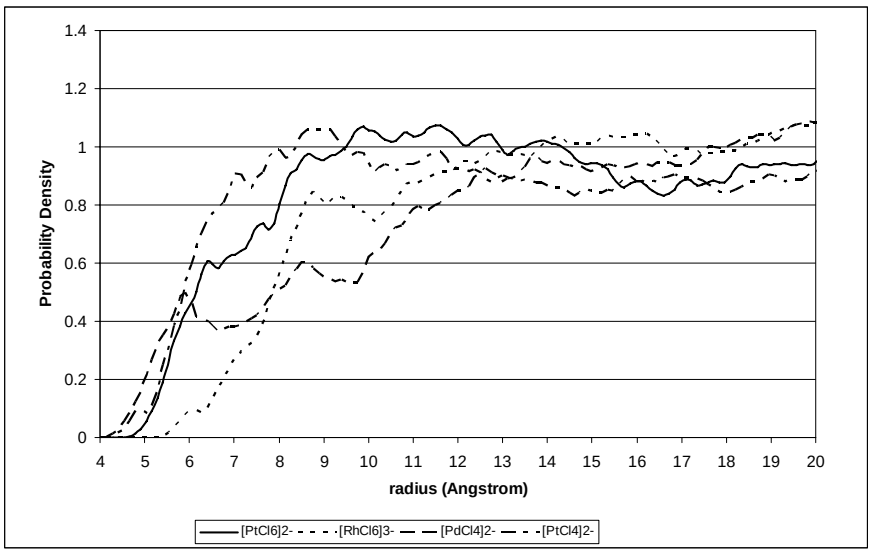

Fig 4.21: RDF's of all the relevant complexes.

(2) Pair Distribution Functions of the Oxygen Atoms in the Water Molecules to the PGM complex Metal Center

As before a radially averaged probability density distribution (radial distribution function) was used to describe the structural arrangement of water around the complex chloro-anions of Pt(IV), Pt(II), Pd(II) and Rh(III). The objective of this study is to compare the results from the pure PGM complex solutions (section 4.2) with that obtained in a system containing polymer (PEO) chains. The radial distribution functions (RDFs) of the square planar $[PdCl_4]^{2-}$ and $[PtCl_4]^{2-}$ complexes can be seen in fig 4.22 and 23. As before the pair distribution functions, g(r) for the metal···O(water) configurations, for these two complexes indicate a similar solvent structure. The RDFs indicate similar regions to those discussed in section 4.2. The results for the two octahedral complexes, $[PtCl_6]^{2-}$ and $[RhCl_6]^{3-}$, are again almost exactly the same as in section 4.2 (see fig 4.24 and 25 respectively). The slight differences which can be observed between the two probability density functions (with and without polymer) of the $[PdCl_4]^{2-}$ complex (fig 4.22) are not significant in terms of the degree of solvation of this complex. This is because the differences occur at a level below bulk probability. In general there is a strong indication that the polymer (PEO) chains do not significantly interfere with the solvation of these complexes in water. From this we can conclude that there is no direct interaction between the polymer (PEO) chains and the PGM chloro-complexes. Any interactions are therefore between the polymer (PEO) and the solvated PGM complex. This interaction does not disturb the structure of the hydration shells. There is no electrostatic incentive for the PGM anions to interact with the ether oxygen atoms in the poly (ethylene oxide) chains, because both have partial negative charges. The forces which act on these species, when random diffusion brings them relatively close together, is therefore repulsive in nature.

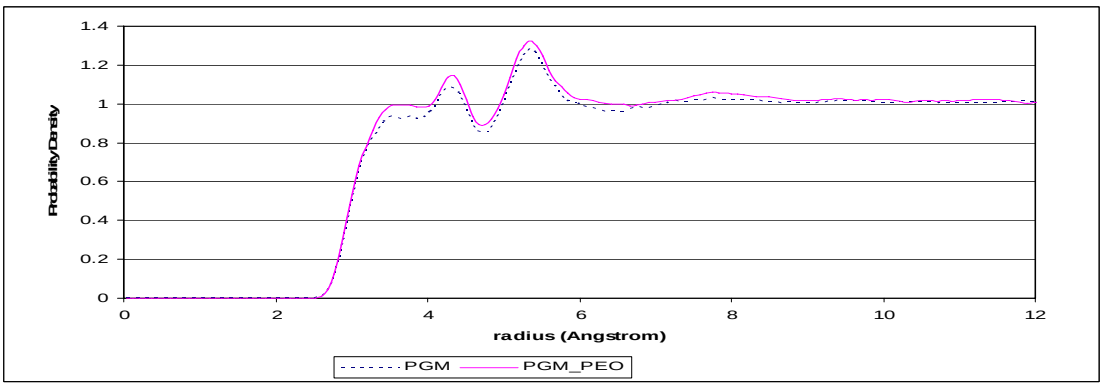

Fig 4.22: The pair distribution functions, g(r), of the metal··O(water) configuration in $[PdCl_4]^{2-}$ with and without the polymer (PEO) present.

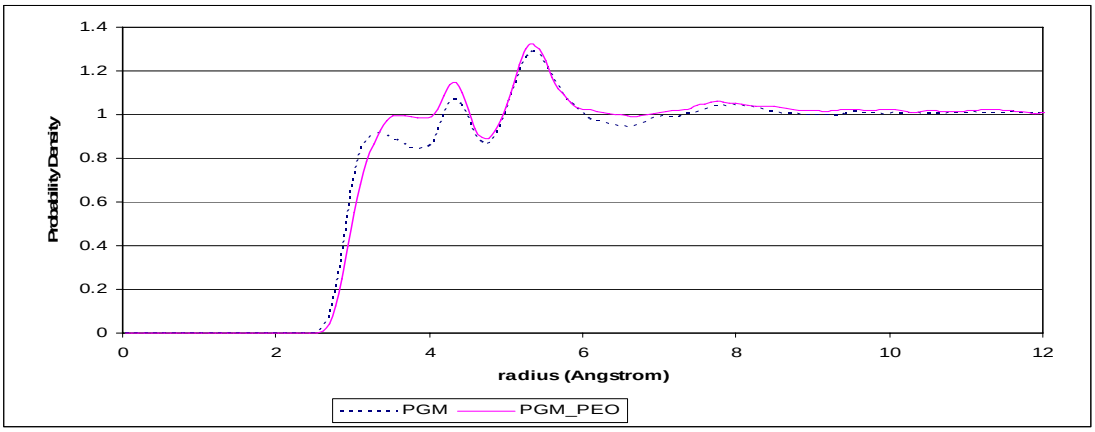

Fig 4.23: The pair distribution functions, g(r), of the metal··O(water) configuration in $[PtCl_4]^{2-}$ with and without the polymer present.

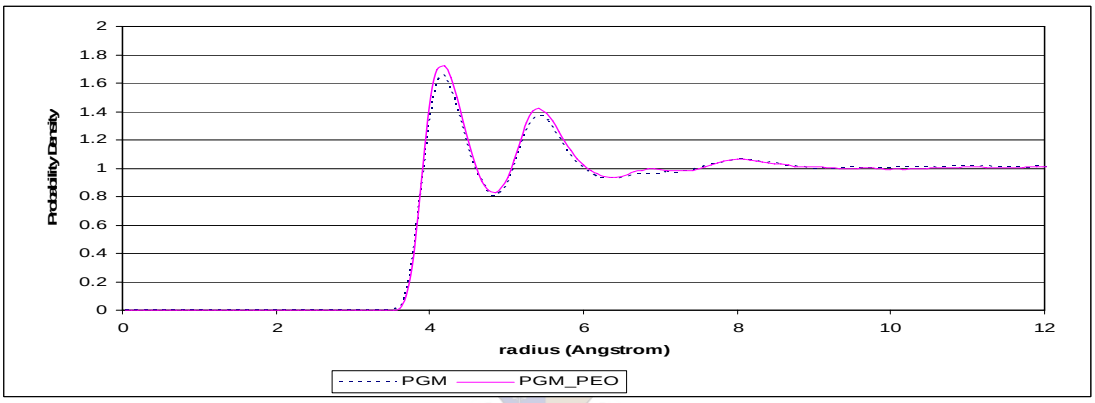

Fig 4.24: The pair distribution functions, g(r), of the metal··O(water) configuration in $[PtCl_6]^{2-}$ with and without the polymer present.

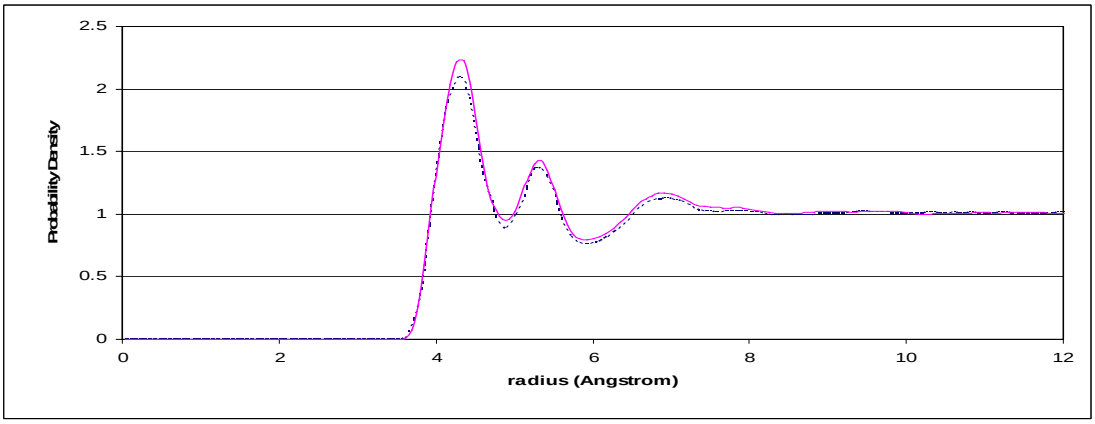

Fig: 4.25: The pair distribution functions, g(r), of the metal··O(water) configuration in $[RhCl_6]^{3-}$ with and without the polymer present.

4.3.3 Water Probability Density Calculations

The probability densities were calculated anisotropically in order to gain detail about the hydration shell symmetries and how or if they vary at all from those results obtained in section 4.2. The NPT trajectory data was used to perform the spatial probability density calculations exactly similar to those done in section 4.2. The results obtained were almost identical and any differences are negligible. Again, only the metal···oxygen isoprobability surfaces were calculated and the metal···hydrogen surfaces were ignored. The isoprobability density surfaces were analyzed at levels of 0%, 5%, 15%, 30%, 50% and 100% greater than that found in bulk water. These surfaces can be seen in fig 4.26 to 29, which are printed on the pages that follow. At bulk density it is clear that the oxygens are distributed in normal bulk fashion. The lack of an even distribution of the oxygens at 5% greater than bulk can be attributed to the asymmetrical presence of the polymer chains as well as the counter ion positions. The solvation shell structure at levels 15% and 30% are remarkably symmetrical, though very diffuse. In terms of geometry as well as relative probability, the results at level 50% and 100% greater than bulk are exactly similar to those obtained in section 4.2. This is true for both the octahedral and square planar complexes. This is yet another indication that the polymer chains do not significantly interfere with the solvation shells or structure of these complexes. From this it is clear that the repulsive interactions between the PGM chloro-complexes and the polymer (PEO) chains do not disturb the geometry of the hydration shells of these complexes. Therefore, the solvation shells remain in tact, despite the interactions with the polymer (PEO) chains.

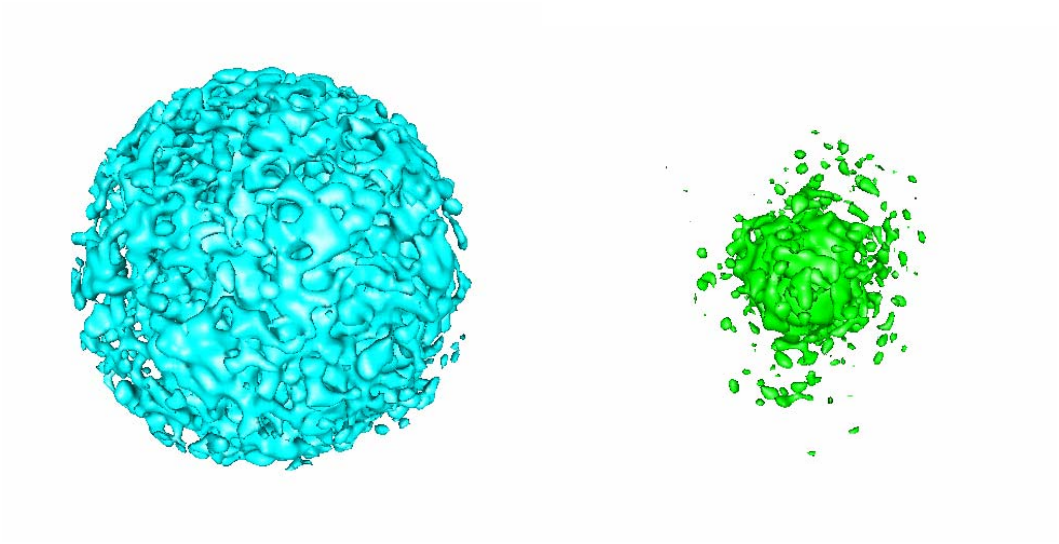

a b

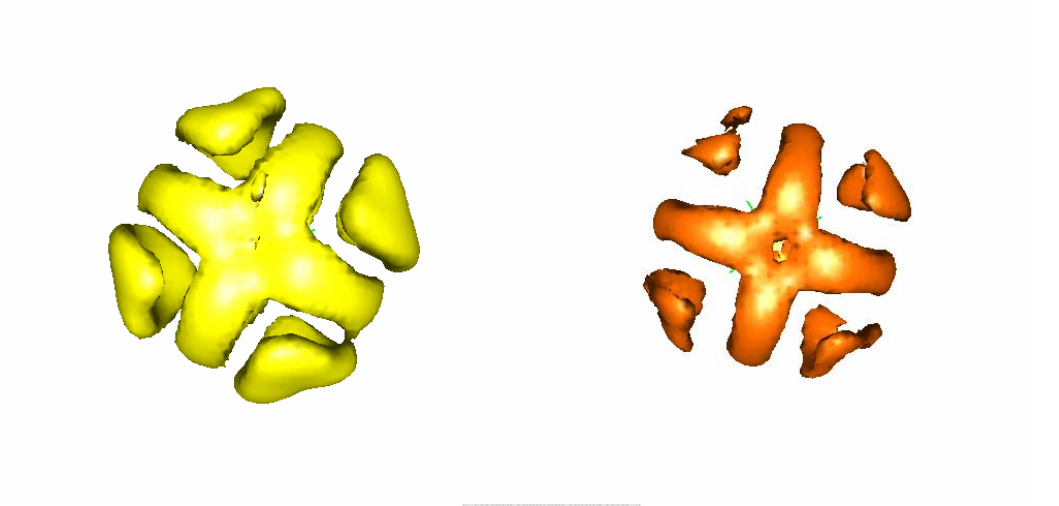

c d

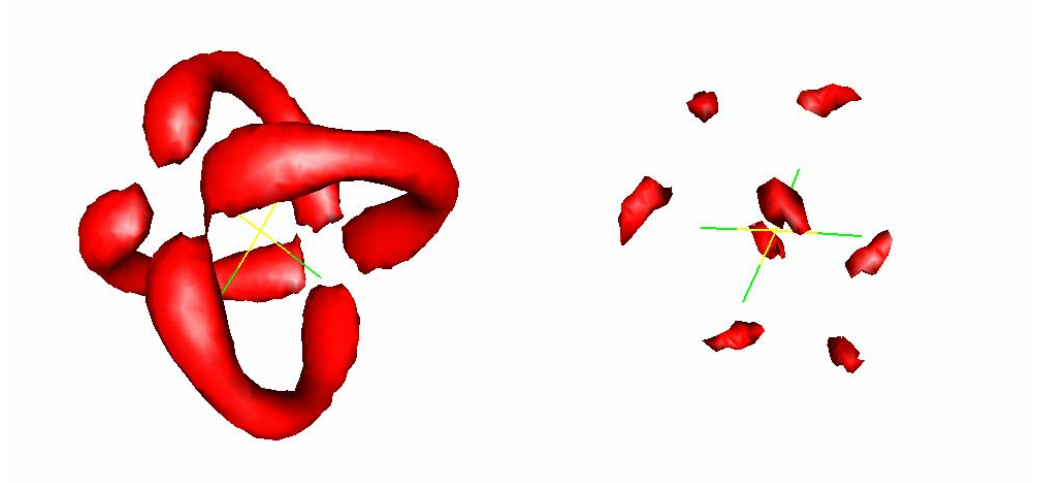

e f

Fig 4.26: The isoprobability density surfaces of $[PdCl_4]^{2-}$ at levels of 0%, 5%, 15%, 30%, 50% and 100% greater than that found in bulk water.

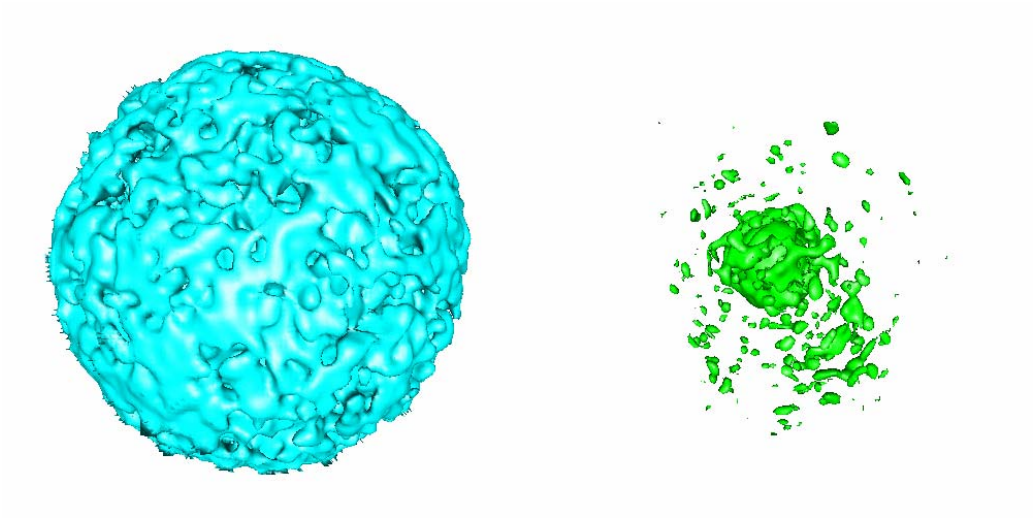

a b

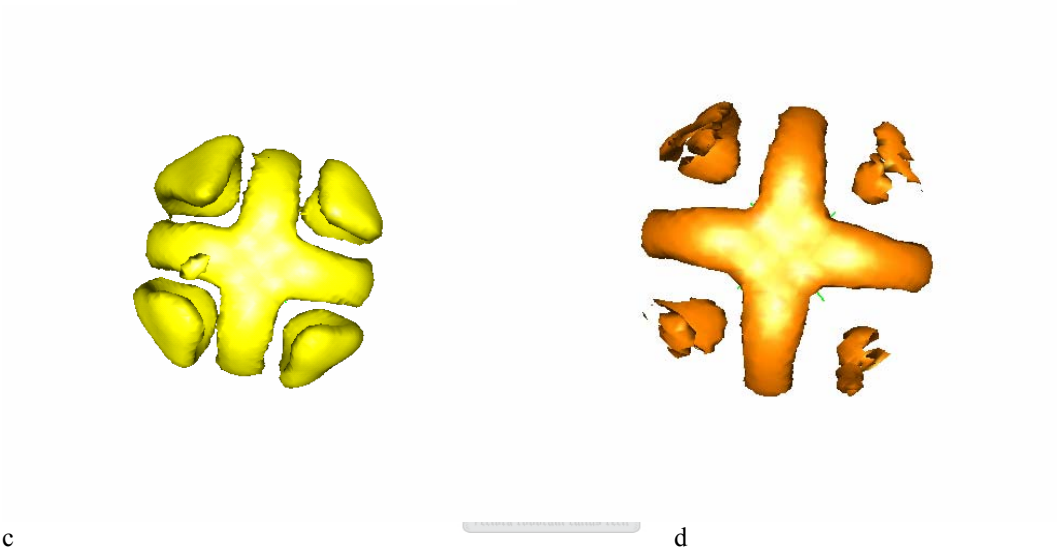

c d

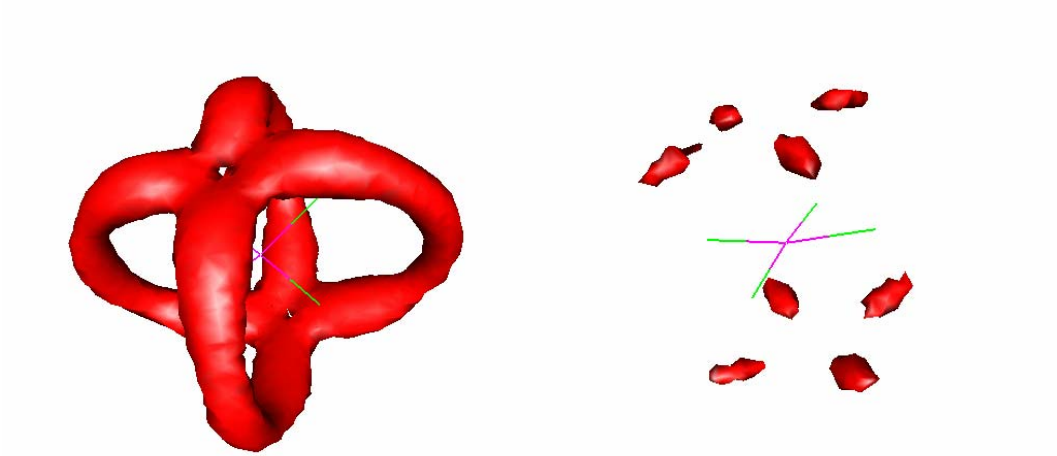

e f

Fig 4.27: The isoprobability density surfaces of $[PtCl_4]^{2-}$ at levels of 0%, 5%, 15%, 30%, 50% and 100% greater than that found in bulk water.

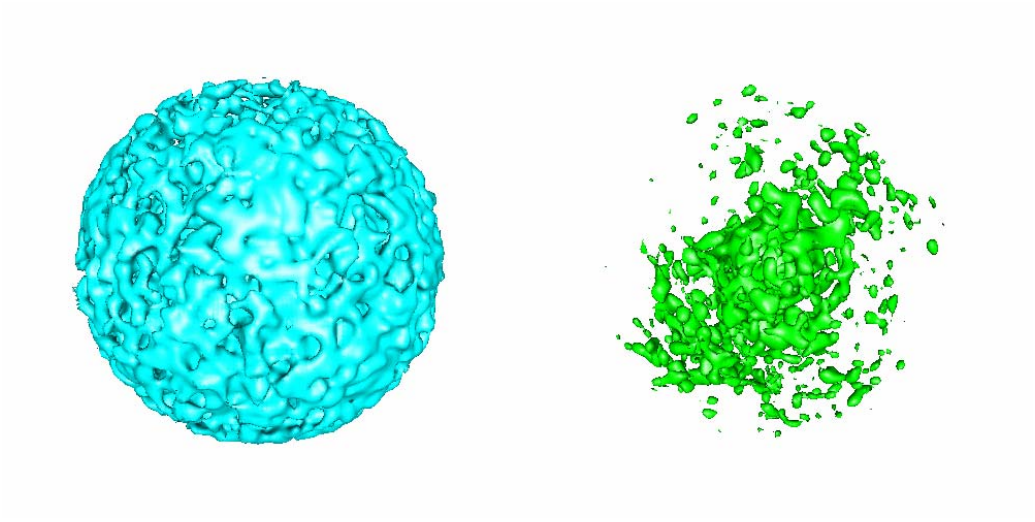

a b

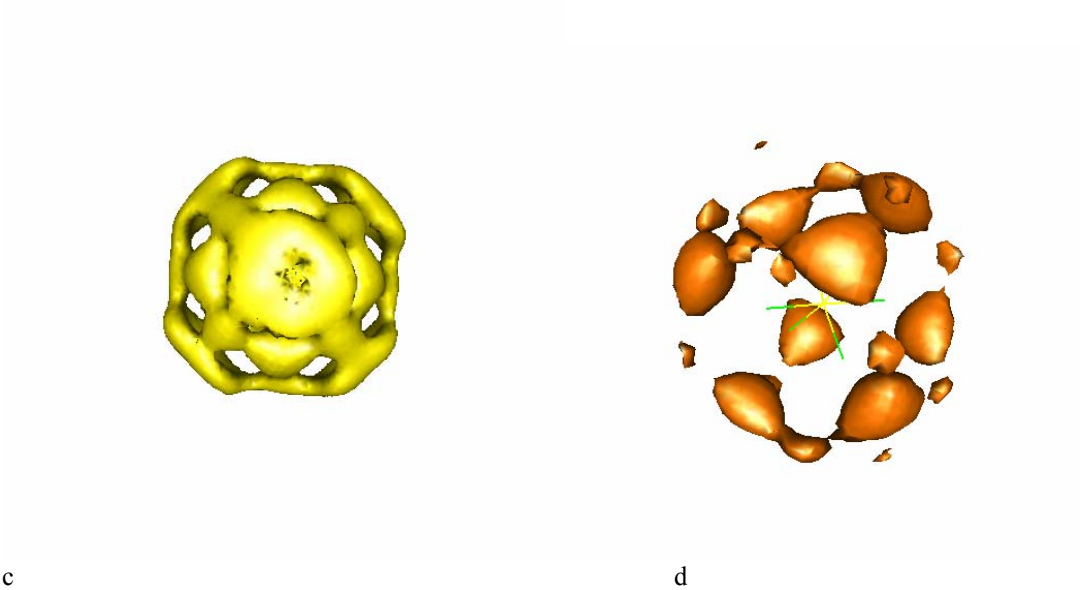

c d

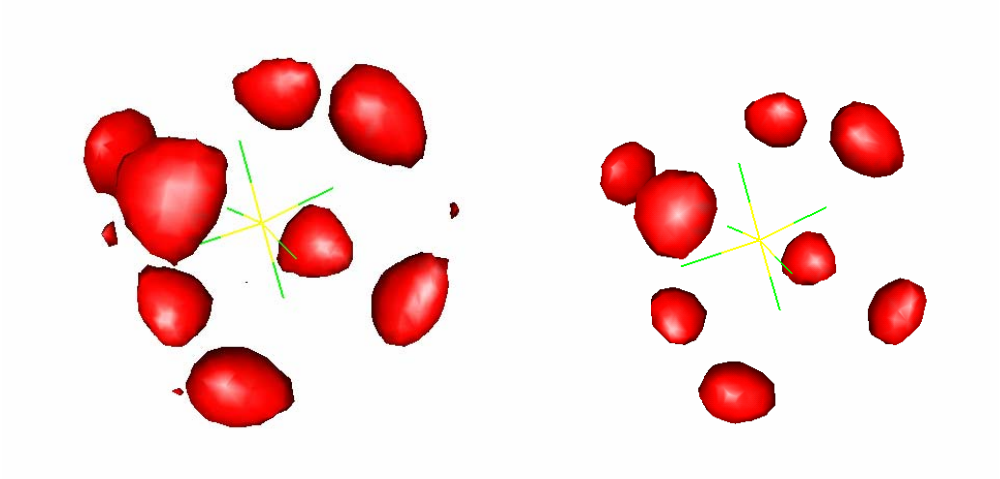

e f

Fig 4.28: The isoprobability density surfaces of $[PtCl_6]^{2-}$ at levels of 0%, 5%, 15%, 30%, 50% and 100% greater than that found in bulk water.

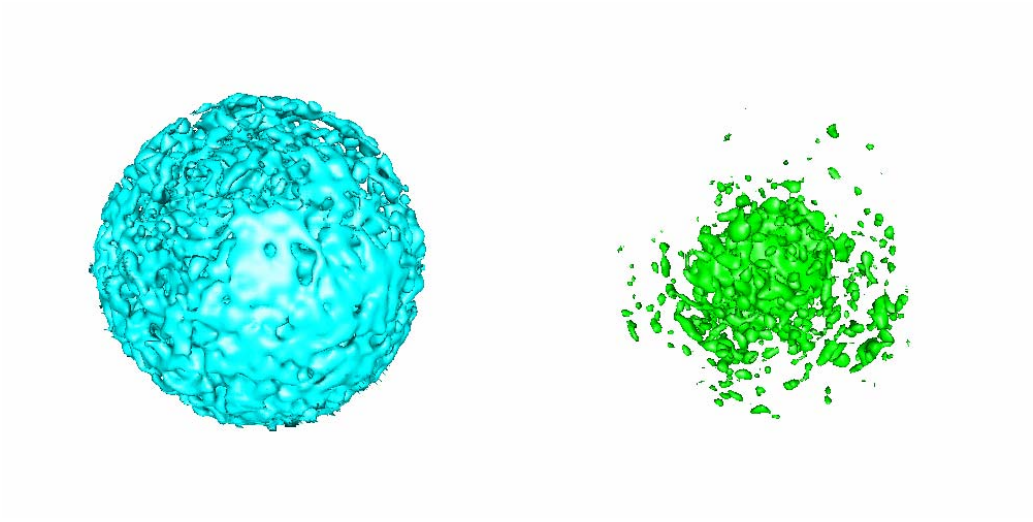

a b

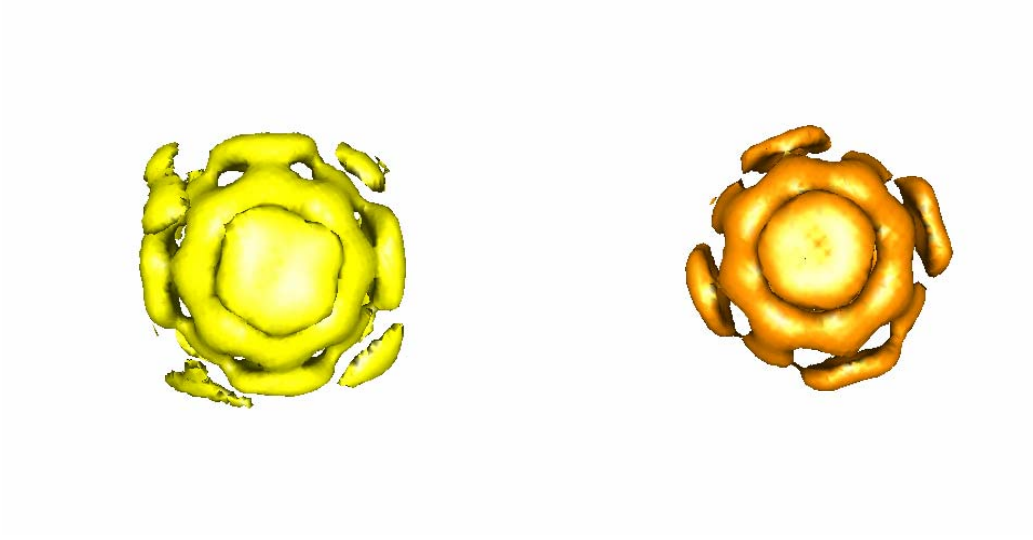

c d

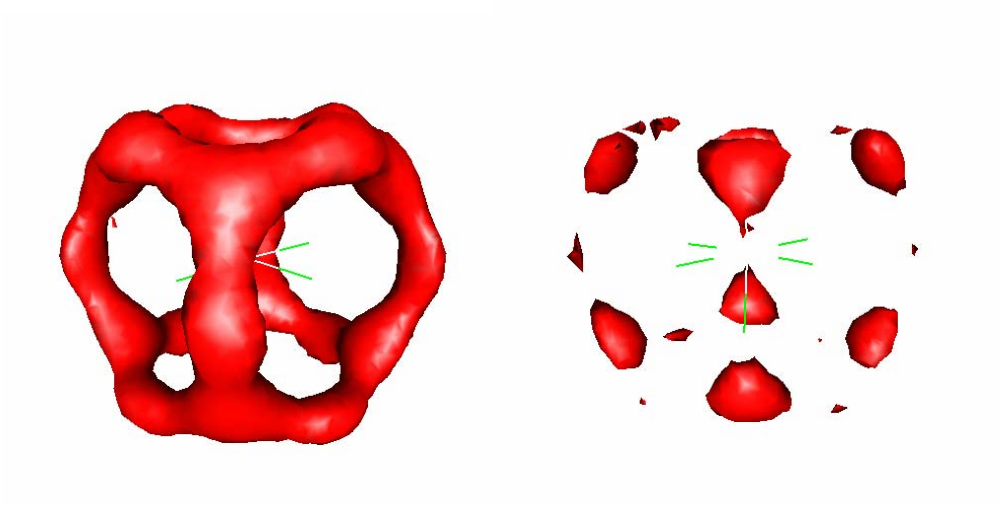

e f

Fig 4.29: The isoprobability density surfaces of $[RhCl_6]^{3-}$ at levels of 0%, 5%, 15%, 30%, 50% and 100% greater than that found in bulk water.

4.4 Speculations Regarding Electrostatic Interactions between the Polymer (PEO) and the Ions in Solution (PGM Chloro-complexes and Sodium Counter-Ions)

The polymer (PEO) chains undergo a variety of interactions with the different species in the solution. Firstly, the polymer (PEO) chains interact with the water molecules. These interactions contribute to the solvation of the polymer (PEO) chains. The presence of the water molecules also results in the solvation of the ions (the PGM chloro-complexes and the sodium counter-ions) in the solution. Because of the conformational characteristics of the ether linkages in the poly (ethylene oxide) chains, the polymer (PEO) chains are very flexible (see section 4.1 and 4.2) and can therefore fold and unfold with relative ease. Secondly, it is speculated that the polymer (PEO) chains interact with the sodium counter-ions in the solution. Therefore, the manner in which the polymer (PEO) chains fold is also expected to be effected by the electrostatic interactions with the sodium counter-ions. The potential exists for folding to result in crown ether formations. These crown ether formations form complexes with the Na^+ ions in the solution. In turn, these complexes, which are positively charged, would interact and associate with the negatively charged PGM chloro-complexes. The figure below illustrates a crown ether complex and its association with a PGM chloro-complex.

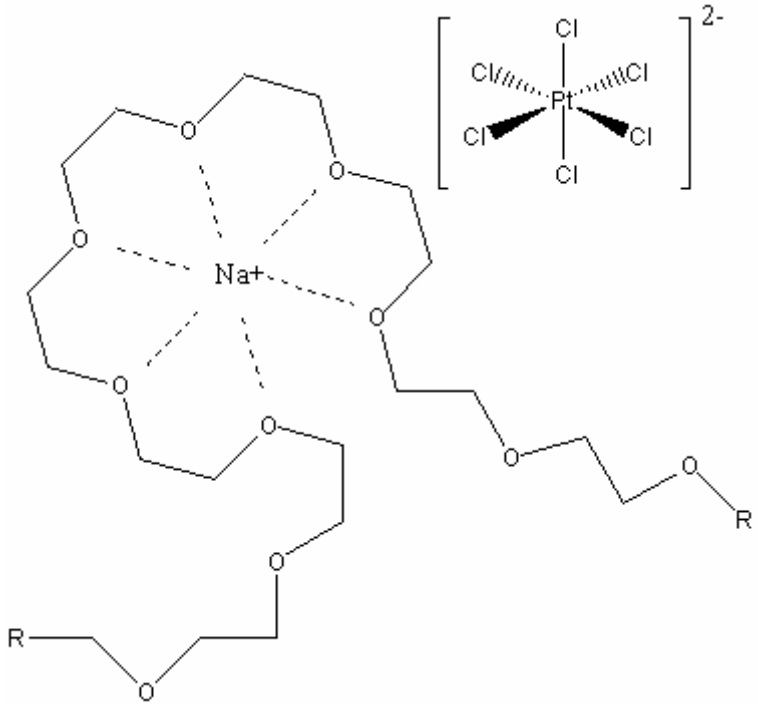

Electrostatic repulsions between the polymer chains and the solvated PGM chloro-complexes might also influence the folding of the polymer (PEO). Due to the low concentration of these ionic species in solution (0.013mol/liter), it is less likely for these interactions to be observed within the relatively short time period of the Molecular Dynamics simulation (1.5 ns).

4.5 Other General Conclusions

The structural information needed for the theoretical calculation of transport properties (diffusion coefficients in Chapter 5) was generated in this chapter. The average structures needed to perform the thermodynamic property analysis (free energies of solvation in Chapter 6) were also obtained. A conformational study of the two dihedral angles in a PEO chain (-C-O-C-C- and -O-C-C-O-) was performed and the extreme flexibility of the polymer were confirmed. Dihedral angle distributions of the two dihedral angles were calculated which can now serve as maps that would enable us to generate starting structures for the polymer chains. The end-to-end distance time series were calculated and we

were able to establish a quantitative framework for the time scale of motion. This motion is slow as is expected for a polymer of this chain length. The solvation geometries of the PGM complexes were confirmed for the NPT ensemble. These results do not vary significantly from those in the system where the polymer is present. From this we can conclude that the effect of the polymer on the structure and degree of solvation is negligible. This confirms our suspicion that there is no real affinity between the PGM chloro-anion and the PEO chain.

References:

1. K.J. Naidoo and J.W. Brady, *The application of simulated annealing to the conformational analysis of disaccarides.* Chem. Phys., 1997. **224**: p. 263-273.
2. A.R. Leach, *A survey of methods for searching the conformational space of small and medium-sized molecules.* Comp.Chem.II, 1991: p. 1-55.
3. L. Verlet, *Computer "experiments" on classical fluids. I. Thermodynamical Properties of Lennard-Jones Molecules.* Phys. Rev., 1967. **159**: p. 98-103.
4. D. Rigby, H. Sun, and B.E. Eichinger, *Computer Simulation of Poly(ethylene oxide): Force Field, PVT Diagram and Cyclization Behaviour.* Polymer International, 1997. **44**(3): p. 311-330.
5. F.P.S.C. Gil, A.M.A. Costa, and J.J.C. Teixeira-Dias, *Conformational analysis of C(m)H(2m+1)OCH2CH2OH(m=1-4):The role of CH-O Intramolecular interactions.* J.Phys.Chem., 1995. **99**: p. 8066-8070.
6. H. Dong, J.K. Hyun, C. Durham and R.A. Wheeler, *Molecular dynamics simulations and structural comparisons of amorphous poly(ethylene oxide) and poly(ethylenimine) models.* Polymer, 2000. **42**(18): p. 7809-7817.
7. F. Muller-Plathe and W. van Gunsteren, *Computer simulation of a polymer electrolyte:lithium iodide in amorphous poly(ethylene oxide).* J.Chem.Phys., 1995. **103**(11): p. 4745-4757.
8. B.R. Brooks, D. Janezic, M. Karplus and R.M. Venable, *CHARMM:A program for macromolecular energy,minimization,and dynamics calculations.* J. Comput. Chem., 1983. **4(2)**: p. 187-217.
9. A. Lienke, G. Klatt, D.J. Robinson, K.R. Koch and K.J. Naidoo, *Modeling Platinum Group Metal Complexes in Aqueous Solution.* Inorg. Chem., 2001. **40**: p. 2352-2357.
10. J.D. Adams, *On the use of the Ewald Summation in Computer Simulation.* J. Chem. Phys., 1982. **78**(5): p. 2585 - 2590.
11. H. Dufner, M. Schlenkrich, and J. Brickmann, *Ewald Summation contra Direct Summation of Shifted-Force Potentials for the Calculation of Electrostatic Interactions in Solids: A quantative study*, . 1994, Techische Hochschule: Darmstadt.
12. D.M. Heyes, *Electrostatic potentials and fields in infinite point charge latices.* J. Chem. Phys., 1981. **74**(3): p. 1924 - 1929.
13. J.E. Roberts and J. Schnitker, *Boundary Conditions in Simulations of Aqueous Ionic Solutions: A Systematic Study.* J. Phys. Chem., 1994. **99**(4): p. 1322 - 1331.
14. D.E. Williams, *Accelerated Convergence of Crystal-Lattice Potential Sums.* Acta. Crystallogr., 1971. **A27**: p. 452 - 455.
15. D. York, T. Darden, and L.G. Pedersen, *Particle mesh Ewald: An Nlog(N) method for Ewald sums in large systems.* J. Chem. Phys., 1993. **98**(12): p. 10089 - 10092.
16. K.J. Naidoo, G. Klatt and K.R. Koch, *Geometric Hydration Shells for Anionic Platinum Group Metal Chloro Complexes.* Inorg. Chem., 2002. **41**: p. 1845-1849.

Chapter 5

THERMODYNAMIC PROPERTIES OF PGM CHLORO-COMPLEXES IN WATER

This chapter describes the procedures and results obtained from two independent computational techniques which were used to calculate certain thermodynamic properties of the solute molecules in PGM systems. The systems on which these thermodynamic analysis were performed involved a variety of PGM Chloro-Complexes ($[PdCl_4]^{2-}$, $[PtCl_4]^{2-}$, $[PtCl_6]^{2-}$ and $[RhCl_6]^{3-}$) with the appropriate number of counter ions in a water solution. The unique challenges (from a computational point of view) are discussed for each method as well as the level of precision associated with its application. Thermodynamic properties (particularly free energy of solvation values) were calculated which provide insight into the structural characteristics observed in chapter 4 (solvation shell volume and geometry) as well as the diffusion rates as reported in chapter 6. The thermodynamic results can be used to clarify the observed trends or phenomena and offer possible explanations for their occurrence. This chapter therefore complements chapter 4 and chapter 6 by validating the structural and diffusion results and offering unique mechanistic insight. The focus in this chapter is, however, on the correlation between the structural characteristics of these solvated anions and their thermodynamic properties. The focus in chapter 6 is on explaining the interdependence between all three properties (structure, thermodynamics and diffusion). The reader is encouraged to pay particular attention to the procedural specifications of each method as many of the practical difficulties due to the chemical systems involved were solved by careful selection and optimization of these parameters. The theoretical foundation of the two techniques used in this chapter was described in chapter 3. As always, a thorough understanding of these theories facilitates a better appreciation of the accuracy and relevance of the results and conclusions.

5.1 Thermodynamic Integration results

5.1.1 Introduction

This explicit solvent free energy simulation method is computationally very demanding, but delivers results which are very reliable compared to alternative computational techniques, such as the Poisson-Boltzmann method. The relative accuracy of this method stems from its independence from empirical data and other approximations as well as the explicit and dynamic way in which it treats the solvent molecules. A big advantage of this method is that it accurately calculates the entropic component of the free energy. The differences in the solvation free energies of two PGM chloro-complexes can be calculated with this technique. In the context of this chapter the $\Delta\Delta G$ value obtained can be used to compare with the same difference in values calculated by using the Poisson-Boltzmann (PB) method. If these values correlate, it would serve to validate the use of the PB method for these systems. A component analysis was performed to establish whether the solvation free energy difference is dominated by enthalpic or entropic effects. In this section the difference in the free energy of solvation was calculated between the two square planar complexes ($[PdCl_4]^{2-}$ and $[PtCl_4]^{2-}$).

5.1.2 Simulation Procedure

A 24.67Å by 24.67Å by 24.67Å cubic box containing 512 waters was generated. The $[Pd/Pt(Cl_4)]^{2-}$ hybrid molecule was defined in the residue topology file. No internal coordinate energy terms involving both reactant (Pd) and product (Pt) atoms were listed. Specific non-bonded exclusions were specified between reactant (Pd) and product (Pt) atoms. This hybrid molecule was generated and all overlapping water molecules (those water molecules within a 2.5 Å distance of the hybrid molecule) were deleted. The Chemical Perturbation parameters which are described in this section were chosen to guarantee maximum precision. The reactant atom selection was Pd and the product atom selection was Pt. The hybrid Hamiltonian in this implementation was defined as:

$$H(\lambda) = V(environment) + \left((1-\lambda)^N\right)V([PdCl_4]^{2-}) + \left(\lambda^N\right)V([PtCl_4]^{2-})$$

where N equals 1 because a linear path progression is appropriate for this system. The λ pathway was constructed with 0.1 λ intervals. This increment size insures that effective integration takes place, as subsequent energy jumps are closer than one would get with wider intervals. The entire λ-range was covered (0.1, 0.2, …., 0.9).

The DONT [1] command was used for both the reactant and the product selection. This command excludes the bond and angle internal energy terms from the perturbation. These interactions were therefore ignored and not factored by λ or 1-λ to contribute to the $V([PdCl_4]^{2-})$ and $V([PtCl_4]^{2-})$ values. This is because these terms are generally not related to the interactions of interest (solvation) and no significant affect in the free energy differences results from this exclusion. These interactions were however treated in full as part of the V(environment) term. The COLO [2] function was employed to facilitate the change in partial charge that occurs on the chlorine ligands during the $[PdCl_4]^{2-}$ to $[PtCl_4]^{2-}$ transition. Despite the vd Waals characteristics and atom type remaining unaltered though out a transition, some atoms change partial charge as the reactant value is perturbed to the product value. MD simulations of 500 ps equilibration and 500 ps production were performed at each λ point. The parameters chosen in both equilibration and production were the following: a NPT ensemble, using the Nose-Hoover thermostat was simulated. The constant pressure calculation was performed using the extended system algorithm. The mass of the pressure piston was 500 amu and the Langevin piston collision frequency was specified as 5 per picosecond. A Nose-Hoover reference temperature of 300 K was used, while the mass of the thermal piston was 1000 $kcal.ps^2$. The equilibration process was therefore performed at 300 K. The temperature deviation to be allowed from the desired temperature was specified as ± 5 K. A time step of 0.001 ps was chosen for the dynamics run. A step frequency of 100 was used for stopping the rotation and translation of the molecule during dynamics. The images were updated every 10 steps. Averages and root mean square fluctuations were calculated every 100 steps.

The non-bonded interaction list was regenerated every 10 steps and the following non-bonded specifications were used: due to the presence of ions in solution the Ewald summation method was invoked to deal with these long-range interactions. The width of the Gaussian distributions used when calculating the Ewald summation was 0.32 Å. It is convention to choose this value as 4/CTOFNB which will be defined later. The Particle Mesh Ewald algorithm was employed for the reciprocal space summation. The number of grid points for the charge mesh was specified as 54 for the x, y and z directions. The order of the ß-spline interpolation was 6. The spline algorithm was used for calculating the complimentary error function, erfc(x). Atom electrostatics were employed which means that interactions were computed on an atom-atom pair basis. The radial energy functional form was chosen as that of the constant dielectric where the electrostatic energy is proportional to 1/R. The distance at which the switching function takes effect is 10 Å. The shifting function which smoothly reduces the energy to zero takes effect in the 11 Å to 12 Å interval. The distance cutoff involved in generating the list of atom pairs was therefore 12 Å. The distance specified function acts per atoms and not per group which improves the accuracy of the interaction calculations. The dielectric constant used in the extended electrostatic algorithm was equal to 1 (vacuum), which is of course standard when explicit solvent models are used. The exclusion list, which prevents certain energy terms from being included in the energy calculations, was specified as 1 and 2 bond interactions. Therefore, both vd Waals and electrostatic interactions between a bonded atom pair or an atom pair separated by 2 bonds were excluded from the calculation of the energy and the forces. No scaling factor was applied to electrostatic interactions involving atom pairs separated by 3 bonds.

Post Processing Implementation:

The Thermodynamic Integration (TI) method [3-6] was used to calculate the relative free energies and relative temperature derivative properties. The ensemble averages as a function of λ was used to fit a cubic spline polynomial function. This function was then analytically integrated over the limits specified by the upper and lower λ values.

5.1.3 Free Energy Differences of Solvation Results

Fig 5.1 shows the integrated $\Delta\Delta G_{solvation}$ values for every consecutive λ point along the pathway which describes the conversion from the pure $[PdCl_4]^{2-}$ complex (when λ is equal to 0) to the pure $[PtCl_4]^{2-}$ complex (when λ is equal to 1). This conversion happens via a hybrid complex which is non-physical. Extrapolation to the end points (λ = 0 and λ = 1) provides the values for calculating $\Delta\Delta G_{solvation}$. The hybrid Hamiltonian in this implementation was defined as:

$$H(\lambda) = V(environment) + (1-\lambda)V([PdCl_4]^{2-}) + (\lambda)V([PtCl_4]^{2-})$$

Note that this technique does not calculate the actual values of the individual free energies of solvation separately ($\Delta G_{solvation}([PdCl_4]^{2-})$ and $\Delta G_{solvation}([PtCl_4]^{2-})$. Only the difference between these two free energy values is determined. The method accomplishes this by exploiting the fact that free energy is a state function. This means that the free energy difference between any two physical states (such as a solvated $[PdCl_4]^{2-}$ and a solvated $[PtCl_4]^{2-}$ complex) can be determined by integrating over any pathway which converts one state into the other. These conversion pathways can be non-physical (not physically or chemically possible) and therefore the most convenient pathway (in terms of computational processing) can be chosen.

As can be seen from fig. 5.1, the $[PtCl_4]^{2-}$ complex forms a more thermodynamically stable solvated system than that of the solvated $[PdCl_4]^{2-}$ complex. Therefore, the process of transferring the $[PtCl_4]^{2-}$ complex from vacuum to a water solution is more thermodynamically favorable than the process of transferring the $[PdCl_4]^{2-}$ complex from vacuum to water.

$$\Delta\Delta G = \Delta G([PtCl_4]^{2-}) - \Delta G([PdCl_4]^{2-}) = -12.27 kcal/mol$$

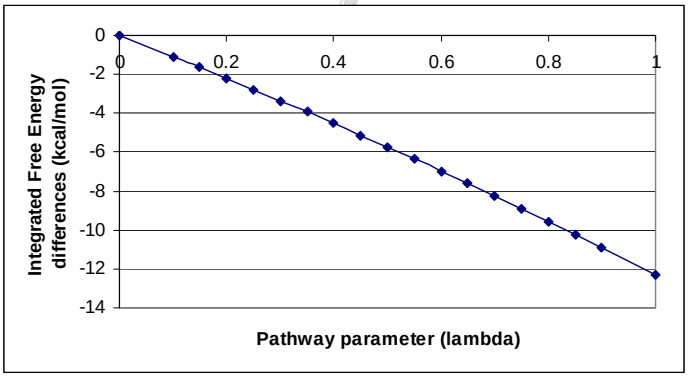

Fig. 5.1: This graph shows the progression along the λ pathway of the integrated ΔΔG values as calculated from the Hamiltonian defined as: $H(\lambda) = V_0 + (1 - \lambda)V([PdCl_4]^{2-}) + \lambda V([PtCl_4]^{2-})$.

From these results we conclude that the $[PtCl_4]^{2-}$ complex is significantly more solvated than the $[PdCl_4]^{2-}$ complex. In chapter 4 the relative hydration shell volumes were estimated from the integrated radial distribution functions. At 20% greater than bulk probability the estimated volume of the $[PtCl_4]^{2-}$ complex is 19% greater than that of the $[PdCl_4]^{2-}$ complex. Figure 5.2 is a reproduction of the radial distribution functions presented in chapter 4, with the relevant distributions highlighted for clarification. From this it is clear that the complex which has the greater thermodynamic stability also has the greater solvation shell volume. This correlation is consistent with what is expected. The enthalpic energy gain due to electrostatic interactions and hydrogen bonding is more substantial in the case of the $[PtCl_4]^{2-}$ complex. The SDF studies that were performed and described earlier (see Chapter 4.2.2) are therefore qualitatively consistent with these perturbation results. By investigating Figure 4.16 (b) and (d) it is clear that at 50% greater than bulk probability the $[PtCl_4]^{2-}$ complex has a bulkier solvation shell than that of $[PdCl_4]^{2-}$. For the sake of convenience these pictures are printed below (fig. 5.3 (a) and (b)).

There are also qualitative consistencies when one considers the diffusion coefficients calculated for these two complexes. These results will be presented in chapter 6. The diffusion coefficient of the $[PtCl_4]^{2-}$ complex is less than the value calculated for the $[PdCl_4]^{2-}$ complex. Based on the information obtained in this section, such a trend has merit. The diffusion rate of the highly solvated complex is

retarded because it has to drag its hydration shell with it to some extent. However, when the error margins of the diffusion coefficients are considered this correlation is questionable.

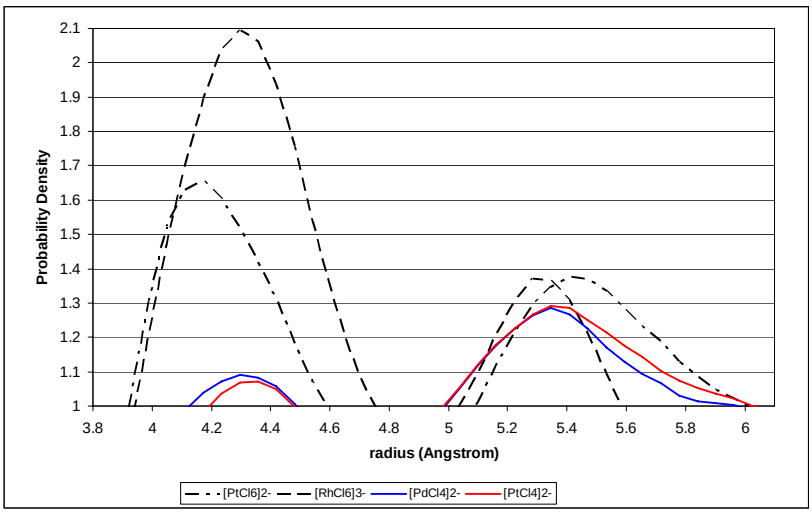

Fig 5.2: The pair distribution functions, g(r), for the metal···O(water) configuration in the following complexes ($[PtCl_6]^{2-}$, $[RhCl_6]^{3-}$, $[PdCl_4]^{2-}$ and $[PtCl_4]^{2-}$).

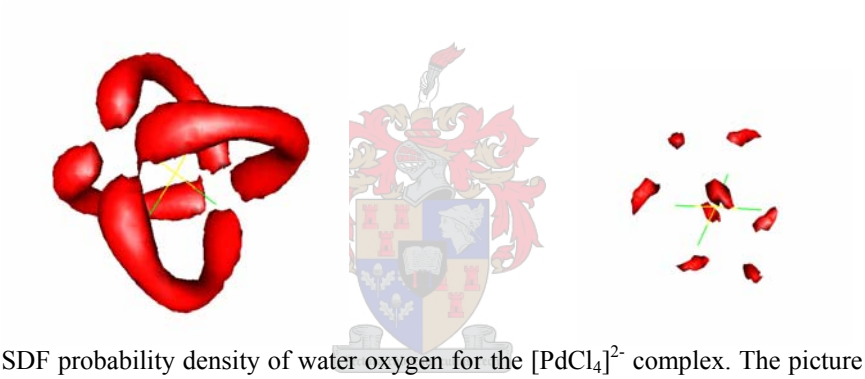

Fig. 5.3 (a) SDF probability density of water oxygen for the $[PdCl_4]^{2-}$ complex. The picture on the left is at 50% greater that bulk probability, while the picture on the right is at 100% greater than bulk probability.

Fig. 5.3 (b) SDF probability density of water oxygen for the $[PtCl_4]^{2-}$ complex. The picture on the left is at 50% greater that bulk probability, while the picture on the right is at 100% greater than bulk probability.

5.1.4 Component Analysis of Free Energy Differences

In order to investigate the dominant thermodynamic factor contributing to this result a component analysis ($\Delta\Delta G = \Delta\Delta H - T\Delta\Delta S$) was performed as part of the thermodynamic perturbation calculation. From fig. 5.4 it is clear that the differences in the enthalpic contribution to the respective solvation processes is dominant in the relevant free energy difference values. The TΔΔS values are almost

negligible in its contribution to the ΔΔG value per λ. This process, which is the chemical perturbation of the solvated reactant ($[PdCl_4]^{2-}$) to the solvated product ($[PtCl_4]^{2-}$), is governed by the enthalpic differences between $[PdCl_4]^{2-}$ and $[PtCl_4]^{2-}$ and not by the respective entropic differences. As stated in section 5.1.3, the enthalpic energy gain due to electrostatic interactions and hydrogen bonding is more substantial in the case of the $[PtCl_4]^{2-}$ complex. In terms of entropy, there is a minor difference in the relative ordering between the two solvated metal complex ions. The solvation shell of $[PtCl_4]^{2-}$ is more ordered than the solvation shell of $[PdCl_4]^{2-}$. The ΔΔH value contributes to a more solvated system in $[PtCl_4]^{2-}$, whereas the TΔΔS values has the opposing influence (to a much smaller extent) on the degree of solvation. This result is consistent with the geometric analysis of the hydration shells as performed in chapter 4 (see section 5.1.3).

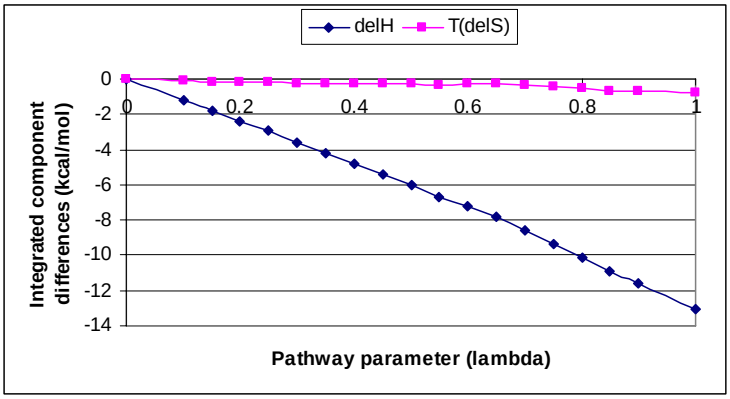

Fig. 5.4 This graph shows the progression along the λ pathway of the integrated ΔΔH and the integrated TΔΔS values.

5.2 Poisson-Boltzmann (PB) Results

The Poisson-Boltzmann (PB) continuum method [7-14] was used to calculate the free energy of solvation values for PGM chloro complexes in water. In this continuum model substances are treated as structureless, homogeneous dielectric media, which can be polarized by electric charges. Therefore, rather than explicitly representing each molecule in the solvent, a dielectric constant is used which is a parameter measuring the bulk polarizability of the media. The numerical solution of the Poisson-Boltzmann equation will incorporate both the effect of varying dielectric media as well as the impact of the ionic strength in solution. The output upon solving the Poisson-Boltzmann equation is the spatial distribution of the electrostatic potential, ø(r) (in units of kTe^{-1}). The solution of the Poisson-Boltzmann equation can be used to calculate the electrostatic contribution to the free energy of solvation. The applicability of the PB method is briefly discussed in contrast with that of explicit perturbation methods. Practicalities concerning the finite difference solution to the PB equation are discussed in detail. The $\Delta\Delta G_{solvation}$ results obtained from the Thermodynamic Integration method (section 5.1) are compared and contrasted with those results obtained from the PB calculations.

5.2.1 Validating the Poisson-Boltzmann Results

There are several reasons why a continuum method is effective in calculating properties for the systems involving PGM chloro-complexes. Due to the size and complexity of the systems it is convenient to use this fast and versatile method. Long range interactions are particularly prominent in ionic systems and these electrostatic effects are dealt with very effectively by the PB method. In the case of the PGM complexes in pure water (no polymer chains present) there are very little conformational change occurring. Also, due to the symmetry of these complexes its surface accessible area stays constant through time. The PB equation was solved for snapshot configurations of these systems. We can however, for the reasons stated above, feel reasonably confident that the results obtained are representative of those over time. To verify this, the ranges of the calculated free energy values were obtained by solving the PB equation for the minimum, maximum and average configurations (as extracted throughout a 1 nanosecond MD trajectory).

The $\Delta\Delta G_{solvation}([PtCl_4]^{2-} - [PdCl_4]^{2-})$ value, calculated in 5.1 (using the thermodynamic integration method), was compared with that obtained by using the PB method (see table 5.1). The values are relatively close provided one uses the average configuration coordinates to generate the PB values. Therefore, both an explicit and continuum method was used independently to calculate this property. The result obtained from the PB method has therefore been confirmed. The reliability of this comparison can be improved by calculating the PB free energy values over a representative sample of the system trajectories and thereby obtaining a reliable confidence interval. It is not really appropriate to use the lower and upper range limits of the free energy values (as calculated in section 5.2.3) to do similar comparisons, as these values could be outliers. Due to limited computational resources it was unrealistic to attempt PB calculations over the entire equilibrated trajectory. Future work would involve automating and optimizing such a process.

Method:	**Water Model:**	$\Delta\Delta G_{solv}\left([PtCl_4]^{2-} - [PdCl_4]^{2-}\right)$
Thermodynamic Integration	Explicit	-12.3 kcal/mol
Poisson-Boltzmann method	Continuum	-11.3 kcal/mol

Table 5.1: The $\Delta\Delta G_{solvation}$ value calculated by using the thermodynamic integration method, compared with that obtained by using the PB method (The specifications of this and other calculations are presented in section 5.2.3).

5.2.2 Parameters and Procedure

5.2.2.1 In order to solve the PB equation the following parameters are needed:

(i) The partial charges on all the atoms in the solute molecules:
These charges were taken from the Topology file used in the molecular dynamics simulations. This ensures consistency with the electrostatic energies calculated by both the explicit and continuum methods.

(ii) The vd Waals radii of all the atoms in the solute molecules:
These values were taken from the Parameter file (non-bonded interaction parameters) used in the molecular dynamics simulations. Firstly, these values are used to determine the molecular surfaces and define grid point positions to resemble this area. A radius for the solvent probe molecule (1.4 Å for water) is used to define the solvent excluded surface. From this it calculates the solvent accessible surface area and similarly assigns grid point positions onto this surface. Grid resolution, expressed in number of grids per Angstrom, has to be high enough so as not to produce surface artifacts. The process of obtaining an appropriate grid size and scale will be described in (5.2.2.3). As discussed in the theoretical chapter (Chapter 3), the solvent accessible surface positions are used when calculating the reaction field energy of the solute molecule. The value of the surface area can also be used to estimate the entropic energy penalty associated with solvent rearrangement on solute insertion. This, however, is a very primitive method of estimating the entropic contribution to the free energy of solvation. As was seen in section 5.2.4, the differences in the enthalpic contribution to the solvation processes are dominant when comparing relative free energy values. The $T\Delta\Delta S$ values are almost negligible in its contribution to the $\Delta\Delta G$ values and entropic estimations are therefore ignored.

(iii) The x, y, z coordinates of all the atoms in the solute molecules:
These coordinates (in standard pdb file format) represents the snapshot configurations that will be used when solving the PB equation. The partial charges mentioned in (i) are placed (according to atom type) onto these three dimensional coordinate positions. The minimum and maximum energy (total internal energy) configurations were extracted from a 1 nanosecond equilibrated MD trajectory. These trajectories were those generated to determine structural properties, as described in Chapter 4. CHARMM was used to obtain these coordinates as well as the average structures as sampled over 1 nanosecond.

(iv) The dielectric constants of all the species in the system:

The PGM chloro-complexes are very symmetrical and therefore no re-orientation of fixed dipoles exists. For these anions only electronic polarizability are assumed (ie. $\varepsilon = 2$). The same applies to the

sodium cations. The PEO strands can undergo both electronic and dipolar polarization. The reorientation of the molecular dipoles is however explicitly represented. Therefore only the electronic polarizability is accounted for by the dielectric constant. The table below shows the values of the dielectric constants of all the relevant species used in the PB calculations.

Species:	Dielectric Constant:
Solvent (water)	80
Solute (PGM complex)	2
Solute (Counter ions: Na's)	2
Solute (PEO)	2

(v) The ionic strength of the solution:
In order to investigate the effect of ionic strength on the free energy of solvation the PB equation has to be solved twice with the following specifications: (a) Solving the linear PB equation with ionic strength of I = 0.0 mol/liter. (b) Solving the non-linear PB equation with ionic strength of I = x mol/liter. The lattice points which are inaccessible to these solvent ions are determined in a similar way to that of the solvent excluded surface. To achieve this, the parameter IONRAD is defined which plays the same role as PRBRAD (see (ii)). A value of IONRAD = 2.0 Å was used. This is the suggested value for sodium chloride.

5.2.2.2 The Focusing Procedure

The points at the boundary of the grid present a problem, because these grid points have no outside neighbors. The accuracy of the entire electrostatic potential map is therefore influenced by these boundary effects. The focusing procedure is an attempt to deal with this problem. In general the procedure works as follows: An initial calculation is done with the molecule very far from the grid boundary and occupying a small percentage of the entire grid volume. This calculation results in a very coarse electrostatic potential map. A number of focusing calculations follow this initial step. With each consecutive step the molecule occupies a larger percentage of the grid volume. This is done in such a way that the new grid is internal points of the previous, coarser grid. The potential values from the coarse grid acts as estimates of the boundary values of the focused grid.

The focusing procedure was implemented as follows: (Note that the values used below were determined after the three resolution tests (see 5.2.2.3) were performed.) An initial calculation was done with grid size of 155 and a scaling factor of 0.25. This means the 0.25 grid points fit into 1 Å on the lattice. Therefore the size of 1 grid point is 4 Å by 4 Å by 4 Å. The first focusing step was done with a grid size of 155 and a scaling factor of 0.5. This step increases the resolution of the grid by a factor of 2 in each dimension. The last two focusing steps follow the same pattern as the fist two. Step 3 has grid size 155 and scale 1.0 and finally step 4 has grid size 155 and scale 2.0. This means that the final resolution is at two grid points per Angstrom. These grid sizes and scaling factors were designed so that the final box size would be 50 % bigger than the box size used in the MD calculations. This was done to ensure that both the PGM complex and the counter ions never find themselves too close to the grid boundary.

5.2.2.3 Procedure to determine the right grid resolution

Three tests were performed to ensure that the final grid resolution was fine enough and resolution errors were insignificant. The first test was similar to a focusing procedure where the energy values of each consecutive focusing step were compared. When no significant improvement in accuracy was observed between steps, the final step was seen as redundant. The second test involved centering and rotating the solute molecules slightly differently in the grid box. The size of the lattice resolution errors can be accessed in this manner. The third test, although only a qualitative indication, can be quite useful. This test involves viewing the contour maps of the electrostatic potentials. A qualitative confirmation that no resolution artifacts occurred can be made. This test is also very valuable to check that the boundary conditions were dealt with effectively. Fig 5.2 (a) and (b) are examples of electrostatic potential contour maps.

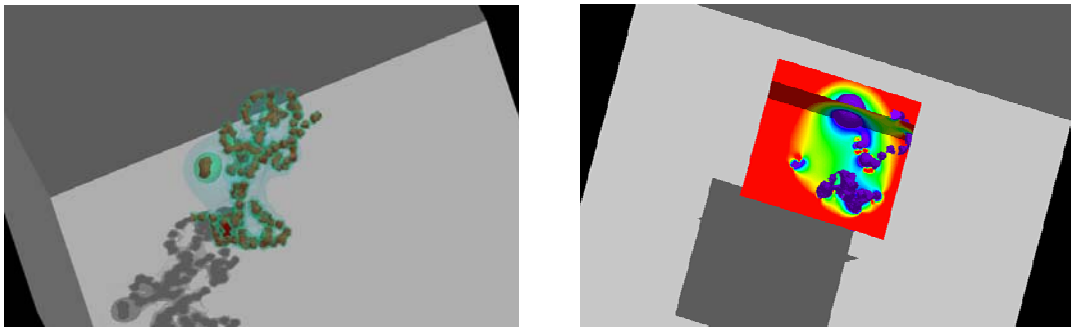

a b

Fig 5.2: These figures are examples of electrostatic potential maps calculated for the $[PdCl_4]^{2-}$ in the presence of a polymer (PEO).

5.2.2.4 Linear vs. non-linear Poisson Boltzmann

The zero ionic strength systems were all solved with the linear Poisson Boltzmann equation. All systems where the ionic strength was greater than zero were solved with the non-linear Poisson Boltzmann equation. (Future work will involve the effect of different ionic strengths on the solvation free energies of the PGM complexes).

5.2.3 PGM Chloro-complexes in Pure Solvent (water)

5.2.3.1 Free Energy of Solvation (The Electrostatic (ES) Contribution)

(A) Comparing two methods of calculation

The free energy of solvation of a molecule is understood as the transfer of the molecule from vacuum to water. Both the Grid Energy Method (less accurate) and the Reaction Field Method was used to calculate the electrostatic contribution to the free energy of solvation. The theory and relative merits behind these two methods were discussed in chapter 3, section 3.3.2.4 (c) and (d). The theoretical discussion was done in the context of the finite difference approximation method. These calculations were performed at zero ionic strength and using the average structures of the respective systems. The other parameters and procedures were as described in 5.2.2.1. As can be seen from Table 5.2, these two methods deliver very similar results, although the Grid Energy Method results are consistently higher. Based on this we feel confident that the results from the Reaction Field Method can be trusted.

Salt=0.0M			
Average conformations			
	Grid Energy Method: (kcal/mol)	Reaction Field Method: (kcal/mol)	Error Margin
$[PtCl_4]^{2-}$	-330.12	-332.86	-0.8%
$[PdCl_4]^{2-}$	-315.99	-321.55	-1.7%
$[PtCl_6]^{2-}$	-337.14	-340.14	-0.9%
$[RhCl_6]^{3-}$	-669.35	-680.81	-1.7%

Table 5.2: Summary of the free energy of solvation (ES) results performed by two different methods.

(B) Free Energy of Solvation (ES) at zero Ionic strength

The Reaction Field Method was used to calculate the free energy of solvation for all four PGM complexes at zero ionic strength. Of these PGM complexes the minimum, average and maximum energy structures were used as coordinate input. The main structural reason for these energy differences is the relative distances of the counter ions (sodium) from the PGM anion. As observed in Charter 4.2.1, the counter ions very rarely get close enough to the PGM complex for it to radically

affect the energy. Due to the lack of salt, the linear PB equation was solved in each case. A maximum number of 800 iterations were allowed in order to achieve conversion. The parameters and focusing procedure were similar to that described in 5.2.2. The PB converged successfully in all cases. Table 5.3 is a summary of the results obtained.

Salt=0.0 mol/litre		
Minimum conformations		
	kT	kcal/mol
$[PtCl_4]^{2-}$	-573.03	-339.24
$[PdCl_4]^{2-}$	-557.68	-330.15
$[PtCl_6]^{2-}$	-596.84	-353.33
$[RhCl_6]^{3-}$	-1170.30	-692.82
Average conformations		
	kT	kcal/mol
$[PtCl_4]^{2-}$	-562.27	-332.86
$[PdCl_4]^{2-}$	-543.16	-321.55
$[PtCl_6]^{2-}$	-574.57	-340.14
$[RhCl_6]^{3-}$	-1150.01	-680.81
Maximum conformations		
	kT	kcal/mol
$[PtCl_4]^{2-}$	-551.1	-326.2
$[PdCl_4]^{2-}$	-532.6	-315.3
$[PtCl_6]^{2-}$	-561.5	-332.4
$[RhCl_6]^{3-}$	-1133.1	-670.8

Table 5.3 Free energies of solvation at I = 0.0 mol/liter. The minimum, average and maximum energy structures were used as coordinate input.

From Table 5.3 the following observations can be made regarding the validation of the PB method:

(i) The free energies of the minimum conformations are consistently lower than that of the average conformations. Similarly the free energies of the maximum conformations are consistently higher than that of the average conformations. Remember that these snapshot structures were extracted from the respective MD trajectories based on their Total Internal Energy values. From the consistencies above we can therefore conclude that the electrostatic effects in these systems govern the overall differences we observe. There is a clear qualitative correlation between the MD and the PB energies. From all this it is clear that the degree of solvation of the system is directly related to the total energy of the system and visa versa. From these values a range of the possible free energies can be determined. These results are presented and summarized in table 5.4 as well as figure 5.5. Notice that these ± limits represents only a small percentage variation from the average (1-3%).

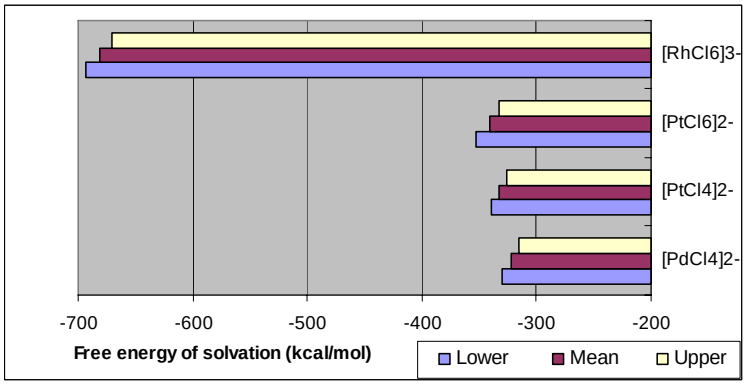

Fig 5.5: A graphic presentation of the electrostatic component of the free energy of solvation values of all the relevant PGM complexes. The lower and upper range values are also included.

	Lower	Mean	Upper
$[PdCl_4]^{2-}$	-330.2	-321.6	-315.4
$[PtCl_4]^{2-}$	-339.3	-332.9	-326.3
$[PtCl_6]^{2-}$	-353.3	-340.1	-332.4
$[RhCl_6]^{3-}$	-692.8	-680.8	-670.8

Table 5.4: The range of the free energy of solvation values for the PGM chloro-complexes.

(ii) The difference in the solvation free energies of $[PdCl_4]^{2-}$ and $[PtCl_4]^{2-}$ were calculated before using the Thermodynamic Integration method. As mentioned in 5.2.1, this $\Delta\Delta G = -12.27 kcal/mol$ value compares very well with that calculated using the PB method.

$$\Delta\Delta G_{PB}([PtCl_4]^{2-} - [PdCl_4]^{2-}) = -332.86 - (-321.55) = -11.31 kcal/mol$$

(iii) Although the PB method is used more often to obtain values that give a qualitative indication as to the relative degree of solvation, it also produces quantitative ΔG results. Note that these calculated ΔG values were produced by solving the linear PB equation for the anion system alone (no counter ions present). This was necessary because the calculated free energy of solvation values would otherwise have included the free energy of solvation of the counter-ions (Na^+) as well.

5.2.4 Comparing Calculated and Experimental Results

Free energy experimental data related to solvation is normally reported in terms of "solvent medium effects", which is a measure of the total solvation energy of a solute when it is transferred from one solvent (S1) to another (S2) [15]. These values rely on the relative stabilities of the solute in the two solvents. There is a direct relation between the "medium effects" and the standard Gibbs energy of transfer, $\Delta_t G^o$(solute,S1→S2). These transfer results are considered under conditions of infinite dilution of the solute in both solvents, in order to eliminate solute-solute interaction effects. The "medium effect" is therefore a measure of the difference in the total (standard) solvation energy of a solute in two solvents. However, in cases where the solute specie is an electrolyte, unique problems present themselves. In solution an electrolyte dissociates into its ions. The Gibbs energy of transfer relates to the whole salt, and is therefore connected to the standard solubility product, K_{sp}^o, of the electrolyte in the two solvents (see equation below).

$$\Delta_t G^\circ(M_{v+}A_{v-}, S1 \rightarrow S2) = 2.303RT \log\left[\frac{K_{sp}^\circ(S1)}{K_{sp}^\circ(S2)}\right]$$

This equation shows that $\Delta_t G^\circ(M_{v+}A_{v-}, S1 \rightarrow S2)$ is a determinable quantity (by measuring the ratio between the two solubility products). These measurements are done by using the techniques of chemical thermodynamic, the description [16] of which is beyond the scope of this section. The experimental determination of the Gibbs energies of transfer can therefore only be determined for molecular solutes, electrolytes and electroneutral combinations of ions. Since conditions of infinite dilution of the electrolytes exit, there is additivity to the individual ionic contributions. If the value of one ion is fixed, the values of all the other ions can be obtained from appropriate thermodynamic cycles. However, the Gibbs energies of transfer of single ions can only be determined by making "extrathermodynamic" assumptions [15]. These are assumptions which are outside the realm of thermodynamics. The role of these assumptions is to split the measurable property of the electrolyte into its (nonmeasurable) ionic contributions. Almost all these assumptions for estimating $\Delta_t G$(ion) are based on insights derived from the Born equation. The Born equation suggests that ions of low charge-to-radius ratios have low solvation energies. The "extrathermodynamic" assumption used which is most reliable is called the Reference Electrolyte Assumption. This approach assumes that the Gibbs energy of transfer (measurable) of a suitable electrolyte can be split between its cation and anion. A suitable electrolyte for this purpose has cations and anions with low charge/radius ratios and a "buried" charge which are as chemically similar as possible. The salt which is used most often for this purpose is that of tetraphenylarsonium tetraphenylborate (Ph_4AsBPh_4, TATB [15]).

When the $\Delta_t G$(ion) values of multivalent ions are estimated, there are several obstacles however. This is partly due to ion pairing which can affect the $\Delta_t G$ values for salts containing multiply charged ions.

Determination of the $\Delta_t G$(ion) values for these ions show great variation and sometimes produce patterns which are contradictory. The table below presents the Standard Molar Gibbs energy values of transfer from water to methanol at 298.15 K for certain cations. Note that these values are all positive, which means that the more favorable solvation process is that of the water medium.

Ion:	$\Delta_t G$(ion,water→methanol) kJ/mol (molarily scale) [15]	Assumption Method: [15]
Li^+	3.0	TATB
Na^+	7.0	TATB
K^+	8.4	TATB
Cs^+	9.7	TATB
Rb^+	11.3	TATB
Mg^{2+}	2.0	TATB
Ca^{2+}	11.2	TATB
Sr^{2+}	7.1	TATB
Ba^{2+}	17.2	TATB
Cd^{2+}	31.4	TATB
Pb^{2+}	10.3	TATB

The $\Delta_t G$(ion,water→methanol) values for the alkali metals (Li^+, Na^+, K^+ etc) follows the pattern as expected, based on the Born principle. The effect of the ionic radius is therefore very prominent for the interactions of these hard ions with hard solvents. The free energy values for these ions are increasingly positive, and this happens parallel to the increase in the ionic radii. The $\Delta_t G$(ion,water→methanol) values for doubly charged metals (Mg^{2+}, Sr^{2+}, Ca^{2+} etc) do not however follows the pattern as expected, based on the Born principle. In this series the Sr^{2+} ion is anomalous and not easily explained. As with the other cations, the $\Delta_t G$(ion,water→methanol) values for the Pb^{2+} and Cd^{2+} ions are both positive, which means that both ions are more soluble in water than in methanol, and would therefore resist the transfer process. If the Born pattern applied (relation of $\Delta_t G$ results to charge density) we would have expected that $\Delta_t G(Pb^{2+}$,water→methanol) > $\Delta_t G(Cd^{2+}$,water→methanol). From the experimental results in the table above, it is clear that this is not the case. This implies that electrostatic interactions are not the only important factor to be considered when estimations these free energy values. Future work is needed to establish the exact mechanism of transfer. Computational studies might assist us in this quest.

Table 5.5 lists the calculated and the experimental free energy of solvation results. The experimental results available in the literature were not generated under comparable experimental conditions to those used in the computer simulations of the same systems. The only experimental results found which match the same conditions (species, solvent, temperature etc.) is that of the $[PtCl_6]^{2-}$ and $[PdCl_4]^{2-}$ complexes. The experimental technique in both cases calculated the standard molar Gibbs energy of hydration (using the TATB assumption [15]) and listed the uncertainty as 9% and 18% respectively. The fact that all these ions are multiply charged means that the experimental result could have been affected by ion pairing. This could possibly account for the inconsistencies with the computational results.

Free Energies of Solvation (kcal/mol)		
Calculated vs. Experimental		
	Calculated (PB)	Experimental
$[PtCl_4]^{2-}$	-332.9	Not available
$[PdCl_4]^{2-}$	-321.6	-175.3 [16]
$[PtCl_6]^{2-}$	-340.1	-163.7 [16, 17]
$[RhCl_6]^{3-}$	-680.8	Not available

Table 5.5 Free energies of solvation (calculated vs. experimental values). Both calculated and experimental values represent the free energies of solvation of the PGM anion alone.

(C) Discussion of the relative values of the Free Energy of Solvation (ES) of the four PGM complexes.

The free energy of solvation results can partially be explained by correlating them with the structural properties of these PGM complexes obtained from the Molecular Dynamics studies performed in chapter 4. During this discussion we assume that the differences between the entropic contributions to the free energies of solvation of the relevant PGM chloro-complexes are insignificant compared to the differences due to enthalpic contributions. As would be expected, due to its -3 charge, the $[RhCl_6]^{3-}$ complex is most solvated (has the lowest solvation free energy). The other three complexes all have a charge of -2. The Born model (chapter 3, section 3.3.2.1) presents the clear correlation between the free energy of solvation (electrostatic component) of an ion (assumed to be spherical) and the charge of the ion. The $[PtCl_6]^{2-}$ complex is second most solvated (has the second lowest solvation free energy). These two octahedral complexes ($[PtCl_6]^{2-}$ and $[RhCl_6]^{3-}$) both have two solvation shells each, which was confirmed by the radial distribution studies discussed in chapter 4 (see fig 5.6). This phenomenon indicates the high solvent density around these complexes, which implies a strong affinity for the solvent molecules (water) in the form of hydrogen bonds and electrostatic interactions. Based on this structural data it is expected that the enthalpic contribution to the free energy of solvation of these two complexes should be higher than that of the two square planar complexes. The high symmetry of these systems (O_h) also enhances the formation of the cages of water molecules around the PGM chloro-complexes. These structured cages optimize the number of hydrogen bonds with the PGM chloro-anion. In the case of the square planar complexes (a lower degree of symmetry) it is not possible for the water molecules to structure themselves as effectively, and the number of hydrogen bonds is less. This means that the enthalpic contributions to the free energy of solvation of the square planar complexes are less than that of the two octahedral complexes. The square planar $[PtCl_4]^{2-}$ complex is the third best solvated, with $[PdCl_4]^{2-}$ the least solvated. It was observed that the relative density of the solvation shells of the $[PtCl_4]^{2-}$ complex is slightly higher than that of the $[PdCl_4]^{2-}$ complex. As explained above, this implies a greater enthalpic contribution to the free energy of solvation. The SDF studies (see chapter 4) also provide visual confirmation of the solvation shells and the probabilities of locating the solvent molecules around the complexes.

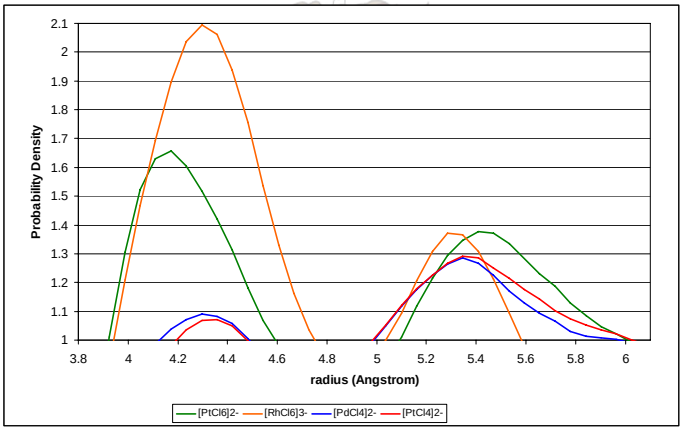

Fig 5.6: The radial distribution functions provide us with actual Metal…Oxygen inter-atomic distances. From this the relative density of the solvation shells can be determined.

By comparing the quantitative order of the free energy of solvation results with the order of the relative volumes of the solvation shells, as calculated in chapter 4, we observe a strong consistency. As mentioned in section 5.2.3, the relatively narrow range the values of the free energies of solvation of these PGM complexes ($[PtCl_6]^{2-}$; $[RhCl_6]^{3-}$; $[PdCl_4]^{2-}$ and $[PtCl_4]^{2-}$) enables us to make conclusive comparisons. There is consistency with the theory that the extent of the volume of the solvation shells corresponds to the degree of the free energy of solvation. As the hydration shell volumes increase, the values of the free energies of solvation increase. These hydration shell volumes were calculated and discussed in chapter 4. Figure 5.7 presents these solvation sphere volume results. A full explanation of the procedural details as well as a thorough discussion of these results can be found in chapter 4, section 4.2.

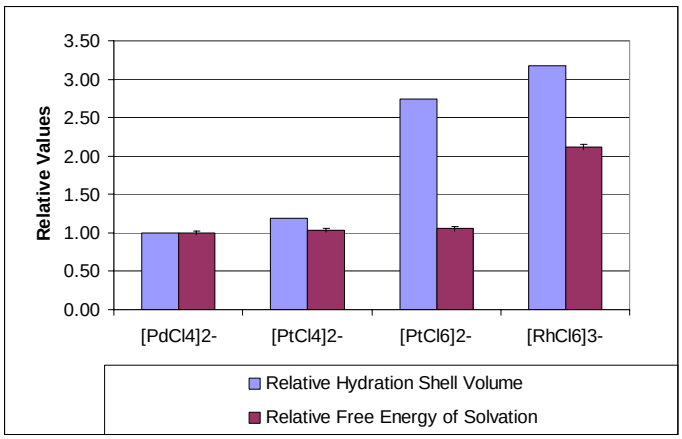

Fig 5.7: A graphic presentation of the relative values of the physical and thermodynamic properties of the respective PGM complexes and how they relate to each other. (1) The electrostatic component of the free energy of solvation values. (2) The hydration shell volumes.

References:

1. C.L. Brooks III and D.J. Tobias, *Thermodynamics and mechanism of alpha helix initiation in alanine and valine.* Biochemistry, 1991. **30**: p. 6059-6070.
2. B.R. Brooks, D. Janezic, M. Karplus and R.M. Venable, *CHARMM:A program for macromolecular energy,minimization,and dynamics calculations.* J. Comput. Chem., 1983. **4(2)**: p. 187-217.
3. M. Mezei, *The finite difference thermodynamic integration, tested on calculating the hydration free energy difference between acetone and dimethylamine in water.* J. Chem. Phys., 1987. **86**: p. 7084-7088.
4. D.A. Pearlman and P.A. Kollman, *Free energy perturbation calculations:problems and pitfalls along.* J.Chem.Phys., 1994. **94**: p. 101-118.
5. H. Schäfer, W.F. van Gunsteren, and A.E. Mark, *Estimating Relative Free Energies from a Single Ensemble: Hydration Free Energies.* J. Comput. Chem, 1999. **20**(15): p. 1604]1617.
6. U.C. Singh, F.K. Brown, P.A. Bash and P.A. Kollman, *An approach to the application of free energy perturbation methods using molecular dynamics.* J.Am.Chem.Soc, 1987. **109(6)**: p. 1607-1614.
7. M.E. Davis and J.A. McCammon, *Solving the finite difference linearized Poisson-Boltzmann equation:A comparison of relaxation and conjugate gradient methods.* J.Comput.Chem., 1989. **10**(3): p. 386-391.
8. M.J. Holst and F. Saied, *Numerical solution of the nonlinear Poisson-Boltzmann equation:developing more robust and efficient methods.* J.Comput.Chem., 1995. **16**(3): p. 337-364.
9. J. Mouesca, J.L. Chen and D.A. Case, *Density functional/Poisson-Boltzmann calculations of redox potentials for ion-sulfur clusters.* J.Am.Chem.Soc., 1994. **116**: p. 11898-11914.
10. A. Nicholls and B. Honig , *A rapid finite difference algorithm, utilizing successive over-relaxation to solve the Poisson-Boltzmann equation.* J. Comput. Chem., 1991. **12**(4): p. 435-445.
11. K. Sharp and B. Honig, *Calculating total electrostatic energies with the nonlinear Poisson-Boltzmann equation.* J.Phys.Chem., 1990. **94**: p. 7684-7692.
12. K. Sharp, *Inorporating solvent and ion screening into molecular dynamics using the finite-difference Poisson-Boltzmann method.* J.Comput.Chem, 1991. **12**(4): p. 454-468.
13. J. Shen and A. Quiocho, *Calculation of binding energy differences for receptor-ligand systems using the Poisson-Boltzmann method.* J.Comput.Chem., 1995. **16**(4): p. 445-448.
14. T. Simonson, G. Archontis, and M. Karplus, *Free Energy Simulations Come of Age: Protein-Ligand Recognition.* Acc. Chem. Res., 2002. **35**: p. 430-437.

15. D. Kalidas and Y. Marcus, *Gibbs Energies of Transfer of Cations from Water to Mixed Aqueous Organic Solvents.* Chem. Rev., 2000. **100**(3): p. 820-830.
16. Y. Marcus and G. Hefter, *Enthalpies and Entropies of Transfer of Electrolytes and ions from Water to Mixed Aqueous Organic Solvents.* Chem. Rev., 2002. **102**(8): p. 2773-2836.
17. A. Bianchi, K. Bowman-James, and E. Garcia-Espana, *Supramolecular Chemistry of Anions*. 1997, New York: Wiley-VCH.

Chapter 6

PRELIMINARY DIFFUSION STUDIES

6.1 Introduction

The relative diffusion coefficients of PGM chloro-complexes in water and polymer media are of major importance when considering chromatographic and solvent extraction separation techniques. In chromatographic terms the resolution is dependent on the column efficiency (*N*), the selectivity efficiency (α) as well as the retention factors (k) [1, 2]. The column efficiency can be expressed by the HETP-value [1, 2]. The Height Equivalent to a Theoretical Plate (*H*) is a theoretical concept that indicates the length of a column segment in which a perfect equilibrium exists between a component in the mobile phase and the stationary phase. The HETP-value is a measure of the band broadening that takes place during the elution process. In order to achieve maximum column efficiency this value should be as small as possible. The HETP-value is dependant on the extent of the longitudinal diffusion, the resistance to mass transfer as well as the average linear velocity of the eluent. All these factors are either directly or indirectly related to the diffusion coefficient in the mobile phase and/or the diffusion coefficient in the stationary phase. The exact nature of these dependences is described elsewhere [1].

There are several experimental methods available to investigate the molecular motion in liquids. Relaxation time measurements in NMR and ESR can be used to interpret the mobility of molecules [3, 4]. This chapter describes the use of computational methods to simulate and analyze the diffusion processes, and thereby gain insight into the mechanisms involved. A brief theoretical overview is given in section 6.2. The influence of physical and thermodynamic properties on the diffusion coefficient is described in this section. Special attention is given to those properties which can be calculated computationally. Section 6.3 describes the correlations and trends which would occur based on this theory. The results from the computational analysis are reported and discussed in section 6.4.1 and 2. The two systems types which are investigated in this chapter are (1) the PGM chloro-complexes in water and polymer (PEO) solution, and (2) the PGM chloro-complexes in water solution. The chapter concludes with comments on the accuracy of the calculated diffusion coefficients as well as the legitimacy of the mechanistic speculations. Suggestions are made regarding possible future improvements to the computational method.

6.2 A Theoretical description of diffusion

6.2.1 The concepts used in a computational analysis of diffusion coefficients

Molecular dynamics is used to calculate the trajectories of all the particles under the influence of the intermolecular potentials. Newton's second law of motion is used to determine where each particle will be after a short time interval (0.001 ps). This time interval is chosen to be shorter than the average time between intermolecular collisions. For each time step the net force on the molecule (which arises from all the other molecules present in the system) is calculated. The theoretical details of how the MD trajectory data can be used to determine the diffusion coefficients were described in chapter 2. This section briefly highlights the relevant concepts needed to understand the discussion that follows.

The derivation of the Einstein equation, eq. (1), on which this analysis is based was fully discussed in chapter 2. This equation is significant because it directly connects the mean-square displacements to the diffusion coefficient [3, 5, 6]. This is valuable, as the mean-square displacements can easily be calculated from the trajectory data generated in the MD simulations.

$$< [x(t) - x(0)]^2 >= 2Dt \qquad (1)$$

The three-dimensional version of eq. (1) is: $< [r(t) - r(0)]^2 >= 6Dt$

Note that eq. (1) is a linear equation where the slope is 2D and the line cuts through the origin. A simple strategy to calculate the diffusion coefficient would therefore be to calculate the mean-square displacements for different time delays, and plotting the linear equation (least square fit) over these time delays. The slope of this line is then used to get the value for the diffusion coefficient. To prevent distortions resulting from atom-atom collisions, it is important that the time delays considered when calculating the slope must be as large as possible relative to average collision times.

6.2.2 The theory behind the effects of physical and thermodynamic properties on the diffusion of ions in a liquid

There are certain properties of the solvent molecules and the ion which affects the movement of the ion in the solution. This section describes these concepts. The relationships of these properties to the diffusion coefficient are discussed and possible weaknesses in the application of the theory are highlighted. It should be emphasized that the systems we investigated are at equilibrium. That implies that no concentration gradient or the presence of a net electric field exists which could bias the motion through the solution. We focus therefore on those factors which affects the random motion of the ion.

An ion moving through a solvent experiences a frictional retarding force, $F_{friction}$ [7, 8]. This force is directly proportional to the following: (1) the speed, s, of the ion, (2) the size of the ion (expressed as a radius, a, for the sake of simplicity), (3) the viscosity, η, of the solvent media.

$$F_{friction} = f.s \qquad where \qquad f = 6\pi.\eta.a$$

The Stokes-Einstein equation [8, 9], eq. (2), can be derived which expresses the diffusion coefficient in terms of these physical properties (the radius of the ion and the viscosity of the solvent media).

$$D = \frac{kT}{f} \qquad D = \frac{kT}{6\pi\eta a} \tag{2}$$

This equation provides us with a relationship between the diffusion coefficient, the viscosity coefficient and the radius of the ion. An important feature of eq. (2) is that it makes no reference to the charge of the diffusing species. Therefore, the equation also applies in the limit of very small charge or neutral molecules. It should be emphasized that the usefulness of this rule is limited by the role of solvation. Different solvents solvate the same ions to different extents, so both the hydrodynamic radius and the viscosity change with the solvent. This flaw can be corrected however by incorporating the solvation effects into the estimation of these properties. How this is accomplished will be discussed later in this section. The Stokes-Einstein equation is useful because it allows us to predict the diffusion coefficient based on the physical properties of the system, namely the (1) viscosity of the solvent and the (2) radius of the ions. What follows is a discussion of these two properties and how they can be estimated using computational techniques. As mentioned above, it is important that these estimations incorporate the solvation effects.

The radius refers to the hydrodynamic radius, which means it is the effective radius in the solution taking into account all the solvent molecules the ion carries in its solvation sphere. Small ions results in stronger electric fields than large ones. (The electric field at the surface of a sphere is proportional to ze/r^2). Therefore, small ions are more extensively solvated than big ions. Thus, an ion of small ionic radius may have a large hydrodynamic radius because it drags many solvent molecules through the solution as it migrates. The hydration H_2O molecules are very labile, however, and NMR and isotope studies have shown that the exchange between the coordination sphere of the ion and the bulk solvent is very rapid [7]. It should be noted that the hydrodynamic radius is reliant on characteristics of the solvent as well as characteristics of the solute. In chapter 4 the volume of the hydration shells were calculated and reported. The relative sizes of these shells were also discussed in terms of their ionic radii, their charges and the potential interference in the degree of solvation due to the presence of a polymer. From this we can estimate the values of the hydrodynamic radii for all the PGM chloro-complexes.

The following paragraphs illustrate the connection between the viscosity coefficient and the free energy of solvation. Once again it should be noted that the viscosity coefficient and the free energy of solvation are both concepts which are reliant on characteristics of the solvent as well as characteristics

of the solute. Different solvents solvate the same ions to different extents, so both the hydrodynamic radius and the viscosity change with the solvent. A solute molecule (in this case an ion) must acquire at least a minimum energy to be able to escape from its neighbors. Only then can the molecule move though the liquid. There are two physical extremes which need to be considered in this scenario. The first extreme is that the ion must rupture the hydrogen bonds within its immediate solvation sphere in order to facilitate motion. The other extreme is that the ion possesses a stable and structured solvation shell which has to be dragged along if the ion is transported. In this case the solvent molecules had to rearrange in such a way that the maximum enthalpic benefit is gained from the solvation process. This implies a disturbance in the local solvent structure surrounding the fully solvated ion. It should then be seen as though the solvated structure has to sever the hydrogen bonds (between the solvation shell and the bulk solvent surrounding the shell) as well as suffer the entropic penalty of further solvent rearrangement to allow transport. Only then can the ion with its solvation shell be transported in bulk solution. In reality the hydration H_2O molecules are very labile and the exchange of the solvent molecules making up the solvation shell and the bulk solvent is very rapid. As mentioned, this has been shown in NMR and isotope studies [7]. Suppose the minimum energy levels necessary which would allow the ion (first extreme) and the solvated ion (second extreme) to rupture these hydrogen bonds are $E_{a(ion)}$ and $E_{a(solvated\ ion)}$ respectively. The probability that a molecule obtains an energy level of E_a is proportional to $e^{-Ea/RT}$. The respective *mobilities* of the ion (first extreme) and the solvated ion (second extreme) can be described in terms of this probability [7, 8].

$$mobility_{ion} \propto e^{-E_{a(ion)}/RT}$$

$$mobility_{solvated\ ion} \propto e^{-E_{a(solvated\ ion)}/RT}$$

It is also true that the viscosity coefficient, η, is inversely proportional to the mobility of a particle.

$$mobility \propto \frac{1}{\eta}$$

This means that it is possible to write the viscosity coefficient as an expression of E_a.

$$\eta_{ion} \propto e^{E_{a(ion)}/RT} \quad (3)$$

$$\eta_{solvated\ ion} \propto e^{E_{a(solvated\ ion)}/RT} \quad (4)$$

From equation (3) and (4) it is clear that the viscosity coefficient decreases with increasing temperature. The activation energy needed to release a particle from its neighbors is dependent on the mean potential energy contributed by the intermolecular interactions. Therefore, the magnitude of E_a is governed by the intermolecular forces between the solute and the neighboring solvent molecules. It is very difficult to calculate these E_a values experimentally however, and that is where computational chemistry can play an important role. The free energy of solvation values can be calculated by using the Poisson-Boltzmann method. The enthalpic component of the free energy of solvation is a quantitative measure of the intermolecular (electrostatic) interactions involved in the hydration process. As was described in chapter 5, the enthalpic energy of solvation is the difference in the potential energy of the ion in solution and the potential energy of the ion in vacuum. The enthalpic component of the reverse process, namely the process of desolvation, can be seen as the energy needed to release the ion from its intermolecular interactions. From this it is clear that the E_a values are related to the enthalpic component of the desolvation process.

$$ion_{solution} \xrightarrow{\Delta G(desolvation)=\Delta H(desolvation)-T\Delta S(desolvation)} ion_{vacuum}$$

The free energy of solvation values of the PGM chloro-complexes was calculated, reported and discussed in chapter 5. From these values we can extract the enthalpic components to the desolvation processes. By substituting these values into equation (3) we can estimate the viscosity coefficient of the first extreme scenario as described above.

The following section attempts to make a connection between the principles discussed in section 6.2.2 and the trends observed in the computational calculation of these properties. In theory, the relative rates of diffusion of these complexes are expected to be dependant on the degree of solvation of these species [10-12] . It is reasonable to expect that the solvent molecules (water) within the solvation shell have a relatively high residence time in the vicinity of the solute molecule. If we assume that the extent

of the residence time is directly related to degree of solvation we can attempt to rationalize the diffusion rates in terms of the free energy of solvation.

6.3 A qualitative prediction of the order of the diffusion coefficients based on physical and thermodynamic properties

The electrostatic components of the *free energies of solvation* were calculated and discussed in Chapter 5. In this chapter we shall refer to these values qualitatively. As to the details of the calculation parameters and procedures we refer the reader to Chapter 5, Section 5.2. The diffusion rate of a highly solvated complex is retarded because it has to drag its hydration shell with it to some extent. The relative values of the free energy of solvation, as determined in Chapter 5, are as follows:

$$[PdCl_4]^{2-} < [PtCl_4]^{2-} < [PtCl_6]^{2-} < [RhCl_6]^{3-} \quad (5)$$

A qualitative approach to rationalize the diffusion rates is by correlating the diffusion coefficients with the estimated *hydration sphere volume* of the complexes as determined in Chapter 4. The relative volumes of the solvation shells, as determined in Chapter 4, are as follows:

$$[PdCl_4]^{2-} < [PtCl_4]^{2-} < [PtCl_6]^{2-} < [RhCl_6]^{3-} \quad (6)$$

Based on these two trends, (5 and 6), we would expect the relative order in the diffusion coefficients to have a qualitative order as indicated in trend 7. It should be emphasized that this conclusion is dependant on whether the assumptions made in this section are sound:

$$[PdCl_4]^{2-} > [PtCl_4]^{2-} > [PtCl_6]^{2-} > [RhCl_6]^{3-} \quad (7)$$

Based on results obtained in chapter 4 and 5, and their theoretical significance as described in section 6.2.2, we would expect this trend in the diffusion coefficient values. Section 6.4 reports the procedures and results obtained by doing diffusion coefficient analysis on the MD trajectory data as described in section 6.2.1. These results are compared and discussed in section 6.4.3.

6.4 Computational Analysis of Diffusion Coefficients

The trajectory data extracted from MD simulations were used to calculate the diffusion coefficients of these complexes in two different solutions. Section 6.4.1 reports and discusses the results obtained for systems of PGM chloro-complexes in water and polymer (PEO) solution. Section 6.4.2 describes the results for systems of PGM chloro-complexes in water solution. Procedural details of how these trajectories were generated were described in Chapter 4 (section 4.2 and 4.3 respectively). The mean-square displacements were calculated for different time delays and plotted as a linear equation over time [13] . The theoretical details of this method were described in Chapter 2, Section 2.4. In order to prevent distortions resulting from atom-atom collisions, the time delays considered when calculating the slope were made as large as possible [14, 15] . Choosing these time delays presents a major practical problem. The integrity of the mean-square displacement values calculated at longer time intervals is very weak. This is due to the fact that very few data points are available for these intervals. In order to quantify the error margins involved in these calculations it is imperative that confidence intervals are calculated for the mean-square displacement values. This allows us to get a realistic idea of the accuracy of the calculated diffusion rates. These confidence intervals were calculated from independent data points. This is crucial as the overlap values at longer time intervals obscure the real variation.

6.4.1 Diffusion of PGM chloro-complexes in water and polymer (PEO) solution.

The Cartesian coordinate data extracted from MD simulations (section 4.3) of these systems were used to calculate the mean-square displacements for equilibrated trajectories of 1.1 ns. In order to prevent distortions due to atom-atom collisions a maximum time delay of 335 ps is used. It is important to note that this time delay would only deliver three independent square displacement values. The variation

expected of the calculated mean over these delay regions (100 ps to 335 ps) is therefore large. A linear regression analysis (least square fit) was performed and the slope of the equation was determined between 0 and 335 ps time delays. In each case the lower and upper limits of a 95% confidence interval was calculated and plotted. These confidence intervals clearly reflect the increased variation in the longer time delay regions. Linear lines were also fitted (least square fit) to these confidence interval (upper and lower) results. These graphs can be seen in fig 6.1 (a) to (d).

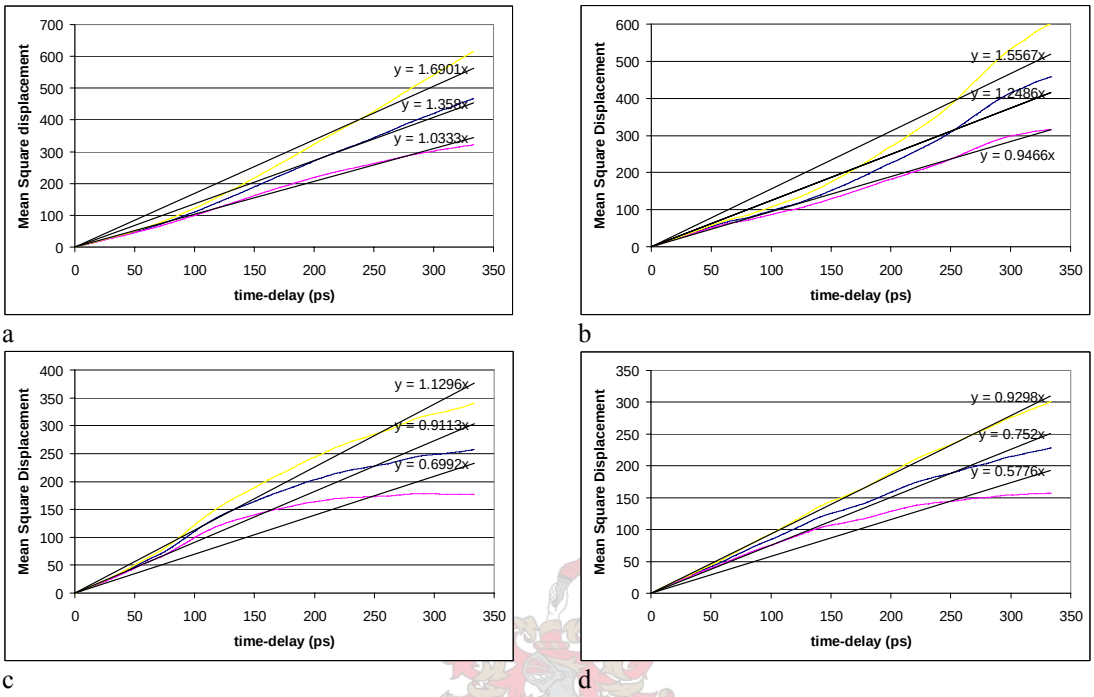

Fig 6.1: Mean Square displacement (MSD) data for the PGM complexes: (a) $[PdCl_4]^{2-}$, (b) $[PtCl_4]^{2-}$, (c) $[PtCl_6]^{2-}$ and (d) $[RhCl_6]^{3-}$. In each case the 95% confidence interval (upper and lower limit) was also plotted.

By investigating fig. 6.1 we get an idea of the uncertainty involved (when calculating the mean square displacements) over the various time delays when using this technique. The increasing sizes of the confidence intervals with increasing time delays are an indication of the lack of reliability at longer time delays. This phenomenon is observed in all four systems. The slopes of the following MSD data were subsequently calculated (least square fit): (1) The slope of the MSD data over a 0-335 ps time delay interval. (2) The slope of the upper confidence interval of the MSD data over a 0-335 ps time delay interval. (3) The slope of the lower confidence interval of the MSD data over a 0-335 ps time delay interval. In each case the intercept was forces to be zero. The results obtained from this analysis and the diffusion coefficients derived from them are summarized in Table 6.1. Figure 6.2 is a graphic presentation illustrating the extent of the 95% confidence intervals.

	95% Confidence Interval Limits: slopes			95% Confidence Interval Limits: Diffusion Coefficients		
	Lower	Mean	Upper	cm^2/sec ($*10^{-5}$) Lower	cm^2/sec ($*10^{-5}$) Mean	cm^2/sec ($*10^{-5}$) Upper
$[PdCl_4]^{2-}$	1.03	1.36	1.69	1.72	2.26	2.82
$[PtCl_4]^{2-}$	0.95	1.25	1.56	1.58	2.08	2.59
$[PtCl_6]^{2-}$	0.70	0.91	1.13	1.17	1.52	1.88
$[RhCl_6]^{3-}$	0.58	0.75	0.97	0.96	1.25	1.62

Table 6.1 Summary of the slopes calculated and the diffusion coefficient results obtained over a time delay of 0 to 335 ps.

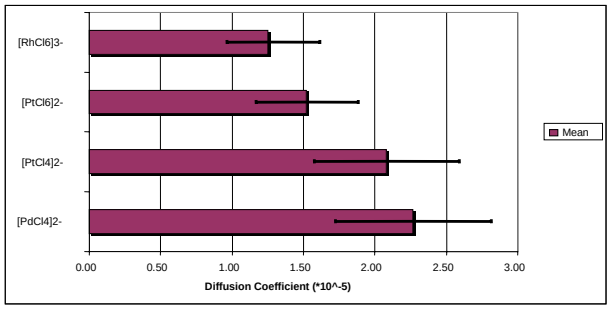

Fig 6.2: A graphic presentation illustrating the diffusion coefficients as well as their respective 95% confidence intervals.

Section 6.2 gave a brief theoretical background of the effect of physical and thermodynamic properties on the diffusion coefficients of ions in a liquid. Based on these principles we can now compare the expected trends, as discussed in section 6.3, and the calculated trends. The discussion below is devoted to this comparison. Fig 6.3 gives a graphical presentation of: (1) The relative electrostatic component of the free energy of solvation values of all the relevant PGM complexes. The lower and upper range values are also included. (2) The relative hydration shell volumes of the PGM complexes. (3) The relative diffusion coefficients as well as their respective 95% confidence intervals of the PGM complexes. Table 6.2 is a summary of the relative values of these properties and might serve as a useful reference. The detailed values, ranges and confidence intervals can be found in chapter 4 (hydration shell volumes) and chapter 5 (free energy of solvation values).

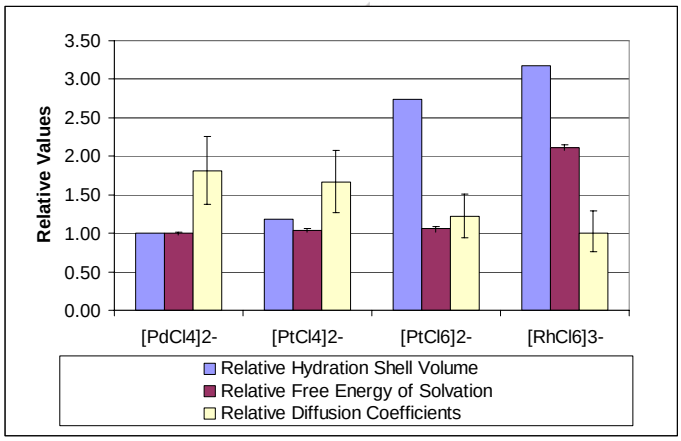

Fig 6.3: A graphic presentation of the relative values of the physical and thermodynamic properties of the respective PGM complexes and how they relate to the relative values of the calculated diffusion coefficients. (1) The electrostatic component of the free energy of solvation values. (2) The hydration shell volumes. (3) The diffusion coefficients and their 95% confidence intervals.

	Relative Hydration Shell Volume	Relative Free Energy of Solvation	Relative Diffusion Coefficients
$[PdCl_4]^{2-}$	1.00	1.00	1.81
$[PtCl_4]^{2-}$	1.19	1.04	1.66
$[PtCl_6]^{2-}$	2.74	1.06	1.22
$[RhCl_6]^{3-}$	3.17	2.12	1.00

Table 6.2: A summary of the following relative values: the hydration shell volumes, the free energies of solvation and the diffusion coefficients.

(i) Comparing Computational and Experimental results:
Due to the uncertainty associated with the calculated diffusion coefficients it is almost impossible to compare these results with those found experimentally. Moreover, no experimental results are available for a system that resembles the system under conditions simulated here. Discussion of these results will

therefore be restricted to a qualitative description. It can be concluded with relative certainty that the diffusion coefficients calculated for the two octahedral complexes ($[PtCl_6]^{2-}$ and $[RhCl_6]^{3-}$) are greater than those of the square planar complexes ($[PdCl_4]^{2-}$ and $[PtCl_4]^{2-}$). There is relatively little overlap of the respective confidence intervals for these two groups. However, when comparing the results of $[PtCl_6]^{2-}$ and $[RhCl_6]^{3-}$, the confidence intervals overlaps so severely that a definite conclusion as to the order of the diffusion rates is impossible. The same applies when comparing the calculated diffusion coefficients of the square planar complexes ($[PdCl_4]^{2-}$ and $[PtCl_4]^{2-}$).

(ii) Comparing the trend of the Computational results with the trend expected based on the Free Energy of Solvation calculations (trend 5 in section 6.3):
Although the relative order of the diffusion coefficients of these PGM complexes ($[PtCl_6]^{2-}$; $[RhCl_6]^{3-}$; $[PdCl_4]^{2-}$ and $[PtCl_4]^{2-}$) are difficult to determine there is some consistency with the theory that diffusion rates are dependant on the degree of solvation of the species in question [10-12]. The electrostatic components of free energies of solvation were calculated and discussed in chapter 5. Figure 6.3 presents these free energy results as well as illustrating the range involved based on minimum and maximum configurational energies. These configurations were extracted from the MD trajectories. A full account of the procedural details as well as a thorough discussion of the results can be found in chapter 5, section 5.2. If we treat these free energies as a measure of the degree of solvation of the complexes, there exits a weak qualitative correlation with what we have postulated. As the values of the free energies of solvation increase, the values of the calculated diffusion coefficients decrease. It should be emphasized that such a correlation was made purely by considering the order of the results. The trend does not, however, conclusively support the expected results (which were based on the argument that the diffusion coefficient of a highly solvated complex is retarded because it has to drag its hydration shell with it to some extent).

(iii) Comparing the trend of the Computational results with the trend expected based on the Volume of solvation shell calculations (trend 6 in section 6.3):
As mentioned above, the variation in the values of the diffusion coefficients of these PGM complexes ($[PtCl_6]^{2-}$; $[RhCl_6]^{3-}$; $[PdCl_4]^{2-}$ and $[PtCl_4]^{2-}$) prevents us from making conclusive comparisons. There is some consistency however with the theory that diffusion coefficients are affected by the volume of the hydration shell of the species in question. As the volumes increase, the values of the calculated diffusion coefficients decrease. These hydration shell volumes were calculated and discussed in chapter 4. Figure 6.3 presents these solvation sphere volume results. A full explanation of the procedural details as well as a thorough discussion of these results can be found in chapter 4, section 4.2. Again, due to the uncertainty involved, the trend does not conclusively support the expected results (which were based on the Stokes-Einstein equation).

6.4.2 Diffusion of PGM chloro-complexes in water

The procedure and analysis performed in section 6.4.1 are repeated in this section, but applied to the Molecular Dynamics data generated from the systems without the polymer present. As before, the mean-square displacements were calculated over equilibrated trajectories of 1.1 ns. A maximum delay time of 335 ps was used. The variation expected of the calculated mean over longer time delay regions (100 ps to 335 ps) is therefore comparable in terms of uncertainty to those in section 6.4.1. A linear regression analysis (least square fit) was performed and the slope of the equation was determined between 0 and 335 ps time delays. In each case the lower and upper limits of a 95% confidence interval was calculated and plotted. Linear lines were also fitted (least square fit) to these confidence interval (upper and lower) results. These graphs can be seen in fig 6.4 (a) to (d).

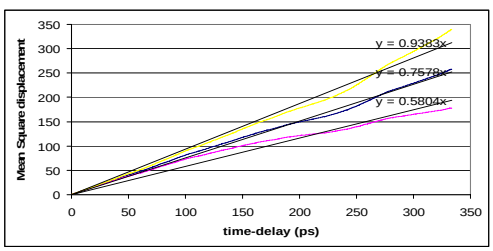

a

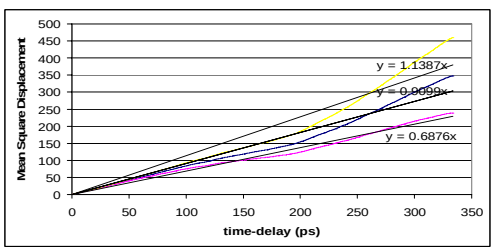

b

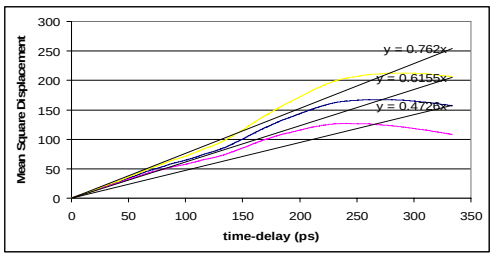

c

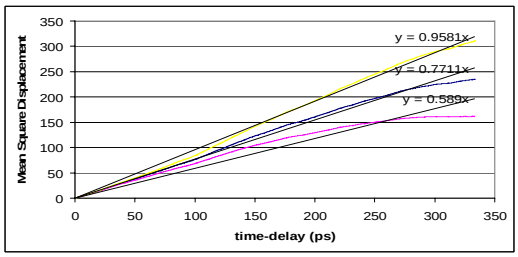

d

Fig 6.4: Mean Square displacement (MSD) data for the PGM complexes: (a) $[PdCl_4]^{2-}$, (b) $[PtCl_4]^{2-}$, (c) $[PtCl_6]^{2-}$ and (d) $[RhCl_6]^{3-}$. In each case the 95% confidence interval (upper and lower limit) was also plotted.

By investigating fig. 6.4 we get an idea of the uncertainty involved (when calculating the mean square displacements) over the various time delays when using this technique. As in section 6.4.1, the increasing sizes of the confidence intervals with increasing time delays are an indication of the lack of reliability at longer time delays. This phenomenon is observed in all four systems. All the appropriate slopes were calculated (least square fit), while forcing the intercept to be zero. The results obtained from this analysis and the diffusion coefficients derived from them are summarized in Table 6.3. Figure 6.5 is a graphic presentation illustrating the extent of the 95% confidence intervals.

	95% Confidence Interval Limits: slopes			95% Confidence Interval Limits: Diffusion Coefficients		
	Lower	Mean	Upper	cm^2/sec ($*10^{-5}$) Lower	cm^2/sec ($*10^{-5}$) Mean	cm^2/sec ($*10^{-5}$) Upper
$[PdCl_4]^{2-}$	0.58	0.76	0.94	0.97	1.26	1.56
$[PtCl_4]^{2-}$	0.69	0.91	1.14	1.15	1.52	1.90
$[PtCl_6]^{2-}$	0.47	0.62	0.76	0.79	1.03	1.27
$[RhCl_6]^{3-}$	0.59	0.77	0.96	0.98	1.29	1.60

Table 6.3 Summary of the slopes calculated and the diffusion coefficient results obtained over a time delay of 0 to 335 ps.

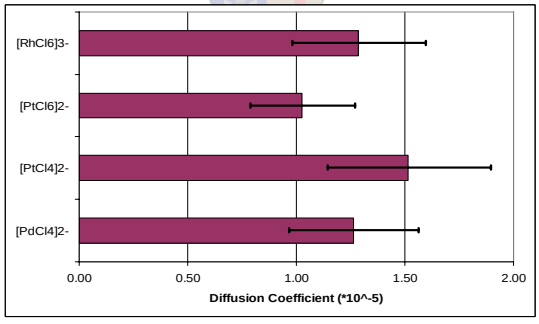

Fig 6.5: A graphic presentation illustrating the diffusion coefficients as well as their respective 95% confidence intervals.

The discussion that follows is aimed at shedding light on the correlations between the calculated diffusion coefficients and the trends we expect due to the effects of physical and thermodynamic properties of the PGM systems. Fig 6.6 gives a graphical presentation of the following relative results: (1) The electrostatic component of the free energy of solvation values of all the relevant PGM complexes. The lower and upper range values are also included. (2) The hydration shell volumes of the PGM complexes. (3) The diffusion coefficients as well as their respective 95% confidence intervals of the PGM complexes. Table 6.4 is a summary of the actual calculated values of these properties and might serve as a useful reference. The detailed values, ranges and confidence intervals can be found in chapter 4 (hydration shell volumes) and chapter 5 (free energy of solvation values).

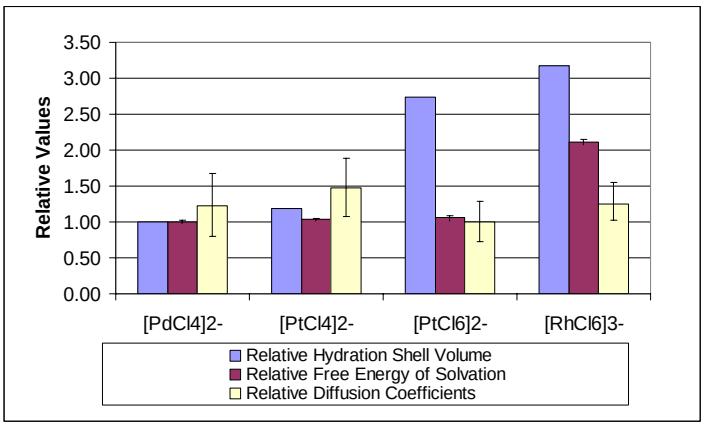

Fig 6.6: A graphic presentation of the relative values of the physical and thermodynamic properties of the respective PGM complexes and how they relate to the relative values of the calculated diffusion coefficients. (1) The electrostatic component of the free energy of solvation values. (2) The hydration shell volumes. (3) The diffusion coefficients and their 95% confidence intervals.

	Relative Hydration Shell Volume	Relative Free Energy of Solvation	Relative Diffusion Coefficients
$[PdCl_4]^{2-}$	1.00	1.00	1.23
$[PtCl_4]^{2-}$	1.19	1.04	1.48
$[PtCl_6]^{2-}$	2.74	1.06	1.00
$[RhCl_6]^{3-}$	3.17	2.12	1.25

Table 6.4: A summary of the following relative values: the relative hydration shell volumes, the relative free energies of solvation and the relative diffusion coefficients.

(i) Comparing Computational and Experimental results:
Due to the uncertainty associated with the calculated diffusion coefficients it is almost impossible to compare these results with those found experimentally. It is clear from fig 6.5 that there is extensive overlap of the respective confidence intervals of the calculated diffusion coefficients of all these PGM complexes. The confidence intervals overlap so severely that a definite conclusion as to the order of the diffusion rates is impossible.

(ii) Comparing the trend of the Computational results with the trend expected based on the Free Energy of Solvation calculations (trend 5 in section 6.3):
There is a weak suggestion in conformance with the theory that diffusion rates are dependant on the degree of solvation of the species in question [10-12]. No definitive conclusions can be made however. Figure 6.6 presents the relative free energy results as well as illustrating the range involved based on minimum and maximum configurational energies. There exits no conclusive evidence of a qualitative correlation, as we have postulated in section 6.3.

(iii) Comparing the trend of the Computational results with the trend expected based on the Volume of solvation shell calculations (trend 6 in section 6.3):
There is almost no consistency with the theory that diffusion coefficients are affected by the volume of the hydration shell of the species in question. These hydration shell volumes were calculated and discussed in chapter 4. Figure 6.6 presents these solvation sphere volume results. There exits no conclusive evidence of a qualitative correlation. Future work is planned to improve the level of accuracy of these results. Ideally the mean-square displacements must be calculated for equilibrated trajectories of at least 5 ns. Although this would require extensive computational resources, it is the only way of narrowing the confidence intervals.

6.4.3 The effect of the polymer (PEO) on the diffusion of PGM chloro-complexes in water

Due to the vast uncertainties involved, it is impossible to make any quantitative observations or comparisons. A few general contrasts were observed, however, which will be discussed. Possible

explanations for these observations will be proposed as well as the context of their interpretation. The figure below represents a combination of fig 6.2 and fig 6.5 which were presented in section 6.4.1 and 2 respectively. When comparing the calculated diffusion coefficients of the $[RhCl_6]^{3-}$ complexes it is clear that the overlap of the confidence intervals is almost exact. This quantitative overlap partially exists for the diffusion coefficients of the $[PtCl_4]^{2-}$ complexes, whereas very little overlap is present for the $[PtCl_6]^{2-}$ complexes. No overlap of the confidence intervals exists, however, for the $[PdCl_4]^{2-}$ complexes. The diffusion coefficients calculated for the systems where the polymer is absent are consistently (apart from the $[RhCl_6]^{3-}$ complexes) lower than those systems where the polymer in present.

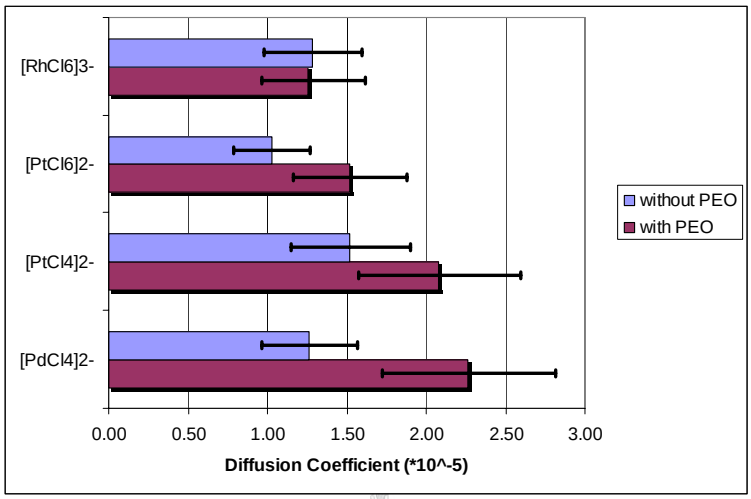

Fig 6.2 and Fig 6.5 combined: A graphic presentation illustrating the diffusion coefficients as well as their respective 95% confidence intervals of the systems with and the systems without the polymer (PEO) present in solution.

The phenomenon described above can partially be explained in terms of differences in the non-bonded interaction parameters chosen for the MD simulations of these two system types (with and without PEO). The reader in reminded that the NPT ensemble was used in both cases, which means that the volume of the box varied slightly during the simulations to maintain constant pressure. The distance cutoff involved in generating the list of atom pairs was chosen as 12 Å for the systems without the polymer (average box size was 24.6 Å cubed) and 14 Å for the systems with the polymer (average box size was 48.7 Å cubed). During the MD simulations of the systems without the polymer there were a number of time frames where the volume of the box went below 24 Å cubed. With the cutoffs chosen at 12 Å it means that for those specific frames the PGM complex was affected by its own image atoms from neighboring boxes (2×12 Å > 23.99 Å). Another factor might be that the lists of atom pairs generated to calculate the non-bonded interactions of the two system types (with and without PEO) are not similar because the cutoff distances differ. The list of atom pairs of the system with the polymer is more extensive than that of the system without the polymer. Future work is planned to eliminate these side effects and improve the simulation consistency so that quantitative comparisons would be possible between the two system types.

As was reported in chapter 4, the concentrations of the systems where the polymer is absent is 8 times greater than the systems where the polymer in present. Both systems are relatively dilute however, and the probability of interference due to concentration is low. The interferences mentioned above however most probably obscure the actual chemical effect of the polymer (PEO) chains on the transport properties of the PGM complexes in the solution. A conclusion as to the influence of the PEO chains on the diffusion of the PGM complexes is therefore impossible.

6.5 Future work

Future work in this area would mostly be focused on improving the accuracy (decreasing the size of the confidence intervals) of the calculations. These inaccuracies are mostly due to insufficient independent data points, specifically *square displacement* values. In order to calculate a reliable *mean square*

displacement value at a specific time delay, there must be enough data points to make the average statistically significant. The more data points exist, the more reliable the statistical conclusions drawn from it become. Figure 6.7 illustrates the number of data points (*square displacement* values) which exits at all the respective time delays. The analysis in this chapter was performed by using MD trajectories which were recorded over 1.1 ns. The maximum time delay period (335 ps) therefore has only 3 (1100/335) independent data points from which to calculate the mean. This implies that the averages calculated over long period time delays are not statistically reliable. As for very small time delays, as is clear from fig 6.7, the statistical reliability increases dramatically. The disadvantage, however, of calculating the slope (using least square fit) over a smaller time delay range is that it increases the probability that the results could be distorted due to atom-atom collisions. Unfortunately, the only way to prevent this problem is to radically increase the total time over which the MD trajectory in recorded. If a total trajectory of 10.1 ns was used for instance, the maximum time delay period (335 ps) would have 30 independent data points. The statistical reliability is increased and the confidence intervals are narrowed.

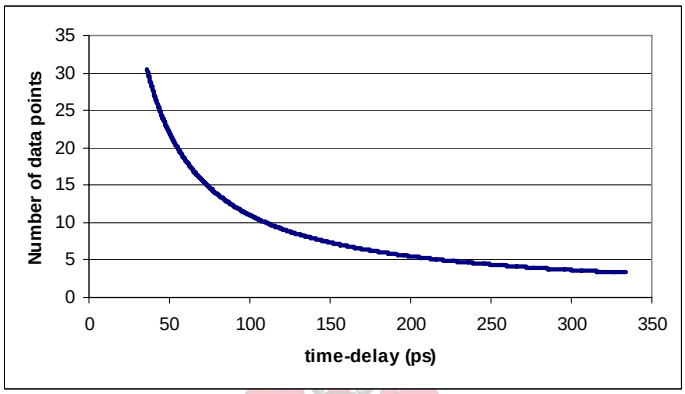

Fig 6.7: A presentation of the number of independent data points per time delay period as calculated over a total trajectory time frame of 1.1 ns.

To compound the problem however, it can be shown that even a maximum time delay period of 335 ps is not long enough to accurately allow for real displacement. If the diffusion coefficient was calculated over a short time delay range, the *mean square displacement* values calculated are more likely to resemble the *mean square distance* traveled. These results would then be of limited practical use from a chemical point of view. It is vital that proper displacement is achieved, which implies that the maximum time delay range must be long enough to insure meaningful results. Theoretically, by calculating the diffusion coefficients over increasing maximum time delay ranges, the calculated values would start to stabilize (approach its constant value, *D*) as the maximum delay reaches sufficiently large period ranges. Figure 6.8 and 9 show the calculated diffusion coefficients based on different maximum time delay ranges for the systems with and without the polymer present respectively. The values of the diffusion coefficients (y-axis) at time delays of 335 ps (on the x-axis) correspond to those values which were reported in section 6.4.1 and 2. Figure 6.8 and 9 illustrates that the calculated diffusion coefficients have not yet stabilized. From this it is clear that proper displacements have not been achieved and that the maximum time delay ranges should be increased in order to insure meaningful results. Again, the solution to this problem is to radically increase the total time over which the MD trajectory in recorded.

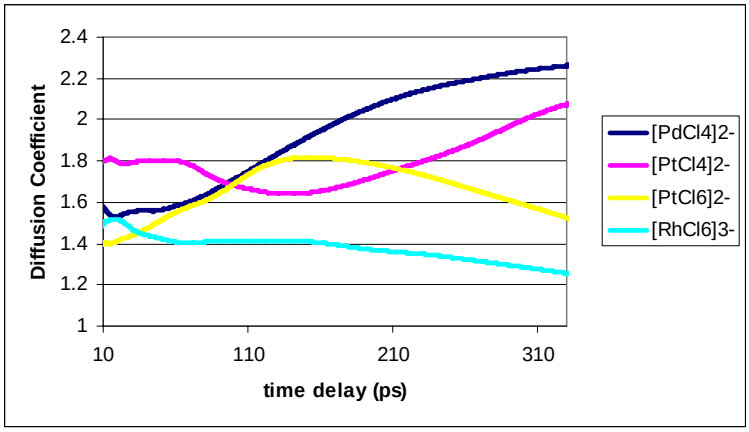

Fig 6.8: The calculated diffusion coefficients based on different maximum time delay ranges (between 10 and 335 ps) for the PGM chloro-complexes in water and polymer (PEO) solution.

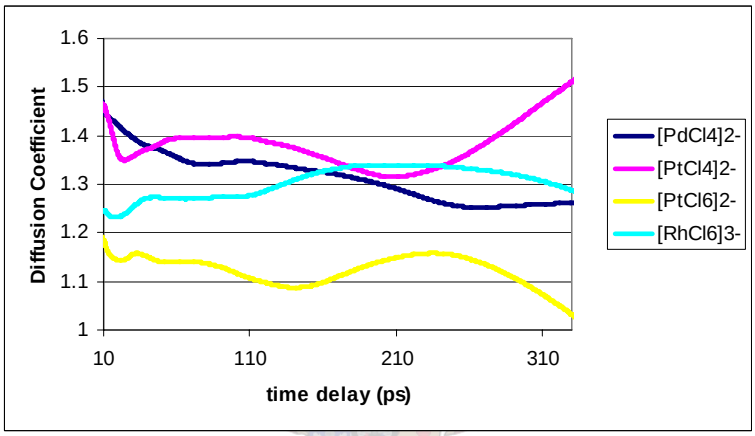

Fig 6.9: The calculated diffusion coefficients based on different maximum time delay ranges (between 10 and 335 ps) for the PGM chloro-complexes in water solution.

References:

1. K.P. Hupe, *The Past 10 Years in Chromatography*. LC GC, 1992. **10**(211).
2. G.D. Christian, *Analytical Chemistry*. 5 ed. 1994, New York: John Wiley & Sons, Inc.
3. G. Lipari and A. Szabo, *Model-Free Approach to the Interpretation of Nuclear Magnetic Resonance Relaxation in Macromolecules. Theory and Range of Validity*. J. Am. Chem. Soc., 1982. **104**(17): p. 4546 - 4559.
4. M.P. Allen and D.J. Tildesley, *Computer Simulation of Liquids*. First ed. 1989, Oxford: Oxford Science Publications.
5. A.R. Leach, *Molecular Modelling: Principles and Applications*, 1996, Singapore: Longman. 595.
6. J. Crank, *The mathematics of diffusion*. 1975, Oxford: Clarendon Press.
7. J.N. Murrell and A.D. Jenkins, *Properties of liquids and solutions*. 1994, New York: Wiley-Interscience.
8. J.S. Rowlinson and F.L. Swinton, *Liquids and liquid mixtures*. 1982, London: Butterworth.
9. Atkins, *Physical Chemistry*. 6 ed. 1998, Oxford: Oxford University Press.

10. I. Klapper, *Focusing of electric fields in the active site of Cu-Zn superoxide dismutase:effectsof ionic strength and amino acid modification.* Proteins, 1986. **1**: p. 47-59.
11. G.J. Moro, A. Polimeno and J.H. Freed, *A cage model of liquids supported by molecular dynamics simulations.1.The cage variables.* J.Chem.Phys., 1994. **101**(1): p. 693-702.
12. J.L. Willett, *Water sorption and diffusion in starch/polyolefin blends.* Polym. Eng. Sci., 1995. **35**(14): p. 1184-1190.
13. I.M.J.J. van de Ven-Lucassen, T.J.H. Vlugt, A.J.J. van der Zanden and P.J.A.M. Kerkhof, *Molecular Dynamics Simulation of Self-Diffusion Coefficients in Liquid Mixtures of Methanol and Water.* Mol. Simulat., 1999. **23**: p. 79-94.
14. J. Ennari, M. Elomaa, and F. Sundholm, *Modelling a polyelectrolyte system in water to estimate the ion-conductivity,.* Polymer, 1999. **40**(18): p. 5035-5041.
15. J. Ennari, I. Neelov, and F. Sundholm, *Estimation of the ion conductivity of a PEO based polyelectrolyte system by molecular modeling.* Polymer, 2001. **42**(19): p. 8043-8050.